ISSN 0038-531X

*Russian Original Vol. 55, No. 1, July, 1983*

January, 1984

SATEAZ 55(1) 441-504 (1983)

PEEL HERE

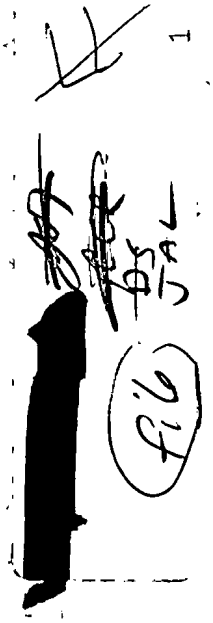

# SOVIET ATOMIC ENERGY

АТОМНАЯ ЭНЕРГИЯ
(ATOMNAYA ÉNERGIYA)

TRANSLATED FROM RUSSIAN

c/b CONSULTANTS BUREAU, NEW YORK

# SOVIET ATOMIC ENERGY

*Soviet Atomic Energy* is abstracted or indexed in *Chemical Abstracts, Chemical Titles, Pollution Abstracts, Science Research Abstracts, Parts A and B,, Safety Science Abstracts Journal, Current Contents, Energy Research Abstracts,* and *Engineering Index.*

Mailed in the USA by Publications Expediting, Inc., 200 Meacham Avenue, Elmont, NY 11003.

**POSTMASTER:** Send address changes to *Soviet Atomic Energy,* Plenum Publishing Corporation, 233 Spring Street, New York, NY 10013.

*Soviet Atomic Energy* is a translation of *Atomnaya Énergiya,* a publication of the Academy of Sciences of the USSR.

An agreement with the Copyright Agency of the USSR (VAAP) makes available both advance copies of the Russian journal and original glossy photographs and artwork. This serves to decrease the necessary time lag between publication of the original and publication of the translation and helps to improve the quality of the latter. The translation began with the first issue of the Russian journal.





Consultants Bureau journals appear about six months after the publication of the original Russian issue. For bibliographic accuracy, the English issue published by Consultants Bureau carries the same number and date as the original Russian from which it was translated. For example, a Russian issue published in December will appear in a Consultants Bureau English translation about the following June, but the translation issue will carry the December date. When ordering any volume or particular issue of a Consultants Bureau journal, please specify the date and, where applicable, the volume and issue numbers of the original Russian. The material you will receive will be a translation of that Russian volume or issue.

Subscription (2 volumes per year)
Vols. 54 & 55: $500 (domestic); $555 (foreign)
Vols. 56 & 57: $560 (domestic); $621 (foreign)

Single Issue: $100
Single Article: $7.50

**CONSULTANTS BUREAU, NEW YORK AND LONDON**

c/b
233 Spring Street
New York, New York 10013

Published monthly. Second-class postage paid at Jamaica, New York 11431.

# SOVIET ATOMIC ENERGY

A translation of *Atomnaya Énergiya*

January, 1984

Volume 55, Number 1 July, 1983

## CONTENTS

# CONTENTS

(continued)

Engl./Russ.



**The Russian press date (podpisano k pechati) of this issue was 6/27/1983. Publication therefore did not occur prior to this date, but must be assumed to have taken place reasonably soon thereafter.**

# PHYSICAL CHARACTERISTICS OF THE BN-600 REACTOR

Yu. A. Kazanskii, M. F. Troyanov,
V. I. Matveev, A. Ya. Evseev,
A. V. Zvonarev, A. I. Kiryushin,
B. A. Vasil'ev, S. P. Belov,
I. P. Matveenko, Yu. S. Kulabukhov,
V. A. Chernyi, V. G. Dvukhsherstnov,
A. T. Bakov, A. P. Ivanov,
P. L. Tyutyunnikov, and G. M. Pshakin

UDC 621.039.526

The BN-600 reactor with a design power of 600 MW (elec.) was built for the third unit of the I. V. Kurchatov Beloyarsk nuclear power plant [1-3]. It has an integral arrangement (with the pumps and the intermediate heat exchangers in the reactor vessel) and a three-circuit heat-removal system. Each circuit consists of three loops; the three generators develop up to 200 MW each.

The fuel elements of enriched uranium dioxide have stainless steel cladding and are contained in hexahedral fuel-element assemblies (FEA).

The principal technical characteristics of the BN-600 reactor are as follows:

| | |
|---|---|
| Thermal power, MW | 1470 |
| Core volume, liters | 2570 |
| Core height, mm | 750 |
| Core diameter, mm | 2058 |
| Maximum neutron flux, neutrons/cm$^2$·sec | $0.77 \times 10^{16}$ |
| Maximum core power density, kW/liter | 806 |
| FEA size "under key," mm | 96 |
| No. of fuel elements in core FEA | 127 |
| Diameter and thickness of core fuel element cladding, mm | 6.9 ×0.4 |
| No. FEA in low enrichment zone (LEZ) | 215 |
| Composition of fuel in LEZ | $UO_2$, 21% enriched |
| No. FEA in high enrichment zone (HEZ) | 154 |
| Composition of fuel in HEZ | $UO_2$, 33% enriched |
| No. fuel elements in FEA of side blanket | 37 |
| Diameter and thickness of cladding of fuel elements of side blanket, mm | 14.1 ×0.4 |
| No. assemblies of inner blanket | 161 |
| No. assemblies of outer blanket | 218 |
| Thickness of end blankets (combined in one tube with active part of fuel element), mm | 400 |
| Material of side and end blankets | Depleted $UO_2$ |
| No. automatic control (AC) rods (europium oxide) | 2 |
| No. shim rods (SR) (europium oxide) | 19 |
| No. emergency shut down rods (ESR) ($B_4C$, 80% enriched) | 6 |

The assembly of the reactor, the adjustment of all control and power measurement systems, and the checking of the shield were completed in December, 1979. The loading of the BN-600 was begun on December 28, 1979 with the installation of the start-up neutron source (SNS) and the FEA of the side blanket. The reactor went critical on February 26, 1980 with a minimum critical mass, and on April 8, 1980 was brought up to a 30% power level.

Translated from Atomnaya Énergiya, Vol. 55, No. 1, pp. 9-14, July, 1983. Original article submitted December 28, 1982.

0038-531X/83/5501-0441$07.50  

In this period, all the studies specified by the program of physical start-up were performed. The critical core parameters were determined for various positions of the shim rods; the start-up core loading was built up; measurements were made of the effectiveness of the control and safety rods (CSR), reactivity effects related to variations in the technological parameters (sodium temperature, pump speed, pressure in the reactor vessel cavity), the power distribution, and the ratios of the average cross sections for the basic reactions; and the effectiveness of the biological shield was investigated.

In the present article we present the main results of the study of the neutron-physical characteristics of the reactor, and compare them with design values.

## Reactor Loading and Critical Parameters

To monitor the chain reaction during loading of the FEA, a start-up neutron source (SNS) having a strength of $1.5 \times 10^9$ neutrons/sec was made with ampoules of $^{239}$Pu—Be in a special cassette. Since the strength of the SNS is ~100 times lower than that of a regular Sb—Be photoneutron source, the start-up sensors — SNM-18 and SNM-14 neutron counters and a KNK-56 chamber — were mounted on a special bracket attached to a small rotatable plug. With this arrangement the neutron flux in the reactor could be confidently monitored from the instant the SNS was placed in the reactor. Before the initial loading of the FEA, the reactor was filled with sodium; steel FEA mockups were located in the reactor.

The reactor was loaded in the following order. First the SNS was placed in a cell near the reactor center, and then the FEA of the inner side blanket, the ESR, the AC rods, and the central shim rod (SRC) were loaded. After this, loading of FEA of the LEZ was begun from the core center, and then the HEZ.

In the process of loading FEA, the SRC and ESR-1 and ESR-5 were periodically withdrawn by using the refueling mechanism. This permitted the state of the reactor to be predicted with confidence.

The drives were not coupled to the rods loaded into the core until 123 FEA of the LEZ had been loaded, when they were surrounded by the ESR.

Subsequently, the extrapolated value of the minimum critical mass was found by coupling two rods with their drives, when 208 FEA of the LEZ and 215 FEA of the LEZ + 14 FEA of the HEZ were in the core. After the loading was completed, the reactor was brought to the critical state.

The minimum critical mass for a sodium temperature of 245°C when the ESR, the AC rods, the SRC, and SR-4 were at the upper ends was achieved with 215 FEA in the LEZ + (36 ±1) FEA in the HEZ.

The indeterminacy of the number of FEA in the HEZ is related to the error in extrapolating the critical mass to the state when the SRC was withdrawn to the upper end.

After reaching the minimum critical mass, the remaining compensators were loaded into the core, and the loading of FEA of the HEZ was continued. When 107 FEA of the HEZ had been loaded, the rods were coupled to the CSR drive mechanisms, and the reactor was brought to the critical state by raising the SR. At 245°C the critical state was achieved by raising 18 SR by 300 mm. Extrapolation to a state in which the SR are completely inserted and the ESR, the AC rods, and the SRC are at the upper ends gave the following value of the critical mass: 215 FEA of the LEZ + (128 ±1) FEA of the HEZ.

If the core were loaded with FEA of the initial enrichment with nominal dimensions of the LEZ and the HEZ, the reactor would be supercritical. Therefore, in accord with design, 13 constant reactivity compensators (CRS), which are FEA with depleted uranium dioxide, were placed in the reactor to compensate the excess reactivity, and the remaining FEA of the HEZ were loaded. For this so-called start-up loading of the core, the critical state at 225°C was achieved by positioning 18 SR at a level of 100 mm from the lower edge of the core and the remaining ESR, AC rods, and SRC at the upper ends, with a core composition of 213 FEA in the LEZ + 143 FEA in the HEZ + 13 CRC.

If in this state all 18 SR are inserted to the lower ends, at 245°C the reactor will have a negative reactivity of $-(0.15 \pm 0.01)\%$ $\Delta k/k$. The critical state of the reactor with the start-up load at a sodium temperature of 380°C is achieved with the rods at the 220-mm level.

To compare the results obtained with the design parameters, we consider the design concept which was used in determining the critical reactor parameters during planning. The core was analyzed in the steady refueling regime. The enrichment of fresh fuel in the FEA of the LEZ and HEZ was determined by requiring excess reactivity for burnup in the initial cycle, and optimum flattening of the power distribution during the whole cycle between refuelings.

The basic calculations were performed in the multigroup diffusion approximation in one-dimensional geometry using nuclear data from BNAB-70 [4]. The enrichment of fresh fuel found in this way was 21% for FEA of the LEZ and 33% for FEA of the HEZ. Subsequently, during modeling of the reactor on critical assemblies, the possible errors of the methods, programs, and nuclear data were determined. With respect to $K_{ef}$ this error was estimated as ±1.2% Δk/k [5].

The criticality of the reactor in the initial state was calculated by determining the number of CRC necessary to compensate the excess reactivity of the fresh fuel. In this way it was found that in the initial state of the reactor it was necessary to load 13 CRC into the core at locations chosen to give the best flattening of the power distribution in the initial state: 11 CRC in the first row of the HEZ and 2 CRC in the LEZ. According to calculations, the SR should be raised 305 mm from the lower edge of the core in the critical state at a core temperature of 380°C and zero power. This raising of the SR was a result of the excess effectiveness of this system, estimated to be 1.5% Δk/k, which it was decided to retain until reactor start-up. In reducing this state to experiment by using the calculated graduation of the characteristics of the SR, the difference in $K_{ef}$ between the realized and design state of the core was 1.3% Δk/k. Analysis showed that part of this difference (+0.5% Δk/k) results from the difference between the actual and design loading of the reactor, arising from a certain increase in the average density of the fuel pellets. Another part (+0.8% Δk/k) comes from the error of the computational methods and the nuclear data, and lies within the limits of error estimated earlier on the basis of experimental modeling of the reactor.

Excess Reactivity. Control Rod Effectiveness

As already noted, the reactor with a start-up core at a sodium temperature of 225°C was in the critical state with 18 SR almost completely inserted and the remaining SRC, ESR, and AC rods withdrawn.

Thus, 18 SR produce excess reactivity for compensating temperature and power reactivity effects in bringing the reactor to the design power level, and the loss of reactivity during reactor operation between two refuelings.

It is impossible to measure the excess reactivity directly. Therefore, various estimates of the effectiveness of the 18 SR were made by using experimental and design data.

In the start-up range the effectiveness of the system was measured by moving the rods into the core from the 240 mm mark to their lower ends. Assuming that the calibration characteristics of the 18 SR correspond to the calibration characteristics of the remaining SR, the effectiveness of the whole system was determined for the displacement of the rods from the 240 mm mark to their upper ends. The total effectiveness of the system of 18 SR calculated in this way was (5.9 ±0.3)% Δk/k.

A procedure for finding rod effectiveness by making outside estimates regarding interfering and noninterfering rods was developed earlier. To do this it is necessary to know the effectiveness of the individual rods of the system in the presence (measurement with the start-up loading) and in the absence (measurement with the minimum critical mass) of the other rods. Appropriate computational corrections were introduced into the effectiveness of the rods measured with the minimum critical mass to take account of the difference in core configurations with minimum critical mass and with the start-up loading. The effectiveness of the system of 18 SR found by the method of outside estimates was (6.0 ±0.3)% Δk/k.

Finally, the effectiveness of the system of 18 SR was determined from measurements of the effectiveness of single rods in the start-up core and calculated interference coefficients. This procedure is rather convincing, since the interference coefficients are relatively small (15-20%) and, consequently, the computational error is small. The effectiveness of the system determined in this way was (5.7 ±0.3)% Δk/k. All three methods gave nearly the same value of the effectiveness of the system; the differences were within the limits of experimental errors.

TABLE 1. Comparison of Measured and Calculated Effectiveness of CSR, %Δk/k

| Rod | Experiment | Calculation |
|---|---|---|
| SR-1 | 0,461±0,018 | 0,521 |
| SR-3 | 0,456±0,018 | 0,497 |
| SR-5 | 0,395±0,016 | 0,437 |
| SR-14 | 0,319±0,013 | 0,328 |
| SR-18 | 0,334±0,013 | 0,372 |
| SRC | 0,470±0,019 | 0,505 |
| AC-1 | 0,278±0,011 | 0,313 |
| AC-2 | 0,273±0,011 | 0,309 |
| ESR-2 | 0,482±0,019 | 0,587 |
| ESR-4 | 0,490±0,020 | 0,591 |
| ESR-5 | 0,519±0,021 | 0,561 |
| ESR-P | 0,279±0,011 | 0,243 |

The design effectiveness of the SR system was determined from reactor calculations in hexagonal geometry in the two-group diffusion approximation. The two-group neutron cross sections were obtained from multigroup calculations of the reactor in two-dimensional (r, z) geometry. The design effectiveness of the system of 18 SR was 5.73% Δk/k. Thus, the measured and design values of the effectiveness of the SR system agreed within the limits of experimental error.

The results obtained permitted a comparison of the experimental and design values of the excess reactivity. Thus, for the start-up state of the BN-600 reactor the experimental excess reactivity was +5.70% Δk/k;* the calculated value for the design composition of the fuel gave +4.41% Δk/k, and for the actual fuel composition 4.91% Δk/k. In the realization of the design, the systematic (0.8% Δk/k) and technological (0.5% Δk/k) errors were positive, and compensated the excess in the effectiveness of the SR system, increasing the excess reactivity of the reactor by ∿1.3% Δk/k.

The effectiveness of the ESR in the start-up state of the reactor was measured by two methods. The rod-drop method consists in processing the neutron density decay curves after dropping the ESR, using special processing programs which take account of calculated variations in detector efficiency. The second method is similar to one used to obtain the SR effectiveness. The effectiveness of the ESR system was found by measuring the effectiveness of single ESR by the rod-drop method and introducing a calculated correction for the interference of the rods. The first method gave (3.2 ±0.2)% Δk/k for the effectiveness of the six ESR, and the second method, taking account of an interference correction of 1.16, gave (3.14 ± 0.12)% Δk/k. The design effectiveness of the ESR system was 3.98% Δk/k. The appreciable difference between the calculated and experimental results (20%) exceeds the ∿10% error of the computational methods and nuclear data estimated earlier on critical assemblies. The causes of this difference require further analysis. From the point of view of reactor operation, this decrease of effectiveness of the ESR system is admissible, since it does not diminish the safety of the operation of the installation.

It should be noted that one more requirement of the design and rules of nuclear safety [6] is satisfied in the start-up core: When the ESR are withdrawn, the subcriticality of the reactor is 1.0% Δk/k. Table 1 compares the calculated values of the effectiveness of individual rods with those measured in the start-up core.

Asymptotic Temperature Coefficient of Reactivity (ATCR)

The effects of temperature on reactivity were measured in the reactor core with the start-up load. As a result of the operation of the primary and secondary circuit pumps, the temperature in the reactor vessel increased from 220 to 380°C. Measurements were performed by two methods. In the first method the reactivity was recorded continuously with a digital reactivity meter operating in the real time scale, and the average sodium temperature in the reactor vessel was determined. The temperature dependence of the ATCR was obtained from these readings. The ATCR did not remain constant, but decreased somewhat with increasing sodium temperature.

*The average of the values obtained by the three methods of measurement at a core temperature of 245°C.

TABLE 2. Relative Power Distribution in Midplane of Core

| Cell No. | Experiment (E) | Calculation (C) | (E − C)/C, % |
|---|---|---|---|
| | Low enrichment zone | | |
| 18—19 | 1,00 | 1,00 | 0 |
| 10—10 | 0,78 | 0,78 | 0 |
| 18—18 | 0,98 | 1,00 | −2 |
| 21—25 | 0,83 | 0,85 | −2 |
| 14—14 | 0,89 | 0,89 | 0 |
| 17—09 | 0,69 | 0,73 | −5 |
| 12—12 | 0,84 | 0,86 | −3 |
| 16—18 | 0,95 | 0,95 | 0 |
| 18—16 | 0,95 | 0,94 | +1 |
| 15—13 | 0,91 | 0,93 | −2 |
| 21—27 | 0,73 | 0,73 | 0 |
| 13—09 | 0,78 | 0,76 | +2 |
| | High enrichment zone | | |
| 07—07 | 0,76 | 0,76 | 0 |
| 12—07 | 0,95 | 0,97 | −2 |
| 11—05 | 0,64 | 0,65 | −2 |
| 27—27 | 0,79 | 0,83 | −5 |
| 08—08 | 0,97 | 0,98 | −1 |
| 26—26 | 1,03 | 0,99 | +4 |
| 23—11 | 0,72 | 0,65 | +11 |
| 11—23 | 0,72 | 0,67 | +8 |
| 17—07 | 0,77 | 0,73 | +6 |
| 19—28 | 0,70 | 0,69 | +2 |
| 19—23 | 0,70 | 0,68 | +3 |
| 05—11 | 0,68 | 0,67 | +1 |
| 10—08 | 1,01 | 1,00 | +1 |
| 08—06 | 0,77 | 0,71 | +8 |

The average value of the ATCR for the temperature range considered was $-(3.6 \pm 0.08) \times 10^{-5}$ $\Delta k/k/degC$.

In the second method reactor states were compared for stabilization of the temperature at 220, 320, and 380°C. In this case the ATCR was determined from the change in position of the CSR, whose effectiveness was found experimentally. The average value of the ATCR for temperatures in the range 220-380°C was $-(3.79 \pm 0.08) \times 10^{-5}$ $\Delta k/k/deg$ C, which is in line with the above.

The value of the ATCR calculated in the design stage as a function of the position of the SR was $-(2.1\text{-}2.8) \times 10^{-5}$ $\Delta k/k/deg$ C. This strong dependence of the calculated values on the position of the rods is related to the effect of europium oxide on the neutron spectrum. Calculation overestimates this effect, since a one-dimensional model of the reactor was used in which the rods were homogenized into two annular regions. Calculations were performed by first-order perturbation theory in one-dimensional geometry, using nuclear data from BNAB-70. A rather detailed description of the method used can be found in [7], where an analysis of reactivity effects in the BN-350 reactor is given. It is shown in [7] that the procedure underestimates the temperature effect. For this reason the value of the ATCR was increased 20% in calculating the reactivity balance of the BN-600. But even in this case the experimental ATCR turned out to be 10-20% higher than the calculated value. One of the reasons for this divergence has been discovered: During warmup of the reactor there is a relative displacement of its structures, including a change in the position of the control rods relative to the core. According to preliminary estimates, this effect is ∿10% of the measured value. This was not taken into account in the calculations.

In addition, the reactivity effect related to the change in pressure in the gas cavity of the reactor was measured. This barometric effect was measured with a digital reactivity meter in the real time scale for a change in gauge pressure of the gas from 0.04 to 0.45 atm (1 atm = $1.01 \times 10^5$ Pa). In order to obtain reliable data, the sodium temperature in the reactor vessel was stabilized (drift no more than 0.5 degC/h). The primary circuit pump speeds were 250 and 400 rpm. The change in reactivity normalized to a pressure increase of 1 gauge atm in the gas cavity was $(1.00 \pm 0.03) \times 10^{-4}$ $\Delta k/k/$gauge atm at 250 rpm, and $(1.00 \pm 0.05) \times 10^{-4}$ $\Delta k/k/$gauge atm at 400 rpm. The values obtained apparently result mainly from the displacement of the SR due to heating of the reactor cover with a pressure change in the gas blanket.

Hydrodynamic Reactivity Effect

The hydrodynamic effect is related to the displacement of the core FEA as a result of a pressure change in the space between the FEA, and a change in the transverse displacement of the guide tubes and sleeves of the CSR resulting from the sodium flow. These displacements develop with a change in the primary circuit pump speed.

The hydrodynamic effect was determined with a digital reactivity meter operating in the real time scale for an increase and decrease in the primary circuit pump speed. The sodium temperature in the reactor vessel was determined continuously, and appropriate corrections were introduced. The various operating conditions of the primary circuit pumps were as follows:

| Operating Condition of Pumps | Change in Reactivity, %Δk/k |
|---|---|
| Increase in pump speed from 250 to 970 rpm.... | —0.032 ±0.001 |
| Increase in pump speed by steps of up to 50 rpm with 7 min holding after each step..... | —0.023 ±0.001 |
| Shutdown of pumps (coasting from 970 rpm to rest)..... | +0.032 ±0.001 |

The maximum calculated estimate of the hydrodynamic effect is —0.2% Δk/k.

Power Reactivity Effect

The power reactivity effect was measured while bringing the reactor to various power levels. The following readings of the regular apparatus were recorded: the temperature at the inlet and outlet of the intermediate heat exchangers, the position of the control rods, and the reactor power determined from the heat balance.

The total power reactivity effect has been obtained up to the present time. According to a preliminary estimate it is —(1.1 ±0.1)% Δk/k. Depending on the model of the axial expansion of the core, the calculated value is —(0.72-0.87)%Δk/k; in accordance with the recommendation in [7], the design value was increased 15%, but there remains a difference of 10-25% between the measured value and that predicted on the basis of a BN-350 experiment on power reactivity effects. One of the causes of this difference is the fact that the calculation did not take account of the displacement of the control rods with respect to the core as a result of the thermal expansion of the drive rods.

Reactivity Effect Due to Fuel Burnup

The reactivity loss due to fuel burnup was determined in two ways: 1) during reactor shutdowns by the position of calibrated rods at minimum controllable power levels; 2) during prolonged operation of the reactor at a constant power level by the displacement of AC rods. In both cases corrections were introduced to take account of variations of the coolant temperature and the neptunium reactivity effect (the effect caused by the retardation of the formation of $^{239}Pu$ from $^{238}U$.

The measured value of the reactivity loss in the first 100 effective days of reactor operation (—(0.0071 ±0.0003) Δk/k/month) is fairly close to the calculated value (—0.0065 Δk/k/month).

Power Distribution over Reactor Volume

Sufficiently representative data on the power distribution were obtained by measuring the intensity of γ radiation from fission fragments ($^{140}La$) accumulated in FEA after their operation at a 30% power level for a month. To do this a collimator with a slit width of ∿0.1 mm was mounted in the refueling box shield. Using the refueling mechanism, the FEA under investigation was placed in a proper position in front of the collimator. A Ge (Li) detector on the other side of the collimator was used to measure the intensity of the induced activity.

Table 2 lists the experimental and calculated relative average values of the power distribution for the midplane of a FEA. The results were normalized to one of the central FEA (cell 18-19). The calculations in the two-group diffusion approximation in hexagonal geometry on the whole give a quite good description of the power distribution, except for peripheral FEA at the blanket boundary, where they are up to ∿10% too low.

The measured power distribution over the height of a FEA was asymmetric because of the asymmetric location of the SR with respect to the height of the core. However, the calculated and experimental coefficients of nonuniformity of the power distribution were both equal to 1.17.

Thus, the studies performed on the BN-600 reactor at the physical and power start-up stage and during the first stage of operation showed that the main physical characteristics agree with the design values within the limits of error estimated earlier. A certain excess of the actual values of the temperature and power reactivity effects over the design values can apparently be accounted for by the large effects of removing the BN-600 CSR drive rods, or other deformations of the reactor structure which were not taken into account in the earlier calculations. We note that these and other small differences between actual and design characteristics do not affect the normal operation of the reactor.

LITERATURE CITED

1. A. I. Leipunskii et al., "The BN-600 fast reactor, NUCLEX-69," Basel (1969).
2. V. M. Budov et al., "The BN-600 fast reactor — a power facility for the immediate future, NUCLEX-75," Basel (1975).
3. O. D. Kazachkovskii et al., in: Proc. Int. Conf. on Nuclear Power and Its Fuel Cycle, Salzburg 1977, V. I. Vienna IAEA (1977), p. 393.
4. L. P. Abagyan et al., Group Constants for Calculating Reactors and Shields [in Russian], Énergoizdat, Moscow (1981).
5. V. V. Orlov, "Study of a model of the BN-600 reactor on the BFS-2 stand," in: Proc. Second Symposium of SÉV on Fast Reactors [in Russian], Obninsk (1973).
6. Safety Rules for Nuclear Power Plants (PBYa-04-74) [in Russian], Atomizdat, Moscow (1978).
7. V. V. Orlov et al., At. Energ., 42, No. 1, 3 (1977).

# TECHNICAL AND ECONOMICAL PREREQUISITES OF BUILDING SPECIALIZED CENTERS OF NUCLEAR HEAT AND POWER GENERATION

B. B. Baturov, V. M. Boldyrev, V. L. Losev, and M. V. Sigal

UDC 621.311.2:621.039.003

The introduction of nuclear sources in heat-supply centers is an important modern problem [1].

One of the development lines is combined nuclear heat and power generation. Its origin stems from the use of minor unregulated steam bleeding from the condensation turbines of atomic power stations. The first atomic power station with combined heat and power generating turbines was the low-power Bilibinsk Center of Nuclear Heat and Power Generation with EGP-6 water—graphite reactors ($N_{el}$ = 48 MW in condensing operation). The experience which was gathered in the operation of combined heat- and power-generating atomic power stations allowed the transition to a new stage, namely the planning and building of huge centers of nuclear heat and power generation. At the present time, a project of a center of nuclear heat and power generation has been outlined for the European part of the Soviet Union. The project is based on technical solutions used in the construction of nuclear power stations with VVÉR-1000 reactors. Two TK-450/500-60 turbines with regulated vapor release are provided in a block with one reactor of such a center of nuclear heat and power generation. With a generated heat release of 900 Gcal/h per block, the electric power of the block is 900 MW (elec.). Owing to the large "bound" condensation power, such a center of nuclear heat and power generation is basically a mixed condensation-heat and power generating station and can be considered an effective means of increasing the nuclear electrical power obtained through condensation. This approach to technical solutions accepted in the design of nuclear power stations is certainly justified in the present stage, because it is in this way possible to accelerate the introduction of combined nuclear heat and power generation. At the present

Translated from Atomnaya Énergiya, Vol. 55, No. 1, pp. 14-18, July, 1983. Original article submitted July 15, 1982.

0038-531X/83/5501-0447$07.50  

time the construction of such a center of nuclear heat and power generation has been initiated for supplying Odessa with heat.

Nevertheless, the use of technical solutions developed for atomic power stations in centers of nuclear heat and power generation has not made it possible to fully satisfy the requirements to the sources of central heat supplies. Thus, despite the economical advantages resulting from bringing the heat sources close to the user, the stations of this series, for reasons of radiation safety, must be placed at considerable distances from the areas in which their heat is required [2]. Therefore, considerable additional expenses for the transport of the heat are required and it is necessary to use a considerable number of large-diameter tubes which are in short supply. For example, in the case of the Odessa Center of Nuclear Heat and Power Generation, which is far from the foreseeable city limits (at a distance of ∿25 km), up to 60,000 tons of tubing with a diameter of 1000 mm are required. Naturally, under such conditions the efficiency of a center of nuclear heat and power generation is reduced, though these stations as a whole are advantageous from the economic viewpoint. In certain cases, owing to the specific features of a center of nuclear heat and power generation of the type indicated, such centers cannot be used because there exist restrictions to the feeding in of their electric power, the water supply may be insufficient, etc.

The large-scale introduction of the very economical combined generation of thermal and electrical energy on the basis of nuclear fuel makes it necessary to build combined condensation-heat and power supply stations and specialized centers of nuclear heat and power generation which to the greatest possible degree satisfy the requirements to centralized heat supply sources. The term "specialized" which we have introduced in regard to centers of nuclear heat and power generation refers to a set of technological solutions which guarantee that the radiation safety requirements for the population and the personnel are met in accordance with certain specifications so that the station can be placed sufficiently close to the region in which the heat is required and that the type of turbines which are economically most advantageous for a certain region can be employed. The complications which develop in the technical solutions as a consequence of these requirements and in comparison with the centers of nuclear heat and power generation of the first generation naturally imply a corresponding increase in the capital investment to be made in the construction of the stations proper. As will be indicated below, the higher specific capital investments in the construction are justified, because the total projected expenditures are reduced.

The first developments which to a significant degree satisfied the requirements to centers of nuclear heat and power generation of the type considered were made with the water—water VK—500 boiler reactor. The technical solutions adopted made it possible to place the station at a distance of 2-3 km from the region in which the heat was required, i.e., at the same distance as the presently planned nuclear heat-supply stations. Such stations can be developed also with other types of reactors. It should be noted that both the number and the type of the requirements to the reactor of a specialized center of nuclear heat and power generation, which make it possible to build the center close to the region to be supplied with heat, must be evaluated per se. Let us note only that these requirements must particularly consider the following: development of project solutions which preclude the release of radioactive nuclides into the environment as gas—aerosol emissions or as discharge of activated water during the normal operation of the station and in any possible emergency situation; elimination of the need for storing liquid and solid radioactive waste materials and exhausted fuel on the site of the center of nuclear heat and power generation; and development of a technology for taking the reactor setup out of operation after its service life.

Bringing a center of nuclear heat and power generation close to the region in which the heat is required imposes peculiar conditions in regard to ecology and the technical possibilities of supplying the station with water. All this affects the technical and economical parameters of the operation of such a center. Therefore, the turbine profiles which were acceptable for the present concept of developing combined nuclear heat and power supplies with VVÉR-1000 reactors can not be automatically used in the development of projects of specialized centers of nuclear heat and power generation. In atomic centers of combined heat and power generation with VVÉR-1000 reactors, the turbine profile is uniquely defined by the heat and power generation [3] with a large inherent condensation capacity; the generation of electric energy by such an inherent condensation capacity exhibits several disadvantages.

Firstly, when turbines operated with saturated steam are used in nuclear power stations, their nominal consumption is much higher than in modern thermoelectric stations of the same

power rating. This, in turn, makes it necessary to use a greater volume of cooling water which enters into the condenser of turbines of atomic power stations than in large state regional electric power plants, and significantly complicates the problem of supplying the electric power stations with water. When we recall that the water supply problem is solved under conditions of nonuniformly distributed water resources in the USSR territory, it becomes obvious that, in principle, the water supply can be obtained at lower cost in an atomic power station than in a center of nuclear heat and power generation, which, by its very nature, is bound to a region in which heat is needed. Indeed, an analysis of the projects executed has shown that cooling systems with cooling ponds are basically employed in the case of atomic power stations; by contrast, systems with cooling towers are practically indispensable in the case of centers of nuclear heat and power generation. Such systems are complicated, huge engineering projects which require for their construction special equipment, means, and materials. According to the data of project modernization, the differences in the expenses for cooling systems with cooling towers and systems with cooling ponds (for stations with organic fuel) are approximately 10 rubles/kW of rated power.* Since in an atomic power station the specific consumption of cooling water is 1.5-1.7 times greater than in a thermal power generating plant [3], the additional capital investments relative to atomic power stations can amount to ∿15-18 rubles/kW for the expenditures of specialized centers of nuclear heat and power generation considered in the present article. It is therefore logical that the specific capital investments for the associated condensing power of centers of nuclear heat and power generation exceed, under otherwise equal conditions, those of atomic power stations of the same power rating (identical conditions means equal number of power blocks, equal unit power rating, etc.).

Secondly, in the comparison of the capital investments, one must bear in mind that in the case of centers of nuclear heat and power generation the restrictions resulting from the thermal loading caused by the region imply that the number of energy-generating blocks basically does not exceed two, whereas in the majority of atomic power stations currently under construction four, six and, in some cases, even more blocks are provided. Calculations of the corresponding organizations have shown that the transition from atomic power stations with two blocks (with the same unit power rating of a block) to atomic power stations with four blocks reduces the specific capital investments for a fixed power rating by about 3%, the transition from four blocks to six blocks by another 4%, and the transition from six blocks to eight blocks by another 3%. Thus, the transfer of the nominal inherent condensing capacity from a specialized center of nuclear heat and power generation to an atomic power generation center is justified by the additional reduction of specific capital investments in condensing capacity because the enlargement of the atomic power station can be used to advantage.

Thirdly, a certain decrease in the specific capital investments for the nominal electric power rating of an atomic power station relative to that of a specialized center of nuclear heat and power generation is also related to differences in the expenditures for the acquisition of the land which, in the general case, are greater for areas in close vicinity to cities and industrial centers.

Fourthly, cooling systems with cooling towers (the average temperature of the cooling water is 1.4-1.5 times higher than in circulating systems with cooling ponds) determine the characteristics of the low-pressure portion of the turbine and necessitate higher pressures in the condenser ($P_c$) than in atomic power stations working on the basis of condensation. For example, in the case of TK-450/500 turbines, the $P_c$ value averaged over both condensers is $9.0 \cdot 10^{-3}$ MPa in comparison with $P_c = 3.9 \cdot 10^{-3}$ MPa in the case of the K-500-60 turbine. In atomic power stations characterized by relatively low initial parameters of the steam before the turbine, the possible reduction of $P_c$ allows a substantial increase in the generation of electric energy. Calculations show that in the bound condensed flow of steam in the TK-450/500 turbine, the indicated $P_c$ difference leads to the generation of about 10% less electric energy than in the case of the condensing K-500-60 turbine.

Fifthly, ecological considerations speak for abandoning the bound condensing power in specialized centers of nuclear heat and power generation. The cooling towers of huge electric power stations are sources of concentrated thermal steam—water emissions into the atmosphere, which, as the investigations of [4] have shown, can produce atmospheric phenomena (cloud formation, increased precipitation, formation of fog, etc.). Obviously, an increase

*Here and below, all economic indicators correspond to the level of wholesale prices and tariffs of 1981.

in the power of a specialized center of nuclear heat and power generation above a certain level is undesirable.

All this makes it necessary to analyze a version in which T-type turbines with a constant steam consumption in the head portion of the turbine and a minimal (ventilating) passage of steam in nominal operation into a low-pressure cylinder are employed in nuclear heat and power centers of the type considered. In the general case, certain turbines must be incorporated in centers of nuclear heat and power generation because of the technicoeconomical features of the centers, because of regional factors, and, first of all, because of the structure of the electric-energy generating capacity in the overall electric-energy generating system and the expenditures for the generation of the electric energy by the power stations of the net.

When nuclear fuel is employed in a thermal supply as an alternative to a specialized center of nuclear heat and power generation with T turbines, one can consider: centers of nuclear heat and power generation of the first generation developed at the present time on the basis of the VVÉR-1000 reactor and the 2TK-450/500 turbines; nuclear thermal stations; and specialized centers of nuclear heat and power generation with TK turbines.

The extent to which the alternative energy sources are competitive depends upon the total reduced calculated expenditures in the net for a particular energy production with comparable versions.

The following combinations of energy sources can be compared in accordance with the above considerations:

$$\mathrm{CNHE}_{\mathrm{T}}^{\mathrm{sp}} + \mathrm{PB} + \mathrm{APS} \leftrightarrow \mathrm{CNHE}_{\mathrm{TK}} + \mathrm{PB};$$

$$\mathrm{CNHE}_{\mathrm{T}}^{\mathrm{sp}} + \mathrm{PB} \leftrightarrow \mathrm{ATS} + \mathrm{PB} + \mathrm{APS};$$

$$\mathrm{CNHE}_{\mathrm{T}}^{\mathrm{sp}} + \mathrm{PB} + \mathrm{APS} \leftrightarrow \mathrm{CNHE}_{\mathrm{TK}}^{\mathrm{sp}} + \mathrm{PB}.$$

Atomic heat sources (CHNE and ATS) which satisfy the main part of the thermal load curve are considered in conjunction with the organic heat sources, namely the peak-reserve city boiler stations (PB) which satisfy the peak portion of the demand.

The subscripts T and TK refer to the type of turbines used in the center of nuclear heat and power generation; sp denotes a specialized center of nuclear heat and power generation (by contrast to the center of nuclear heat and power generation of the first generation).

When centers of nuclear heat and power generation with T and TK turbines are compared, the corresponding atomic power station (APS) compensates for the difference in the production of electric energy, the difference resulting from abandoning the bound condensing capacity used during the greatest possible number of hours per year ($h_u$). When centers of nuclear heat and power generation (CHNE) and centers of atomic thermal power generation (ATS) are compared, the corresponding introduction of an atomic power plant must provide for the delivery of the same electric energy into the network as a specialized center of nuclear heat and power generation at the same $h_u$ value.

The conditions of competitiveness of centers of nuclear heat and power generation with T turbines can be expressed as follows:

in a comparison with centers of nuclear heat and power generation having TK turbines

$$C_T + C_{tr} + C_{PB} + C'_{APS} \leq C_{TK} + C'_{tr} + C'_{PB}; \quad (1)$$

in a comparison with ATS

$$C_T + C_{tr} + C_{PB} \leq C_{ATS} + C''_{APS} + C''_{tr} + C''_{PB}. \quad (2)$$

In these formulas, $C_T$, $C_{TK}$, $C_{APS}$, $C_{ATS}$, and $C_{PB}$ denote the calculated cost of the energy generation with the corresponding sources, namely $\mathrm{CNHE}_T$, $\mathrm{CNHE}_{TK}$, APS, ATS, and PB (rubles/yr); $C_{tr}$ denotes the calculated cost of the transport of heat (rubles/yr). The costs $C_{PB}$ and $C_{tr}$ are determined from the known relationships of [3], whereas the cost of producing energy with atomic-energy sources in the general case may be defined as

$$C = 1.05\mathrm{Cap}(p + f) + C^{\mathrm{fuel}} + c^f N^{\mathrm{th}} h_u \quad (3)$$

where Cap denotes the total capital investment (rubles) for the building of the station; f, annual write-off of the capital invested; p, standard efficiency factor; $c^f$, fuel component

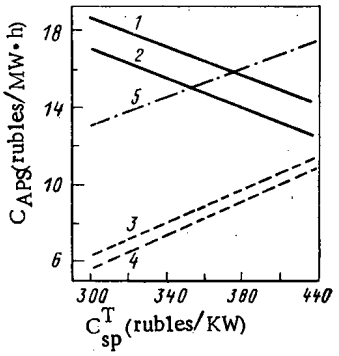


Fig. 1. Relation between the specific rated expenditures $C_{APS}$ for the delivery of electric energy and the specific capital investment for the construction of a specialized center of nuclear heat and power generation with T turbines under equal commercial efficiency of such centers of nuclear heat and energy generation and alternative energy sources: ———) first-generation center of nuclear heat and power generation as an alternative source with specific capital investments $C_{sp}^{CHNE}$ of: 1) 310; 2) 290 rubles/KW; ----) atomic thermal station as an alternative heat source with a specific capital investment $C_{sp}^{ATS}$ of: 3) 120; 4) 130 thousand rubles/Gcal·h$^{-1}$; -·-·-) specialized center of nuclear heat and power generation with TK turbines as an alternative source with specific capital investments $C_{sp}^{TK} = 0.98C_{sp}^{T}$ (curve 5).

of the specific rated expenditures for the energy generation by a nuclear reactor of the corresponding type (rubles/MW·h); $N^{th}$, fixed thermal power (MW) of the source; and $h_u$, annual number of hours during which the fixed power is used.

The coefficient 1.05 in Eq. (3) accounts for the overhead expenditures in the operation of the station and expenditures for salaries. The quantity $C^{fuel}$ determines part of the rated expenditures associated with the cost of the first fuel load and the transport and burial of the fuel waste. The cost of the first fuel charge of a specialized center of nuclear heat and power generation was assumed as identical for the various versions considered in the present article and equal to the corresponding cost in the case of the VK-500 reactor. The same assumption was made for the quantity $c^f$.

We have derived from projects the characteristics of equipping first-generation centers of nuclear heat and power generation, nuclear thermal stations, and specialized centers of nuclear heat and power generation with TK-450/500 turbines which determine the technological and economic performance parameters of such sources. When the performance parameters of centers of nuclear heat and power generation equipped with T turbines were determined, and expected characteristics of such a turbine were assessed by converting the parameters of TK-450/500-60 turbines to the passage of the bound condensing flux into water-network heaters. Calculations have shown that for the climatic conditions of the center of the European part of the USSR, with a hot-water supply fraction $\beta = 0.2$ of the total thermal load and with a thermal heat generation coefficient $\alpha_{CNHE} = 0.6$,* the electric power of a T turbine on the basis of a TK-450/500 changes from 380 (at the rated temperature of the external air) to 500 MW in

*$\alpha_{CNHE} = 0.5$–$0.7$ was recommended for centers of nuclear heat and power generation with T and TK turbines on the basis of the design calculations in [3].

summertime without a district-heating load. The greatest possible release of heat from the turbine amounts to 830 Gcal/h. An analysis of projected centers of nuclear heat and power generation with two blocks containing VK-500 reactors and the evaluation of the capital investment structure in such a station have shown that when the differences in the expenditures for network heating and the corresponding changes in the capacity of the turbine houses, as well as the changes in the expenditures for the heat-release system (within the area) resulting from the exchange of the TK turbine against a T turbine, are taken into account, the increase in the total capital investment in a center of nuclear heat and power generation does not exceed 2%.

When the performance parameters of centers of nuclear heat and power generation and nuclear power stations were determined, it was assumed that the coefficient of using the nominal power rating of the nuclear reactor is $\varphi = 0.74$ [5].

In this study the specific capital investments $C_{sp}$ in a center of nuclear heat and power generation of the first generation were assumed as 290 and 310 rubles/kW,* and 120 and 130 thousand rubles/Gcal·h$^{-1}$ in the case of a district-heating station. When the various versions of equipping a specialized center of nuclear heat and power generation with T and TK turbines were compared, the assumption was made that the specific capital investments in the construction of the station are related by $C_{sp}^{T} = 1.02 C_{sp}^{TK}$.

As indicated above, at the present time the projects of specialized centers of nuclear heat and power generation are in the initial stage, and therefore no reliable information on the capital investments to be made in such stations is available. There also exists some uncertainty about the cost of the electric energy generated by atomic power stations ($C_{APS}$). Under these conditions, the economic advantage of a specialized center of nuclear heat and power generation and the most convenient profile of the turbine set mounted in such centers must be considered when the parameters $C_{sp}^{T}$ and $C_{APS}$ are varied.

In our study we considered the conditions of competitiveness of alternative energy sources for the example of supplying heat to a region with a rated thermal load $Q_r = 1500$ Gcal/h. This makes it possible to undertake a technicoeconomic analysis of the use of both a center of nuclear heat and power generation and a nuclear heating station. The climatic conditions of the region correspond to the conditions at the center of the European part of the USSR. It was assumed that a first-generation center of nuclear heat and power generation is located at a distance of 25 km from the area in which the heat is needed, and that this distance is 3 km in the case of a nuclear district-heating station and a specialized center of nuclear heat and power generation. The thermal load fraction covered by nuclear sources was assumed as $\alpha^{T}_{APS} = 0.55$, $\alpha^{TK}_{CNHE} = 0.6$, and $\alpha_{ATS} = 0.57$ of the overall rated load of the associated region. Gas—oil boiler stations with KVGM-100 boilers were assumed as peak-reserve sources of heat. The temperature curve of the operation of a thermal network fed by atomic sources up to the peak reserve was in all versions assumed to be the same; the fuel cost of gas—oil boiler stations was assumed as 45 rubles/ton of the corresponding fuel.

The economic preference conditions of the left or right combination of energy sources in the versions cited were determined in accordance with the methodological assumptions outlined above. The $C_{APS}$ value at which the left and the right combination of energy sources are identical from the viewpoint of economy was determined for each $C^{T}_{sp}$, i.e., the difference of the rated expenditures was equal to zero:

$$\Delta C\,(C_{sp}^{T},\ C_{APS},\ C_{sp}^{CNHE},\ C_{sp}^{ATS}) = 0. \qquad (4)$$

The functions obtained in this fashion for $C^{T}_{sp}$ and $C_{APS}$ are shown as curves 1-5 in Fig. 1. The curves delimit the regions of economical preference of the left or the right combination of energy sources (the functions were obtained for comparing a specialized center of nuclear heat and power generation with T turbines with each of the alternative energy sources and must not be used for comparing these sources among themselves).

The regions of the $C_{sp}^{T}$ and $C_{APS}$ below curves 1, 2 determine for the corresponding $C_{sp}^{CNHE}$ the area of economic advantage of $CNHE_{T}^{sp}$, whereas the values above these curves

*Since T and TK turbines in condensing operation render the same electric power, here and below the specific capital investments in the construction of a center of nuclear heat and power generation, for the sake of a simplified comparison, were referred to the power of the station in the particular mode of operation.

denote the zone of economic advantage of a first-generation center of nuclear heat and power generation. It follows from an analysis of the data that at the present rated expenditures for the production of electric energy with an atomic power station, i.e., with $C_{APS}$ = 12 rubles/MW·h [5], the specialized centers of nuclear heat and power generation with T turbines are competitive with first-generation centers of nuclear heat and power generation even in the case of specific capital investments exceeding 1.5 times the capital investments in the first-generation centers.

The regions of the $C_{sp}^{T}$ and $C_{APS}$ under curves 3, 4 determine at the corresponding $C_{sp}^{ATS}$ the economic preference of $CNHE_{T}^{sp}$ vis-a-vis atomic thermal stations; below these curves there are the regions where atomic district-heating stations are used to greater advantage. For $C_{APS}$ = 12 rubles/MW·h, an analysis of curves 3, 4 shows that an economic advantage of $CNHE_{T}^{sp}$ is reached at specific capital investments of up to 430-440 rubles/kW.

When it is to be determined whether it is advantageous to install a set of T or TK turbines in a specialized center of nuclear heat and power generation, the conditions of equal economic advantage are described by curve 5. The region of the $C_{sp}^{T}$ and $C_{APS}$ values for which a set of T turbines is to be preferred is below this curve. When in the determination of the conditions of competitiveness of a specialized center of nuclear heat and power generation with T turbines with a first-generation center of nuclear heat and energy generation and an atomic district-heating station an upper limit exists for $C^{T}_{sp}$, a lower limit exists in the comparison of specialized centers of nuclear heat and power generation with T turbines and with such centers with TK turbines. Indeed, the lower the specific capital investments in the construction of a specialized center of nuclear heat and power generation and the closer its performance parameters to the corresponding parameters of an available atomic power station, the more favorable the economic conditions for mounting turbines with bound condensing power in specialized centers of nuclear heat and power generation. It must be recalled that the question of the preference for T or TK turbines in a specialized center of nuclear heat and power generation must be answered not only on the basis of economic considerations, but also with proper regard for ecological concepts.

## LITERATURE CITED

1. L. A. Melent'ev et al., Teploenergetika, No. 8, 10 (1982).
2. "Requirements to the distribution of atomic district-heating stations and atomic heating centers in regard to radiation safety," At. Energ., 49, No. 2, 151 (1980).
3. L. S. Khrilev et al., Optimizing District-Heating Systems and a Centralized Heat Supply [in Russian], Énergiya, Moscow (1978), p. 264.
4. M. Chandrakaut and Bhumralkar, in: Proc. IIASA Climate and Solar Energy Conversion, Workshop, December 8-10 (1976).
5. L. M. Voronin, Features of the Use and Maintenance of Atomic Power Stations [in Russian], Énergoizdat, Moscow (1981), p. 168.

# AN AUTONOMOUS MANEUVERABLE LOW-POWER CENTER OF NUCLEAR HEAT AND POWER GENERATION WITH HEAT STORAGE

M. E. Voronkov, A. T. Glyuza,
Yu. A. Sergeev, V. M. Chakhovskii, and
B. V. Yakovlev

UDC 621.039:658.26:697.328

The accumulation of energy during periods of reduced load and subsequent release of the energy to the consumer during times of peak load is one of the promising methods of covering the variable portion of the electric and thermal load curves. Heat storage in centers of nuclear heat and power generation can cover both the constant and the variable thermal load, including the release of heat when turbines are bleeded to increase their electric power. Of particular interest is the storage of heat accumulated in atomic power stations working in isolated electric and thermal supply systems participating in adjustments of the electric load curves. Such situations are typical in the operation of energy-supplying installations in northerm regions. The Bilibinsk Center of Nuclear Heat and Power Generation can serve as an example. It is a well-known fact that the operation of capital intensive atomic power stations in variable operation implies a deterioration of their economic parameters. This is particularly applicable to low-power atomic power plants. It is therefore necessary to find ways of increasing the economic efficiency of such electric power plants. This is very important for extending their use. Furthermore, several technical difficulties are encountered in the operation of reactor equipment with variable power ratings, and the reliability of providing heat and electric energy to the user may be reduced. Previous investigations and evaluations [1-5] were the basis for adopting certain technological solutions in a heat-storing system used in the low-power "Sever-2" two-block center of nuclear heat and power generation designated for deployment in remote and not easily accessible regions.

The basic technical characteristics of the station are as follows: thermal power rating of one reactor 14.5 MW, nominal steam pressure at the exit of the steam generator 1.6 MPa, and maximum and nominal power rating of the turbine 2.8 and 2.0 MW, respectively. The parameters of the combined heat and power release are: maximum and nominal steam release 16 and 9.4 tons/h; pressure 0.18 MPa; and temperature 114°C [6]. It was assumed that the electric load of the station may be reduced at nighttime to 30% of the nominal power. This time is used for loading the storage tanks of hot water or network water. The electric power of the center of nuclear heat and power generation is spent at night either for increasing the steam consumption from the heat and power supply to the maximum value of network-water tank filling or for reducing the release of live steam to the turbine while a part of the steam is used to fill the hot-water tank. A qualitative control of the thermal load has been introduced for this installation. Depending upon the proposed extent of energy discharge from the station, two versions of the heat-accumulating system are proposed.

Figure 1 shows the basic thermal scheme of the energy block of a center of nuclear heat and power generation with thermal storage and regulation of the electric power by changing the release of steam from the combined heat and power take-off of the turbine. The rotating-piston storage device of the water system is connected to the forward (feeding) and return lines of the thermal network. When the electric load is lowered, the release of steam from the heat and power supply system is increased. At the same time, an additional amount of network water with a temperature equal to the temperature in the return main line is circulated with the pump from the lower part of the line water tank through the boiler. After heating in the boiler, this water is directed from the feeding line of the thermal network into the upper part of the network storage tank. When the electric load is increased, the release of steam from the combined heat and power supply is decreased or fully interrupted by a corresponding decrease or interruption of the circulation of network-line water through the boiler. In this case the water is circulated from the return line of the thermal network into the lower part of the storage tank of the network water. The deficit which appears in

Translated from Atomnaya Énergiya, Vol. 55, No. 1, pp. 19-22, July, 1983. Original article submitted October 10, 1982.

 0038-531X/83/5501-0454$07.50 

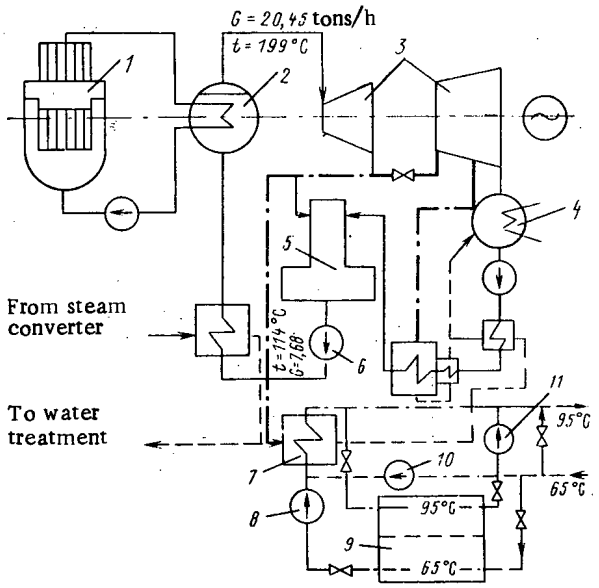


Fig. 1. Basic scheme of the "Sever-2" center of nuclear heat and power generation with network water storage: 1) reactor; 2) steam generator; 3) turbine; 4) condenser; 5) deaerating heater; 6) supply pump; 7) boiler of the network water; 8, 11) pumps of the storage system; 9) network water storage tank; 10) network-water pump.

this case in the release of network water into the forward line is compensated for by admitting hot water from the upper portion of the storage tank of the network water. The large variability range of steam release in the regulated operation of the turbines provided for use with the "Sever-2" center of nuclear heat and power generation makes it possible to change within wide limits the ratio of thermal load to electric load of the station. At the same time, the electric power can be reduced to about 60% of the maximum value while the admission of steam to the turbine is unchanged (nominal).

If a lesser load of the electric power provided by the station is required, the scheme with the hot-water storage tank can be employed (Fig. 2). In this case, part of the steam or the entire steam from the steam generator is directed into the steam-to-water heat exchanger of an intermediate circuit in which the water arriving from the lower (colder) part of the storage tank of the hot water is heated. For reasons of radiation safety, the pressure in the hot-water storage tank must be slightly below the pressure in the hot network.* When the water is heated in the storage tank to 160-170°C, the pressure in the hot network must be maintained above 0.7-1.0 MPa. The charging of the hot-water storage tank, as well as of the network-water storage tank, takes place in the hours of minimum electric load on the station. When the electric load is restored, the release of steam into the heat exchanger is reduced or completely terminated. The network water (part of it or all of it) is directed into a water—water heat exchanger in which the hot water of the hot-water storage tank is heated and fed into the hot network.

One of the basic elements of the thermal storage circuit is the storage tank, which can have the form of a pressure vessel of metal, reinforced concrete, or prestressed concrete. Metal and reinforced concrete can be employed for the structures of the storage tanks when the requirements to the parameters of the water network are not stringent. A possible design of the structure of a high-pressure storage tank of prestressed concrete has been provided in [3]. A detailed comparison of the various versions of the structures requires developments

*It should be noted that in the case of a liquid with a high boiling point being used in place of water as a heat-storage medium, the pressure required in the storage tank can be on the level of the atmospheric pressure or slightly higher than that.

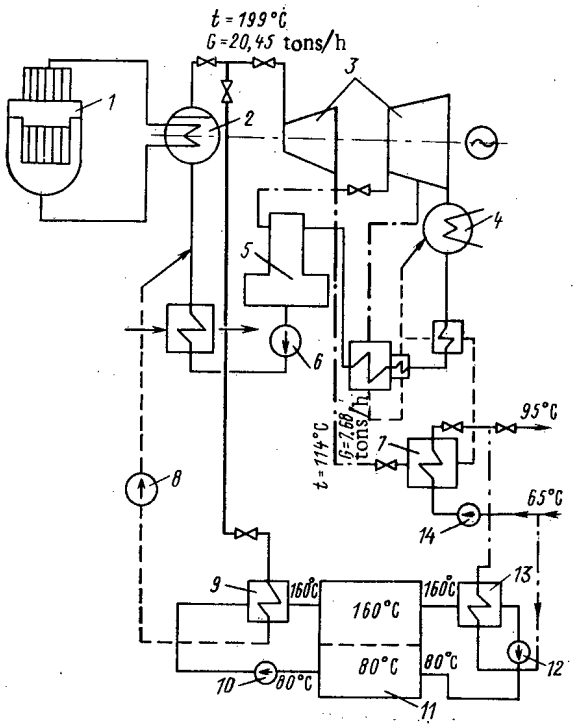


Fig. 2. Basic scheme of the "Sever-2" center of nuclear heat and power generation with an intermediate circuit of heat storage: 1) reactor; 2) steam generator; 3) turbine; 4) condenser; 5) deaerating heater; 6) feeder pump; 7) network boiler; 9) charging steam—water heat exchanger of the storage system; 8, 10, 12) pumps of the storage system; 11) storage tank (hot-water storage); 13) discharging water—water heat exchanger of the storage system; 14) network pump.

to be made by specialized organizations on the basis of technological and economic data. In order to avoid the accumulation of thermal stress in the construction materials of a storage tank, one can employ schemes with separate storage of hot and cold water [1, 3].

Since a variety of conditions and levels of energy demand exist and since the structures of the storage tanks must be unified, the total volume of storage tanks can be obtained by using several containers of standard series. The greater operative volume of storage tanks of the autonomous maneuverable "Sever-2" center of nuclear heat and power generation can reach 1500 $m^3$ in the thermal load range of 9-17 MW in hot-water storage of the intermediate circuit and 6000 $m^3$ in the storage of network water.

The economically reasonable volume of the tanks and their other characteristics can be determined only when the levels and conditions of the energy requirements in the actual autonomous system of energy provision are taken into consideration. Therefore, thermal design calculations of the above-described storage systems were made for some generalized model of energy supply. The electric load curve was assumed to have a minimum at night. The nocturnal thermal minimum load reached a value equal to the load of the hot-water supply (up to 10% of the total). The maximum of the electric load was assumed to be equal to the power of the autonomous center of nuclear heat and power generation in the maximum heat and power supply work in winter time. The annual curve of thermal delivery is basically given by the conditions of the continental strip of the extreme North (village of Olenek, Yakut Autonomous SSR). The temperature curve of the thermal network was assumed as 96/65°C. With these assumptions, the influence of the conditions of operation of the supply system of electric and thermal energy upon the parameters of the autonomous maneuverable center of nuclear heat and power generation with heat storage tanks was studied.

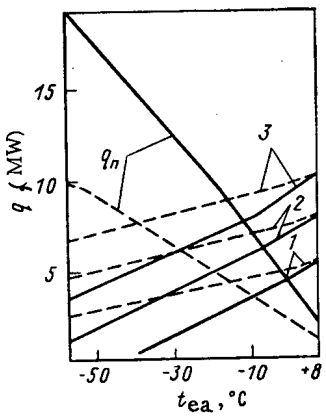


Fig. 3

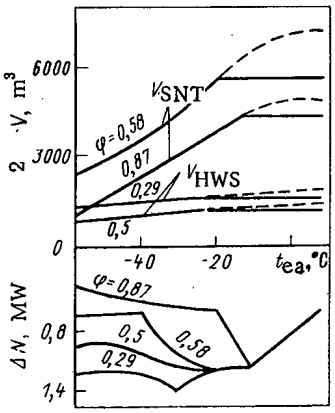


Fig. 4

Fig. 3. Dependence of the consumption of heat for providing heating $q_n$ and of the thermal power of a storage tank during its discharge time $q_a$ (curves 1, 2, 3) upon the temperature of the external air for a calculated maximum (daily average) thermal load of 17 (———) and 9 (– – –) MW. The $q_a$ dependence is shown for load-reduction degree $\varphi$ = 0.87 (curve 1), 0.58 (curve 2), and 0.29 (curve 3) of the station, respectively.

Fig. 4. Dependence of the volumes of the storage tanks ($V_{SNT}$ and $V_{HWS}$) and of the additional electric power $\Delta N$ upon the degree $\varphi$ of load reduction of the station and the external-air temperature $t_{ea}$ for a calculated maximum (daily average) thermal load of 9 MW (the dashed lines indicate the overshooting of the maximum volume of the storage tanks).

Calculations have shown (Fig. 3) that for the load characteristic of the conditions in the continental part of the extreme North (electric power consumption of the autonomous "Sever-2" center of nuclear heat and power generation during nighttime in winter) and for the expected calculated thermal load (6-10 MW) through the heat storage system, one can obtain full coverage of the thermal load during the diurnal maximum in the course of 70-80% of the duration of a space-heating period.

It follows from Fig. 4 that the interrelation of the basic parameters of the autonomous maneuverable "Sever-2" center of nuclear heat and power generation (volumes $V_{SNT}$ and $V_{HWS}$ of the storage tanks, additional electric power $\Delta N$, degree $\varphi$ of load reduction of the station, and temperature $t_{ea}$ of the external air) is rather complicated. Obviously, when the temperature of the outer air increases and the thermal load on the station decreases, the amount of "free" heat which can be stored increases. Accordingly, the required volume of the storage tank must increase. Its maximum volume is given by the condition that the calculated thermal load of the station be equal to the thermal capacity of the storage tank in the reduced-load mode. A further increase in the amount of heat stored and, hence, in the volume of the storage tanks is not sensible for the thermal schemes under consideration.

The additional electric power in the space-heating period increases with decreasing demands to the station at night. Calculations have shown that with a sufficiently large reduction of the load on the center of nuclear heat and power generation (up to 50-60% of the nominal electric power rating and lower) during about half of the space-heating period, the reduced load of the storage tanks can help to provide for an additional electric power during the diurnal maxima of electric load requirements to the station. This power is comparable with the load reduction of the station at night. The useful volume of the hot-water storage tank, which has a volume smaller than that of the network-water storage tank, changes in the course of a year to a lesser extent (at most by 25%) than the corresponding volume of the network-water storage tank. An increase in the designated average daily heat

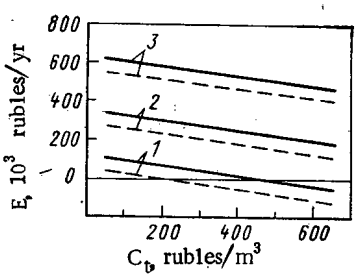


Fig. 5. Savings E in the use of heat-storage systems in dependence upon the cost of storage tanks and of organic fuel of a substituting diesel power plant: 1) 30, 2) 150, and 3) 300 rubles/ton of the corresponding fuel; – – –, ——) use of a previously constructed and a new 740 kW diesel power plant at a specific construction cost of 800 rubles/kW.

load limits the storage of heat and, accordingly, reduces the required volume of the storage tank and the additional electric power of the station.

A transition to higher heat storage parameters with the aid of steam used to heat the stored water (steam directly arriving from the steam generator of the reactor) reduces the calculated volume of the storage tank approximately in proportion to the increase in the difference between the water temperatures in the upper and lower parts of the hot-water storage tank relative to the corresponding difference of the temperatures in the network-water storage tank. However, the electric power of the station is sharply reduced during the loading of the storage tank, since the steam throughput of the turbine decreases and, accordingly, the generation of electric energy decreases in the period of the thermal demands.

It has been established that the accumulation of heat in the autonomous operation of the "Sever-2" center of nuclear heat and power generation facilitates the production of considerable additional electric energy. This leads to an increase in the coefficient of using the stationary power of a center of nuclear heat and power generation, though in the autonomous operation of the station, the storage of heat does not fully guarantee the operation of the reactors with constant power in the course of a year (in the reactor-base mode). Technological and economic calculations have shown that in the autonomous operation of a "Sever-2" center of nuclear heat and power generation, a heat storage tank can provide considerable savings, since the available power of the center of nuclear heat and power generation is substantially raised during the hours of the maximum load on the station.

When a center of nuclear heat and power generation is operated in combination with a diesel power plant or a gas-turbine electric power plant, the maximum of the electric load need not be necessarily covered during the entire year by the center of nuclear heat and power generation. But in this case the storage of heat in the center of nuclear heat and power generation can be an economically advantageous measure, because this makes it possible to stretch organic fuel, which is expensive in the extreme North. The efficiency of storing heat in a center of nuclear heat and power generation depends upon the relation between the costs of the storage system, alternative energy sources, and organic fuel. Calculations have shown that even with a high cost of storage tanks ($C_t \geq 600$ rubles/m$^3$ under the conditions of the extreme North), the use of such tanks in the "Sever-2" center of nuclear heat and power generation for increasing the available power of the station by 740 kW during the maximum electric load period is more efficient than the use of a diesel power plant at an organic fuel cost of 40-60 rubles/ton and more of the corresponding fuel (Fig. 5). In many regions of the extreme North, the cost of organic fuel even exceeds these figures.

The investigations, therefore, have shown that it is promising to use systems of heat storage in low-power centers of nuclear heat and power generation working in isolated energy-producing systems. The main conclusions and results of the investigations can be useful in the development of storage systems for huge centers of nuclear heat and power generation.

LITERATURE CITED

1. A. P. Kirillov et al., Energet. Stroit., No. 2, 33 (1980).
2. M. E. Voronkov, R. M. Sargsyan, and V. M. Chakhovskii, At. Tekh. Rubezhom, No. 9, 3 (1980).
3. A. P. Kirillov et al., Energet. Stroit., No. 1, 2 (1981).
4. V. M. Boldyrev et al., At. Energ., 51, No. 3, 153 (1981).
5. M. E. Voronkov and V. N. Chakhovskii, Express-Information: Operation and Repair of Equipment in Atomic Power Stations [in Russian], Informénergo, No. 3, Moscow (1982).
6. G. V. Merzlikin, I. A. Garbuz, and K. M. Ter-Osipyan, in: Chances of the Development and Improvement of the Fuel-Energy Industry in the Regions of the Extreme North and the Northeast of the USSR on the Basis of Nuclear Energy Sources [in Russian], Izd. Fiz. Énerg. Inst., Obninsk (1978), p. 186.

# USE OF THERMOELECTRIC CONVERTERS WITH LIQUID-METAL ELECTRODES FOR MEASURING THE TEMPERATURE OF LIQUID-METAL COOLANTS

M. N. Arnol'dov, B. V. Kebadze, F. A. Kozlov, Yu. O. Komissarov, and V. I. Lukovenko

UDC 621.36:621.039.52.034.6

One of the most important elements of a liquid-metal loop of an experimental installation or a fast reactor is the temperature-monitoring instrumentation. As large installations with fast sodium reactors are brought into operation, the requirements for reliability, accuracy, and speed of action of the temperature-measuring systems become more stringent.

Recently, the attention of experimenters and designers has been attracted more and more to thermoelectric temperature converters (TTCs), which have one electrode consisting of the liquid-metal coolant itself [1], while the other thermoelectrode is a steel electrode. The scheme of a TTC with a liquid-metal electrode (LME TTC) is shown in Fig. 1. For the closure of the thermoelectric circuit, the system uses a second TTC of the same kind, placed in the same coolant in another zone whose temperature is a known constant value (see Fig. 1a).

The advantage of an LME TTC is its greater speed of action, combined with a lower thermal inertia than in the case of an ordinary TTC with standard thermoelectrodes enclosed in a shell which protects the thermoelectrodes from the action of the molten metal. The reason for this advantage is that the source of the thermo-emf in the LME TTC is situated directly on the interface between the liquid metal and the steel electrode, while in a TTC with standard electrodes it is separated from the monitored medium by the wall of a protective shell whose thermal resistance is one of the main reasons for the high thermal inertia. Moreover, the single-electrode design of the LME TTC is simpler to manufacture and more reliable in operation. Such a converter can also be expected to be less sensitive to the effects of radiation,

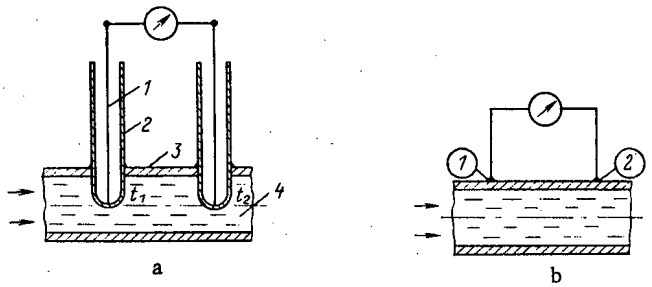


Fig. 1. Scheme of an LME TTC: a) submerged-type TTC; b) surface-type TTC; 1) steel electrode; 2) protective jacket; 3) pipe; 4) liquid metal.

Translated from Atomnaya Énergiya, Vol. 55, No. 1, pp. 22-24, July, 1983. Original article submitted November 10, 1982.

0038-531X/83/5501-0459$07.50  

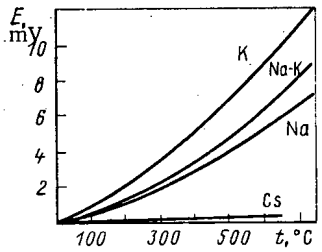


Fig. 2

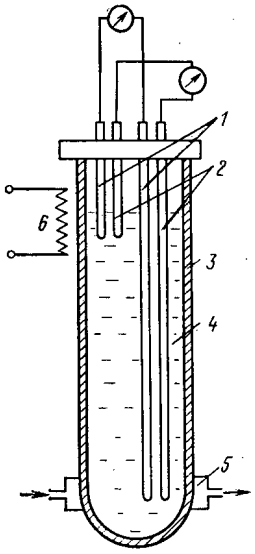


Fig. 3

Fig. 2. Thermo-emf for various combinations of steel and liquid metal as a function of temperature.

Fig. 3. Schematic diagram of the apparatus: 1) CA TTC; 2) LME TTC; 3) wall of the ampoule; 4) liquid metal; 5) water jacket; 6) heater.

since the liquid-metal electrode, consisting of pure metal, exhibits practically no change in its properties when it is irradiated. When an LME TTC of the surface type is used (see Fig. 1b), there is also less error due to heat leakage through the electrodes and less error due to the embedding into the wall of the pipe when there is a temperature drop across it, which is characteristic of ordinary two-electrode TTCs. An LME TTC generates a substantial thermo-emf with respect to a steel electrode (with the exception of cesium). Figure 2 shows the variation of the thermo-emf as a function of temperature for a TTC with respect to an electrode made of 12Kh18N9T steel with a temperature of 0°C at the cold electrode. These curves were obtained in our experiments by means of an apparatus whose theoretical scheme is shown in Fig. 3. If the steel electrode is replaced, e.g., with nickel, there will be an even higher thermo-emf, even in the case of cesium.

In order to explain the shunting effect of the walls of an LME TTC on the signal, we analytically solved the problem of the magnitude of the signal in the simplest TTC, the schematic of which is shown in Fig. 1b. The calculations showed that the received signal

$$U_0 = K_{sh} E_0,$$

where $E_0$ is the value of the thermo-emf, determined by the difference between the temperatures $t_1$ and $t_2$ (see Fig. 1b); $K_{sh}$ is the shunting coefficient (if the electrical contact resistance is disregarded)

$$K_{sh} = \frac{1}{1 + \frac{R_{st}}{R_{Na}}}$$

(here $R_{st}$ and $R_{Na}$ are the resistances of the steel and sodium segments between the electrodes).

The magnitude of the signal is independent of the temperature distribution between the electrodes and is determined only by the temperature at the points where the first and second electrodes are situated.

An LME TTC can be made from a KNMS type heating cable with a steel core whose outer diameter is 1.5 mm or more. When such TTCs are submerged in molten metal, $R_{st} \ll R_{Na}$ and $K_{sh} \approx 1$.

If there are impurities dissolved in the liquid metal, this theoretically affects the coefficient of thermo-emf. However, it can be seen from [2] that for lithium the effects of

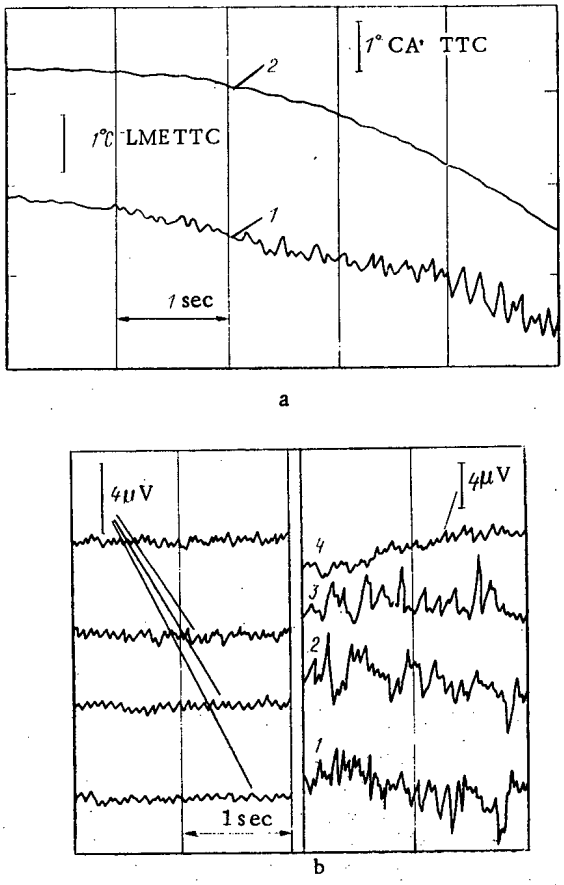


Fig. 4. Record of the readings of TTCs with a sodium electrode: a) temperature pulsation when there is a thermal disturbance after the electric heater is shut off [1) LME TTC; 2) CA TTC]; b) temperature pulsations before and after the injection of water into the sodium [1-3) LME TTC; 4) CA TTC].

the impurities are perceptible when the concentration of dissolved nitrogen is about 1% by mass or higher. Special experiments carried out by the method of [2] with molten sodium and a sodium—potassium alloy of eutectic composition did not reveal any effect of oxygen on the coefficient of thermo-emf when the oxygen was present in concentrations up to 0.1% by mass. Under real conditions, when the dissolved metals in the circulation loops are constantly or periodically removed, the concentration of dissolved impurities (oxygen, nitrogen) does not exceed 0.01% by mass, and therefore under the conditions of circulation loops the impurities should not exert any appreciable effect on the thermo-emf of a liquid-metal electrode.

The presence of such impurities in the form of excess phases deposited on the walls of a TTC may change its signal, owing to the shunting of the electrodes. However, this was not observed for excess-phase concentrations of 10% by mass and higher.

Experimental study of the dynamic characteristics of LME TTCs is difficult, since it is a very complicated matter to ensure that the temperature of the liquid metal varies with a frequency of the order of tens of hertz. For this reason, calculations were carried out on the basis of a simplified model of a TTC which took account of heat exchange between the liquid metal (sodium) and the working junction of the TTC. The calculations showed that for a shell thickness of more than 1 mm, the frequency of the TTC exceeds 40 Hz. This is much higher than the analogous factor for TTCs with standard electrodes.

Thus, the results of the investigations of LME TTCs indicate that they have some favorable features: high speed of action, simplicity and reliability of design, an apparently lower sensitivity to radiation, no error for embedding in the wall of the pipe, simplicity

of measurement of the temperature difference, etc. At the same time, such TTCs also exhibit some drawbacks: nonlinearity of the calibration characteristic, and complexity of the measurement of absolute temperature (relative to 0°C).

We demonstrated the possibilities of LME TTCs on a sodium circulation loop which contained a segment with five LME TTCs built into it. Their design was based on a KNMS heating cable with a steel core having a diameter of 1.5 mm. The working junction was formed by welding together the shell of the cable, the core, and a steel stopper placed in the cable segment near the end face. The TTCs were welded to the segment by means of connectors, perpendicular to the axis of the pipe, so that they projected 5 mm or 8 mm above the inner surface of the pipe (the inner diameter of the pipe was 31 mm).

The thermoelectric circuit was formed by the steel electrodes of two TTCs or one electrode and a segment of pipe wall at the point where the TTC passed through the wall.

Figure 4 shows examples of signals in cases in which electrode-wall type TTCs were included in the circuit; the signals were obtained by means of a signal amplifier and an N-117 light-beam oscillograph. Temperature pulsations with amplitudes of up to 1°C and characteristic times of about 0.1 sec were recorded by the sensors on the measurement segment some time after power had been disconnected from the heating segment (see Fig. 4a). Figure 4b shows the readings of the LME TTCs after the injection of water with a flow rate of 0.12 liters/h into the circulating sodium. The point of injection was 5 m away from the segment. It can be seen that the sensor clearly records this small effect, showing a marked increase in the pulsation amplitude. In both cases (see Figs. 4a, b) we show for comparison the signals from an ordinary TTC with Chromel—Alumel electrodes (CA TTC) of the cable type with an outer diameter of 1.5 mm, set up on the same segment with the same design at the input as the LME TTC. The ordinary TTC showed practically no reaction to rapid fluctuations.

## LITERATURE CITED

1. "A thermocouple for monitoring the fluctuations in the temperature of a nuclear reactor," Japanese Patent No. 51-16596. Cl. G21 c 17 10 of October 17, 1972.
2. V. I. Subbotin, M. N. Ivanovskii, and M. N. Arnol'dov, Physicochemical Foundations of the Use of Liquid-Metal Coolants [in Russian], Atomizdat, Moscow (1970).

# PORE MIGRATION AND ACTINIDE REDISTRIBUTION IN $(U, Pu)O_2$ AT THE BEGINNING OF FUEL-ELEMENT OPERATION

A. N. Bakhteev, Yu. G. Godin, and
V. I. Rybakov

UDC 621.039.54

Redistribution of the components and porosity occurs in the nuclear fuel $(U, Pu)O_2$ on irradiation in a reactor under the action of a sharp temperature gradient, which markedly influences the efficiency of the fuel element [1]. The actinide redistribution occurs both as a result of pore migration and by thermodiffusion in the solid phase. However, according to the estimates of [2], the characteristic thermodiffusion time of actinides is a few years. Hence, this mechanism cannot lead to pronounced redistribution of actinides in the course of a few decades at the initial stage of fuel-element irradiation.

The basic mechanisms causing pore migration are surface diffusion and the mass transfer of material due to evaporation—condensation. Surface diffusion prevails only in the case of small pores of diameter less than 10 μm [3]. Experimental results [4, 5] show that the pore-size estimates of [3] may be too high. Hence, for pores of dimension more than 10 μm (and possibly also for sizes of 1 μm and above [6]), the evaporation—condensation mechanism should dominate at temperatures above 1500°K. Calculations of the rate of pore migration and redistribution of the components on the basis of this mechanism [7] agree with experimental data to a certain extent. However, subsequent analysis [8, 9] shows that a significant deficiency of such calculations is the neglect of the change in actinide concentration at the pore surface due to noncongruent evaporation of the oxide. At the same time, in the models of [8-11], this effect is taken into account, which leads to a smaller actinide redistribution than is observed experimentally. The explanation for this is evidently that in the models of [8-11] no account was taken of actinide diffusion along the grain boundaries, which may make a significant contribution to the redistribution of the fuel components and accordingly require more detailed consideration.

Pore Migration. Large migrating pores are usually lenticular, with a diameter of about 100 μm and a thickness of 10 μm [12]. Without significantly reducing the accuracy of the calculations, a disk-shaped pore may be considered (Figs. 1, 2), with its axis coinciding with the direction of the thermal gradient. Vapor transfer through the gas phase from the "hot" to the "cold" surface of the pore is mainly determined by molecular diffusion, since the thermodiffusional and convective contributions (Rayleigh number $Ra \ll 1000$) may be neglected.

Because of the small pore thickness, only evaporation from the end surfaces will be taken into account, and the vapor migration in the gas phase will be characterized by an effective diffusion coefficient corresponding to the mean temperature $\bar{T} = 0.5(T_1 + T_2)$.

If mixed oxides of U and Pu are regarded as ideal quasibinary solutions $UO_{2+x_1}$—$PO_{2-x_2}$ [13], then the flux of the i-th component may be found from the formula

$$J_j^{(i)} = \int_{S_j} K_j^{(i)} Y_j^{(i)} dS, \qquad (1)$$

where i is equal to 1 and 2 for the more- and less-volatile actinides, respectively; j is equal to 1 and 2 for the cooler and hotter pore surfaces, respectively; $K_j^{(i)}$ is the molar evaporation rate of the i-th component from the j-th surface with unit cationic concentration; $Y_j^{(i)}$, cationic concentration at the j-th surface of the i-th component in the oxide $(U_{Y(i)}$-$Pu_{Y(i\pm1)})O_2$, and $S_j$, area of the end surface of the pore.

Individual oxide grains are represented in the form of cylindrical blocks of radius $a_0$, with their axis perpendicular to the pore surface. As a result of evaporation, the hotter surface of the pore will be denuded of the slightly volatile component, which results in

Translated from Atomnaya Énergiya, Vol. 55, No. 1, pp. 25-29, July, 1983. Original article submitted May 10, 1982.

0038-531X/83/5501-0463$07.50  

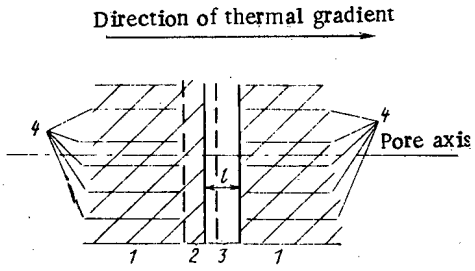


Fig. 1

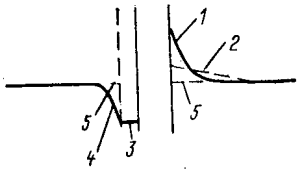


Fig. 2

Fig. 1. Microstructure of oxide in the vicinity of a migrating pore: 1) region with initial structure; 2) monocrystalline layer of material condensing from the "cold" surface of the pore; 3) free volume of pore; 4) grain boundary; the dashed lines indicate the initial position of the pore end surfaces.

Fig. 2. Cationic concentration of plutonium close to the pore: 1, 2) along the central axis of the grain and the grain boundary, respectively; 3, 4) in and close to the condensing layer of material, respectively; 5) initial value.

diffusional redistribution of the components in the oxide volume, including close to the grain boundary. The molar flux of the slightly volatile component from the grain boundary may be estimated from the following formula in this case:

$$J_b = \left(\frac{\rho}{M} Y_N - C_b\right)\frac{dV}{dt}, \tag{2}$$

where $Y_N$ is the cationic concentration of the slightly volatile actinide far from the pore, equal to the initial concentration; $C_b$, molar concentration of the slightly volatile actinide at the pore surface in the region of the grain boundary; V, oxide volume in which pronounced redistribution of actinides occurs; t, diffusional-redistribution time of actinides in the oxide; $\rho$, density of the oxide; and M, molar mass of the oxide.

The value of V may be estimated from the formula

$$V = 2\pi a_0 \sqrt{D_v t}\sqrt{D_b t}, \tag{3}$$

where $D_v$ and $D_b$ are the coefficients of volume and boundary diffusion of the slightly volatile actinide, respectively. Then the molar density of the material flux $j_b$ reaching the pore surface along the grain boundary may be defined as

$$j_b = \frac{\sqrt{D_v D_b}}{\delta}\left(\frac{\rho}{M} Y_N - C_b\right), \tag{4}$$

where $\delta$ is the width of the intergrain region. In this method the flux $J_b$ does not depend on the time when the concentration $C_b$ is constant, which allows the analysis to be reduced to the simpler case of pore migration in the stable state, i.e., migration at constant rate.

Now consider the distribution of the material flux traveling from the grain boundary along an individual grain at the pore surface. The surface-diffusion equation of the slightly volatile component takes the form

$$\frac{1}{r}(D_s\delta)\frac{\partial}{\partial r}\left(r\frac{\partial C_a}{\partial r}\right) + f = \delta\frac{\partial C_a}{\partial t}, \tag{5}$$

where r is the distance from the center of the evaporating surface of the grain; $D_s$, diffusion coefficient of the slightly volatile component over the oxide surface; $C_a$, molar concentration of the slightly volatile component in the absorbed layer; and f, source function.

In the stable state the source function is defined as

$$f = \rho v_2 Y_N + \alpha C_2^{(1)} - \frac{M}{\rho} K_2^{(1)} C_a, \tag{6}$$

where $v_j$ is the migration rate of the j-th surface of the pore; $\alpha = \sqrt{RT/2\pi M}$, kinetic coefficient (the condensation coefficient is assumed to be unity): R, universal gas constant; and $C_j^{(i)}$, molar vapor concentration of the i-th component close to the j-th surface of the pore.

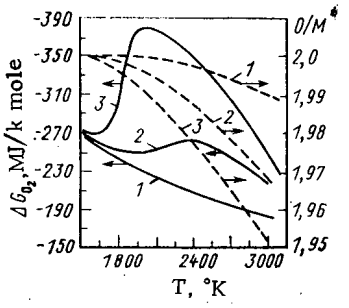


Fig. 3

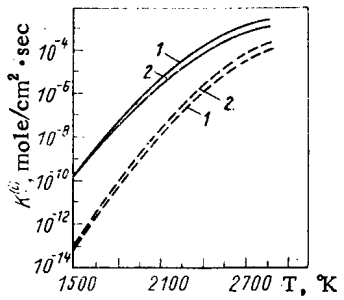


Fig. 4

Fig. 3. Oxygen distribution and its chemical potential $\Delta G_{O_2}$ in the oxide $(U_{0.8}Pu_{0.2})O_2$ in a temperature field with $\overline{O/M}$ = 1.998 (1), 1.990 (2), and 1.981 (3).

Fig. 4. Temperature dependence of the molar evaporation rate of the actinides $K^{(i)}$ for $(U_{0.8}Pu_{0.2})O_2$ with $\overline{O/M}$ = 1.998 (1) and 1.981 (2); the continuous and dashed curves refer to the uranium- and plutonium-containing components of the vapor, respectively.

The boundary conditions are as follows:

$$D_s \frac{\partial C_a}{\partial r}\Big|_{r=a_0} = j_b; \tag{7}$$

$$C_a|_{r=a_0} = C_b. \tag{8}$$

Since the characteristic diffusional-redistribution time of the material over the surface of the grain is very small (according to the formula $\tau_{char} = a_0^2/D_s$ for a temperature above 1500°K, it is less than 1 sec), the solution of Eq. (5) will be sought in the steady approximation: $\partial C_a/\partial t = 0$ . Then

$$C_a = \frac{\rho}{M}\left[\frac{\chi}{1-\chi} I_0(\varkappa r)\left(Y_N - \frac{M}{\rho} C_b\right) + \frac{1}{1-\chi} Y_{2,0} - \frac{\chi}{1-\chi} Y_N\right], \tag{9}$$

where $I_k$ is a modified Bessel function of k-th order; $Y_{2,0}$ is the cationic concentration of the slightly volatile component at the central point of the evaporating surface of the grain on the hotter side of the pore;

$$\varkappa = \sqrt{\overline{M K_2^{(1)}/\rho D_s \delta}}; \tag{10}$$

$$\chi = \frac{\sqrt{\overline{D_v D_b}}}{\varkappa D_s \delta I_1(\varkappa a_0) + \sqrt{\overline{D_v D_b}}\, I_0(\varkappa a_0)}. \tag{11}$$

Taking account of Eqs. (7) and (8), $C_b$ may be determined:

$$C_b = \frac{\rho}{M}\left[\frac{\chi}{1-\chi} I_0(\varkappa a_0)(Y_N - Y_{2,0}) + \frac{Y_{2,0} - \chi Y_N}{1-\chi}\right]. \tag{12}$$

As a result of integrating Eq. (1), taking account of Eq. (9), it is found that the mean flux density of the slightly volatile component evaporating from the hotter surface of the pore, $j^{(1)}_{2,ev}$, is

$$j^{(1)}_{2,ev} = \frac{2}{a_0}\sqrt{\overline{D_v D_b}}\,\frac{\rho}{M}(Y_N - Y_{2,0})\,\frac{1-\chi I_0(\varkappa a_0)}{1-\chi} + \frac{1}{1-\chi} K_2^{(1)} Y_{2,0} - \frac{\chi}{1-\chi} K_2^{(1)} Y_N. \tag{13}$$

Solving the system of equations for the resulting flux densities of the slightly volatile component close to the hotter surface of the pore

$$j^{(1)} = \varepsilon(Y_N - Y_{2,0}) + \frac{1}{1-\chi} K_2^{(1)} Y_{2,0} - \frac{\chi}{1-\chi} K_2^{(1)} Y_N - \alpha C_2^{(1)}, \tag{14a}$$

close to the cooler surface of the pore

$$-j^{(1)}=K_1^{(1)}Y_1-\alpha C_1^{(1)}, \tag{14b}$$

and with molecular diffusion of the vapor in the gas phase of the pore

$$j^{(1)}=D_p\frac{C_2^{(1)}-C_1^{(1)}}{l}, \tag{14c}$$

where $\varepsilon=\frac{2}{a_0}\sqrt{D_bD_v}\frac{\rho}{M}\frac{1-\chi I_0(\varkappa a_0)}{1-\chi}$ ; $D_p$ is the diffusion coefficient of the metal-containing components of the vapor in the gas phase of the pore, and $l$ is the pore thickness, it is found that

$$j^{(1)}=\frac{\eta}{1+2\eta}\left[\varepsilon(Y_N-Y_{2,0})+\frac{1}{1-\chi}K_2^{(1)}Y_{2,0}-K_1^{(1)}Y_1-\frac{\chi}{1-\chi}K_2^{(1)}Y_N\right], \tag{15}$$

where $\eta=\frac{D_p}{l}\sqrt{\frac{2\pi M}{R\bar{T}}}$ .

The flux of the second component is calculated on the basis of this expression, taking account of the relation

$$C_a+C_d=\rho_T/M, \tag{16}$$

where $C_d$ is the volume concentration of the less-volatile component in the adsorbed layer and $\rho_t$ is the theoretical density of the oxide, with the result

$$j^{(2)}=\frac{\eta}{1+2\eta}\left[-\varepsilon\frac{K_2^{(2)}}{K_2^{(1)}}(Y_N-Y_{2,0})+\left(1-\frac{Y_{2,0}}{1-\chi}\right)K_2^{(2)}-K_1^{(2)}(1-Y_1)+\frac{\chi}{1-\chi}K_2^{(2)}Y_N\right]. \tag{17}$$

In addition, if the diffusional flux of cations from the cooler surface into the depth of the oxide is neglected, then

$$\begin{cases} j^{(1)}=v_1\frac{\rho_t}{M}Y_1; \\ j^{(2)}=v_1\frac{\rho_t}{M}(1-Y_1). \end{cases} \tag{18}$$

To determine the concentration of the slightly volatile component at the cool surface of the pore $Y_1$, the balance condition is written for the components in the case of migration of the hotter surface of the pore in the stable state:

$$\begin{cases} j^{(1)}-j_b\frac{2\delta}{a_0}=\frac{\rho}{M}v_2Y_N; \\ j^{(2)}=\frac{\rho}{M}v_2(1-Y_N). \end{cases} \tag{19}$$

Solving the system in Eqs. (14) and (17)-(19) allows an analytical expression for $Y_1$ to be obtained:

$$Y_1=\frac{-b-\sqrt{b^2-4ac}}{2a}, \tag{20}$$

where

$$a=hK_1^{(2)}+\left\{K_1^{(1)}+\frac{Y_N}{1-Y_N}K_1^{(2)}\right\}\left\{\varepsilon\frac{K_2^{(2)}}{K_2^{(1)}}Y_N-\left(1-\frac{\chi}{1-\chi}Y_N\right)K_2^{(2)}\right\}-m\left\{\left(\frac{K_2^{(2)}}{K_2^{(1)}}\varepsilon-\frac{1}{1-\chi}K_2^{(2)}\right)\times Y_N-\frac{1+2\eta}{\eta}\varepsilon(1-Y_N)\right\};$$

$$b=h\left\{\frac{1+2\eta}{\eta}\varepsilon Y_N(1-Y_N)-(1+Y_N)K_1^{(2)}-\varepsilon\frac{K_2^{(2)}}{K_2^{(1)}}Y_N+K_2^{(2)}+\frac{\chi}{1-\chi}K_2^{(2)}Y_N\right\}-\left\{K_1^{(1)}+\frac{Y_N}{1-Y_N}\times K_1^{(2)}\right\}\left\{\varepsilon\frac{K_2^{(2)}}{K_2^{(1)}}Y_N-\frac{1}{1-\chi}K_2^{(2)}Y_N-\frac{1+2\eta}{\eta}\varepsilon(1-Y_N)\right\}+m\left\{\varepsilon\frac{K_2^{(2)}}{K_2^{(1)}}-\frac{1}{1-\chi}K_2^{(2)}+\frac{1+2\eta}{\eta}\varepsilon(1-Y_N)\right\};$$

$$c=h\left\{Y_NK_1^{(2)}-\frac{1+2\eta}{\eta}\varepsilon Y_N(1-Y_N)+Y_N(\varepsilon Y_N\times\frac{K_2^{(2)}}{K_2^{(1)}}-K_2^{(2)}-\frac{\chi}{1-\chi}K_2^{(2)}Y_N)\right\}-m\left\{Y_N(\varepsilon\frac{K_2^{(2)}}{K_2^{(1)}}-\frac{1}{1-\chi}K_2^{(2)})-\frac{1+2\eta}{\eta}\varepsilon(1-Y_N)\right\}.$$

In addition,

$$h=\frac{1}{1-\chi}K_2^{(1)}+\frac{1+\eta}{\eta}\varepsilon+\frac{1}{1-\chi}\frac{Y_N}{1-Y_N}K_2^{(2)}-\varepsilon\frac{Y_N}{1-Y_N}\frac{K_2^{(2)}}{K_2^{(1)}};$$

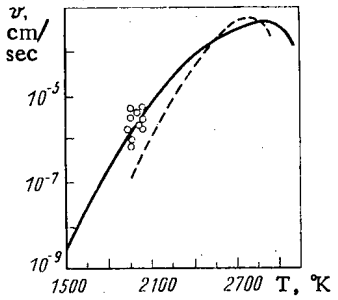


Fig. 5

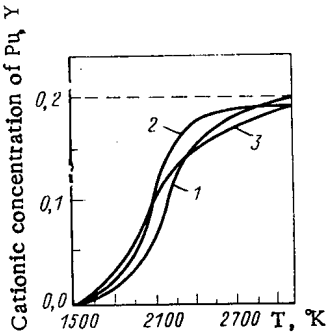


Fig. 6

Fig. 5. Dependence of the migration rate v of the "cold" surface of the pore in the oxide $(U_{0.8}Pu_{0.2})O_2$ on its mean temperature for $\overline{O/M}$ = 1.981-1.998; the continuous curve corresponds to the data of the present work, the dashed curve to the data of [9], and the points to the data of [21].

Fig. 6. Dependence of the cationic plutonium concentration Y at the "cold" surface of the pore on the mean pore temperature in the oxide $(U_{0.8}Pu_{0.2})O_2$ with $\overline{O/M}$ = 1.998 (1), 1.990 (2), and 1.981 (3); the dashed curve corresponds to the initial plutonium concentration in the circle.

$$m = \frac{\chi}{1-\chi} K_2^{(1)} Y_N + \frac{1+\eta}{\eta} \varepsilon Y_N + K_2^{(2)} \frac{Y_N}{1-Y_N} + \frac{\chi}{1-\chi} K_2^{(2)} \frac{Y_N^2}{1-Y_N} - K_1^{(2)} \frac{Y_N}{1-Y_N} - \varepsilon \frac{K_2^{(2)}}{K_2^{(1)}} \frac{Y_N^2}{1-Y_N}.$$

Numerical Example. The relations obtained here were used to analyze the migration of individual pores in a core and the associated redistribution of actinides. The calculations were performed for a fuel element with a core of diameter 6 mm and a central hole of diameter 1.5 mm, with a linear power of 65 MW/m. The grain size of the core was taken to be 5 μm. When $Y_N$ = 0.8, the mean value $\overline{O/M}$ of the oxide (O/M is the oxide:metal ratio in the oxide) was taken successively to be 1.981, 1.990, and 1.998. In this case the temperature drop in the pore ΔT (°K) is described approximately by the formula

$$\Delta T = -28.5 + 91.39 \frac{T}{1000} - 26.85 \left(\frac{T}{1000}\right)^2. \qquad (21)$$

The calculated oxygen distribution and the oxygen potentials in the fuel-element core with such parameters are shown in Fig. 3. The oxygen distribution was found from the data of [14]. The corresponding values of the oxygen potential of the oxide were determined in accordance with the thermodynamic model of the oxide (U, Pu)$O_2$, which was regarded as an ideal solution of nonstoichiometric uranium and plutonium oxides with equal oxygen potentials. The thermodynamic potentials were determined here for $UO_2$ in accordance with the thermodynamic model proposed in [15] and for $PuO_2$ by an analogous mode. On account of the high diffusional mobility of oxygen in (U, Pu)$O_2$, the oxygen potentials are regarded as constant from here on with any changes in the actinide concentration close to the pore. Therefore, the molar evaporation rates $K_j^{(i)}$ also remained constant with changes in the actinide concentration in the oxide close to the pore. They were calculated from the well-known thermodynamic relations on the basis of the activities of the oxide components found in accordance with the thermodynamic model of (U, Pu)$O_2$ using the energy of formation of the gaseous actinide oxides tabulated in [16]. The temperature dependence of $K^{(i)}$ is shown in Fig. 4. In addition, the values of the diffusion coefficients $D_s$ and $D_b$ found in [17, 18], respectively, were used for the calculations. The bulk-diffusion coefficient for a temperature of 1773°K was determined from the graphical dependence on O/M in [19]. For other temperature values, it was calculated taking account of the activation energy Q = 461 MJ/kmole [20]. For comparison with the published calculations [8, 9], the value $D_p \approx 2$ cm²/sec found in [9] was used.

In accordance with the relations obtained and the given initial data, the values of the pore migration rates were calculated, together with the concentration of actinides condensing on the cold surface of the pore (Figs. 5, 6). It is evident from Fig. 5 that the calculated migration rates of the pores are in satisfactory agreement with the experimental data of [21], and also with the values calculated in [9], while the small discrepancy with the latter is due mainly to the nonidentical temperature difference between the pore surfaces.

At the same time, the actinide concentration at the cold surface of the pore in the given calculations is markedly different from the initial value (Fig. 6), whereas in the model of [9], pore migration in the stable state at constant temperatures of the hotter and cooler surfaces did not lead to any change in concentration at the "cold" surface of the pore. At low temperatures the actinide concentration in the condensed layer is close to the value found in [7], and it is only above 2400°K that it tends to the initial value.

Thus, transfer of the slightly volatile component by intergrain diffusion from the depth of the oxide to the evaporating surface of the pore, which was disregarded in [9-11], may make a significant contribution to the actinide redistribution by the evaporation—condensation mechanism at temperatures that are not too high; this mechanism is evidently dominant at the beginning of fuel burnup. In this connection, the previously "inexplicable" [10, 11] results of [2] on actinide redistribution in a field-element core with small burnup becomes understandable.

## LITERATURE CITED


1. R. Meyer, E. Butler, and D. O'Boule, Actinide Redistribution in Mixed Oxide Fuels Irradiated in a Fast Flux, ANL-7929 (1972).
2. J. Bramman and H. Powell, J. Brit. Nucl. Energ. Soc., 14, No. 1, 63 (1975).
3. L. Michels and R. Poeppel, J. Appl. Phys., 44, No. 3, 1003 (1973).
4. M. Gulden, J. Nucl. Mater., 23, 30 (1967).
5. R. Cornell and G. Bannister, Proc. Brit. Ceram. Soc., 7, 355 (1967).
6. F. Nichols, J. Nucl. Mater., 84, 319 (1979).
7. W. Lackey, F. Homan, and A. Olsen, Nucl. Techn., 6, 120 (1972).
8. D. Olander, J. Nucl. Mater., 49, 21 (1973/74).
9. S. Guarro and D. Olander, J. Nucl. Mater., 57, 136 (1975).
10. C. Clement and M. Finnis, J. Nucl. Mater., 75, 115 (1978).
11. C. Clement and M. Finnis, J. Nucl. Mater., 75, 193 (1978).
12. D. Olander, in: Proceedings of Technical Information Center, Energy Research and Development Administration, US Department of Commerce, Springfield, Virginia (1978), p. 273.
13. T. Markin and E. McIver, in: Proceedings of Third International Conference on Plutonium, London (1965), p. 845.
14. C. Sari and G. Schumacher, J. Nucl. Mater., 61, 192 (1976).
15. A. N. Bakhteev and Yu. G. Godin, Izv. Akad. Nauk SSSR, Ser. Neorg. Mater., 16, No. 2, 324 (1980).
16. R. Ackerman and M. Chandraseakharaiah, in: Thermodynamics of Nuclear Materials, Vol. II, IAEA, Vienna (1974), p. 3.
17. E. Hodkin and M. Nicholas, J. Nucl. Mater., 47, 23 (1973).
18. S. Yajima, H. Furuya, and T. Hirai, J. Nucl. Mater., 20, 162 (1966).
19. Hj. Matzke, in: Proceedings of Fifth International Conference on Plutonium and Other Actinides, Baden-Baden, 1975, North-Holland, Amsterdam (1976), p. 801.
20. Hj. Matzke and R. Lambert, J. Nucl. Mater., 49, 325 (1973/74).
21. H. Kawamato et al., J. Nucl. Mater., 68, 48 (1977).

# EFFECTS OF REACTOR IRRADIATION ON CYCLIC STRENGTH IN ZIRCONIUM ALLOYS

V. M. Filatov, V. I. Barsanov,
S. V. Evropin, S. A. Averin, and
Yu. A. Anikhimovskii

UDC 621.039.531:669.296

The working channels in an RBMK reactor are subject not only to static load caused mainly by the internal pressure, but also to cyclically varying stresses related to the changing working conditions. The number of such cycles during the working life of a channel may be more than 1000.

In order to calculate the strength of an evaporation channel it is necessary to have data on the effects of various factors (irradiation, corrosion, hydrogenation, etc.) on the working life of the constructional material, particularly the cyclic strength. It is very laborious to examine the effects of these factors by experiment. In this connection, research on materials used in existing nuclear power stations is of undoubted interest.

At Beloyarsk nuclear power station, two experimental channels were extracted after 1100 effective days of operation, which contained tubes made of Zr +2.5% Nb and Zr +1% Sn +1% Nb + 0.5% Fe alloys of outside diameter 63 mm and wall thickness 4 mm. Table 1 gives the irradiation parameters for the parts of these tubes examined for cyclic strength. The temperatures of the inner and outer surfaces of the tubes were 600 ±5°K.

The mechanical properties [1, 2] show that the strength characteristics increased on average by 25%, while the plasticity (relative extension) was reduced for the Zr +2.5% Nb alloy by a factor of 1.5-1.8 [1] and for the Zr +1% Sn +1% Nb +0.5% Fe alloy by a factor of 2-2.4 [2], while remaining at a fairly high level (10-12%). This change in mechanical properties is due in the main to the effects of the neutron irradiation, because the hydrogen contents had increased only slightly [2].

Tests were performed for few-cycle fatigue with severe symmetrical bending for specimens cut from these tubes at 293°K on an apparatus and by a method as described in [3]. The deformation at the surface of the working part was measured with strain gauges. The occurrence of a fatigue crack was identified visually by means of a system of mirrors and binocular viewer with eightfold magnification, and also from the reduction in the force in the diagram of bending moments against number of cycles. The test results were processed by least squares.

The tests in cyclic loading showed that the irradiated Zr +2.5% Nb alloy becomes weaker on cyclic loading, as it does in the initial state [4], but the extent of this is small. The cyclic weakening for Zr +1% Sn +1% Nb +0.5% Fe alloy was slight.

Figures 1, 2 show curves for the few-cycle fatigue of these materials for Zr +2.5% Nb and Zr +1% Sn +1% Nb +0.5% Fe, correspondingly. For the Zr +2.5% Nb alloy, the stage at which a fatigue crack developed was 10-15% of the total working life (Fig. 1), while for the

TABLE 1. Basic Irradiation Characteristics for Parts of Channels

| Material | Coordinates of parts from base of core, m | Fluence, $\times 10^{-24}$ neutrons / m$^2$ ($E \geq 0,2$ MeV |
|---|---|---|
| Zr+2,5% Nb | 3,0—3,2 | 38 |
| | 6,3—6,4 | 1,6—2 |
| Zr+1% Sn+ | 3,06—3,16 | 36 |
| +1% Nb+0,5% Fe | 6,26—6,36 | 3,8—4,6 |

Translated from Atomnaya Énergiya, Vol. 55, No. 1, pp. 29-31, July, 1983. Original article submitted August 5, 1982.

0038-531X/83/5501-0469$07.50  

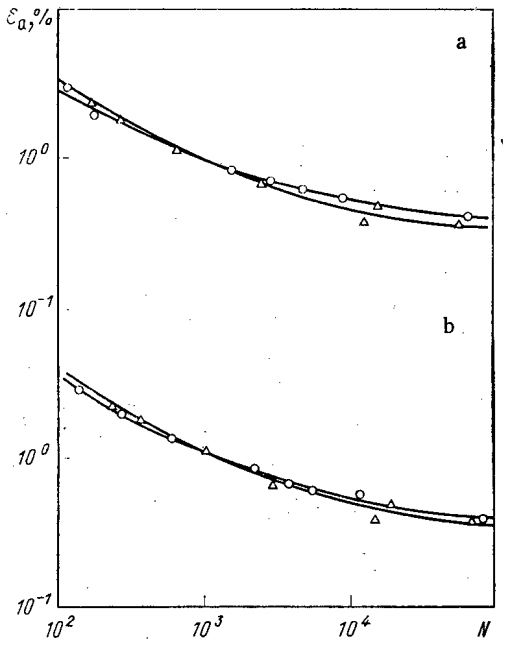


Fig. 1

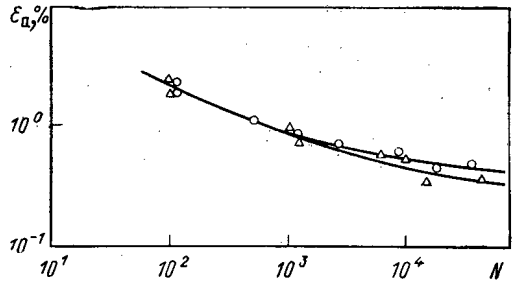


Fig. 2

Fig. 1. Fatigue curves for Zr +2.5% Nb alloy: Δ, ○) $(1.6\text{-}2)\cdot10^{24}$ and $3.8\cdot10^{25}$ neutrons/m$^2$, respectively; a) from moment of crack formation; b) from failure.

Fig. 2. Fatigue curves for Zr +1% Sn +1% Nb +0.5% Fe alloy: Δ, ○) $(3.8\text{-}4.6)\cdot10^{24}$ and $3.6\cdot10^{25}$ neutrons/m$^2$, respectively.

irradiated Zr +1% Sn +1% Nb +0.5% Fe alloy it did not exceed 5%, and in this connection these data are not reflected in Fig. 2.

Figures 1, 2 show that an increase in the neutron fluence by about a factor of ten did not reduce the few-cycle strength of the material when the number of cycles was $N \leq 10^3$; in the region of strain amplitude $\varepsilon_\alpha \leq 0.8\%$, which is of practical interest, the resistance to few-cycle failure in Zr +2.5% Nb alloy and in particular in Zr +1% Sn +1% Nb +0.5% Fe was somewhat raised. These results agree with those of [5]. Comparison of the fatigue curves with those given in [4] for Zr +2.5% Nb in the unirradiated state shows that irradiation does not have a marked effect on the resistance to few-cycle failure in this alloy when allowance is made for the differences in properties for different batches of material.

There is considerable margin for increasing the working life of components by continuing their operation in the stage where cracks are developing, i.e., up to the moment where a through defect is produced or a crack attains a critical size. In particular, an initial crack can grow by cyclic loading. Fatigue-crack growth kinetics for these tubes was examined with a pulsing cycle of severe loading in bending for a specimen of height 10 mm with a V notch on an apparatus previously described [3]. The bending moment was continuously recorded. When it had fallen by not less than 5%, an alcohol-based dye solution was poured into the notch, and after this had dried the tests were continued up to the next fall in load, and then a dye of another color was added. The size of the crack corresponding to a given dye

TABLE 2. Constants C and n in Eq. 2

| Material | Fluence, $\times10^{-24}$ neutrons/m$^2$ | C | n | Mean-square error |
|---|---|---|---|---|
| Zr+2,5% Nb | 1,6—2,0 | $6{,}8\cdot10^{-8}$ | 3,4 | 0,4 |
| | 38,0 | $9{,}6\cdot10^{-9}$ | 3,7 | 0,2 |
| Zr+1% Sn+ +1% Nb+0,5% Fe | 3,8—4,6 | $9{,}4\cdot10^{-7}$ | 3,2 | 0,3 |
| | 36,0 | $4{,}1\cdot10^{-24}$ | 12,3 | 3,0 |

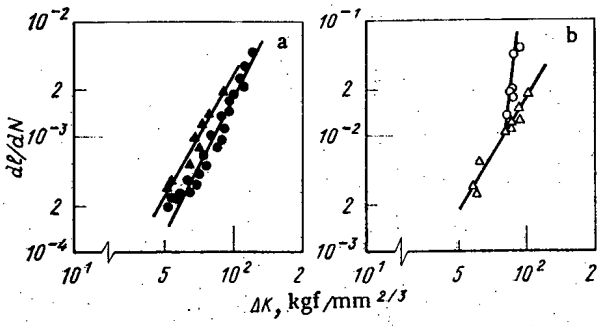


Fig. 3. Rates of crack growth in Zr +2.5% Nb (a) and Zr +1% Sn +1% Nb +0.5% Fe (b) alloys: Δ, •) $(1.6-2)\cdot10^{24}$ and $3.8\cdot10^{25}$ neutrons/$m^2$, respectively; Δ, ○) $(3.8-4.6)\cdot10^{24}$ and $3.6\cdot10^{25}$ neutrons/$m^2$, respectively.

color and bending moment was determined in the fracture of the specimen by an optical method. The spread in the stress-intensity coefficient ΔK was determined [6] from

$$\Delta K = \frac{6\Delta M}{b\,(h-l)^{3/2}}\,g\,(l/h), \tag{1}$$

where ΔM is the spread in the bending moment in the specimen corresponding to a crack length $l = (l_i + l_{i+1})/2$; h, specimen height; b, specimen width; and the values of g(l/h) have been given in [6].

Figure 3 gives results on the fatigue-crack growth kinetics. The experimental points for each alloy and neutron fluence are fairly closely described by a Peris equation:

$$\frac{dl}{dN} = C\Delta K^n, \tag{2}$$

where ΔK is defined by Eq. (1), dl/dN is the crack growth rate, and C and n are constants of the material, which are dependent on the test conditions.

Table 2 gives values of C and n obtained for the curves of Fig. 3, and it is clear from Fig. 3a and Table 2 that the fatigue-crack growth rate in Zr +2.5% Nb alloy is reduced by about a factor of two on increasing the neutron fluence with only a slight change in n. In the case of the Zr +1% Sn +1% Nb +0.5% Fe alloy, an increase in neutron fluence markedly increases the fatigue-crack growth rate (Fig. 3b, Table 2), which indicates that this alloy is more embrittled under working conditions than is Zr +2.5% Nb; this agrees well with the results of [2].

Therefore, an increase in fluence from $(1.6-4.6)\cdot10^{24}$ to $3.8\cdot10^{25}$ neutrons/$m^2$ ($E \geq 0.2$ MeV) does not have a marked effect on the few-cycle strength of tubes from working channels made of Zr +2.5% Nb and Zr +1% Sn +1% Nb +0.5% Fe alloys.

LITERATURE CITED

1. O. A. Shatskaya et al., At. Energ., 47, No. 1, 18 (1979).
2. A. M. Vasnin, "A study of the failure resistance in zirconium tubes from technological channels in water—graphite reactors," Dissertation, Moscow (1980).
3. V. M. Filatov, Yu. A. Anikhimovskii, and S. V. Evropin, Zavod. Lab., 46, No. 2, 169 (1980).
4. E. Yu. Rivkin, B. S. Rodchenkov, and V. M. Filatov, The Strengths of Zirconium Alloys [in Russian], Atomizdat, Moscow (1974).
5. K. Petterson, J. Nucl. Mater., 56, No. 1, 91 (1975).
6. Applied Aspects of Failure Viscosity [Russian translation], Mir, Moscow (1969).

# FISSION CROSS SECTION OF $^{249}$Cf WITH FAST NEUTRONS

V. M. Kupriyanov, G. N. Smirenkin, and B. I. Fursov

UDC 539.173.84

At the present time, because of the practical requirements, an extremely high level of experimental information about the fast-neutron fission cross sections of nuclei in the range from thorium to americium has been obtained. Experimental work in this direction has also made a significant contribution to the development of physical concepts about low-energy fission — with values of the excitation energy comparable with the fission barrier height. The development of research in the transplutonium range of nuclides is interesting because of the possibility of obtaining valuable data about the many urgent problems of describing the probability of fission of nuclei, the present state of which guarantees neither the requirements of practice, nor research into related domains of nuclear physics.

Californium is an element with maximum value of Z, for the two isotopes of which $^{249}$Cf and $^{252}$Cf the dependence of the fission cross section on the neutron energy $\sigma_f(E_n)$ has been measured in the range of energy values up to several MeV. However, with the help of them it is difficult to satisfy the interests of fission physics: for $^{252}$Cf there are the results of single, quite rough measurements [1], and for $^{249}$Cf there are more data [2-5] but they are contradictory. Recently, the fission probability of the nuclei of californium isotopes was investigated by means of direct reactions [6], but only in the near-threshold region of energies.

The fission cross section of $^{249}$Cf with fast neutrons was studied earlier by four experimental groups, including the authors of the present paper, for monoenergetic neutrons [2-4] and by the time-of-flight method with a pulsed single-acting source (nuclear explosion) [5]. The deviations of the results of the first three experiments were astonishing, in which not only single-type neutron sources were used, but also identical fission event detectors (glass). This circumstance stimulated us, when formulating the measurements, to reject the procedure for recording the fission fragments with track detectors, which, moreover, is found to be unsuitable for detailed measurements of the energy dependence of the cross sections. In the present experiment an ionization chamber is used, by means of which the fission cross sections in the same range of energies (from 100 keV up to several MeV) were studied for a wide circle of lighter actinides: from $^{233}$U to $^{241}$Am [7].

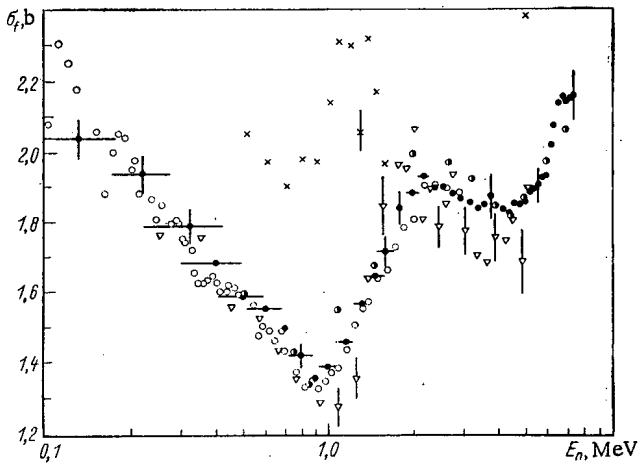


Fig. 1. Fission cross section $\sigma_f$ for the $^{249}$Cf nucleus as a function of the neutron energy E: •) results of present experiment; ○) [5]; ◑) [2]; ×) [3]; ▽) [4].

Translated from Atomnaya Énergiya, Vol. 55, No. 1, pp. 31-34, July, 1983. Original article submitted May 24, 1982.

 0038-531X/83/5501-0472$07.50 

TABLE 1. Measurement Results

| $E_n$, MeV | $\Delta E_n$, keV | $\sigma^{249}/\sigma^{239}$ | $\Delta\sigma^{249}/\sigma^{239}$, % | $\sigma^{239}$, b * | $\sigma^{249}$, b |
|---|---|---|---|---|---|
| 0,13 | 50 | 1,35 | 2,7 | 1,508 | 2,039 |
| 0,22 | 50 | 1,29 | 2,8 | 1,503 | 1,937 |
| 0,32 | 100 | 1,18 | 2,7 | 1,519 | 1,789 |
| 0,40 | 95 | 1,08 | 2,6 | 1,554 | 1,683 |
| 0,50 | 90 | 1,00 | 2,6 | 1,588 | 1,588 |
| 0,60 | 85 | 0,97 | 2,7 | 1,600 | 1,552 |
| 0,70 | 80 | 0,92 | 2,7 | 1,624 | 1,494 |
| 0,80 | 75 | 0,86 | 2,6 | 1,648 | 1,420 |
| 0,90 | 70 | 0,79 | 2,7 | 1,706 | 1,356 |
| 1,00 | 65 | 0,80 | 2,6 | 1,729 | 1,390 |
| 1,15 | 60 | 0,81 | 2,7 | 1,806 | 1,459 |
| 1,30 | 60 | 0,84 | 2,7 | 1,874 | 1,567 |
| 1,45 | 120 | 0,85 | 2,6 | 1,923 | 1,642 |
| 1,60 | 115 | 0,88 | 2,6 | 1,947 | 1,715 |
| 1,80 | 110 | 0,94 | 2,5 | 1,962 | 1,840 |
| 2,00 | 105 | 0,96 | 2,6 | 1,964 | 1,885 |
| 2,20 | 100 | 0,99 | 2,6 | 1,952 | 1,932 |
| 2,40 | 95 | 0,99 | 2,6 | 1,921 | 1,902 |
| 2,60 | 90 | 1,01 | 2,6 | 1,891 | 1,902 |
| 2,80 | 85 | 1,00 | 2,6 | 1,873 | 1,882 |
| 3,00 | 80 | 1,01 | 2,9 | 1,854 | 1,865 |
| 3,20 | 78 | 1,02 | 2,9 | 1,828 | 1,859 |
| 3,40 | 75 | 1,01 | 3,1 | 1,816 | 1,840 |
| 3,60 | 220 | 1,02 | 3,4 | 1,814 | 1,850 |
| 3,80 | 190 | 1,04 | 3,0 | 1,799 | 1,874 |
| 4,00 | 150 | 1,04 | 3,2 | 1,784 | 1,848 |
| 4,20 | 140 | 1,04 | 3,1 | 1,771 | 1,838 |
| 4,40 | 125 | 1,04 | 3,1 | 1,758 | 1,828 |
| 4,60 | 110 | 1,06 | 3,1 | 1,745 | 1,853 |
| 4,80 | 100 | 1,07 | 2,8 | 1,732 | 1,850 |
| 5,00 | 90 | 1,08 | 3,0 | 1,720 | 1,864 |
| 5,20 | 125 | 1,11 | 2,6 | 1,705 | 1,886 |
| 5,40 | 120 | 1,12 | 2,6 | 1,698 | 1,895 |
| 5,60 | 115 | 1,12 | 2,6 | 1,702 | 1,904 |
| 5,80 | 110 | 1,12 | 2,6 | 1,725 | 1,927 |
| 6,00 | 105 | 1,09 | 2,6 | 1,770 | 1,933 |
| 6,20 | 102 | 1,08 | 2,6 | 1,864 | 2,020 |
| 6,40 | 98 | 1,06 | 2,8 | 1,969 | 2,079 |
| 6,60 | 94 | 1,04 | 2,7 | 2,055 | 2,141 |
| 6,80 | 90 | 1,02 | 2,8 | 2,115 | 2,161 |
| 7,00 | 87 | 0,99 | 2,8 | 2,160 | 2,147 |
| 7,20 | 84 | 0,99 | 3,0 | 2,186 | 2,155 |
| 7,40 | 82 | 0,98 | 3,2 | 2,213 | 2,164 |

*1b = $10^{-28}$ $m^2$.

A relative method was used, when the ratio of the fission cross sections of $^{249}$Cf and $^{239}$Pu were measured directly in the experiment, which made it possible to obtain the fission cross section of $^{249}$Cf with an accuracy comparable with the accuracy of the reference cross section. The choice of the fission cross section of $^{239}$Pu as the reference cross section was motivated by the suitability of use of $^{239}$Pu for determining the number of nuclei fissioned in layers by comparison of their $\alpha$ activity. Moreover, since the fission cross section of $^{239}$Pu has been studied intensively in recent years (see, in particular, [7]), the accuracy with which it is known is only slightly worse than the accuracy of the standard — $\sigma_f(^{235}U)$ — usually used in relative measurements.

The measurements were carried out in electrostatic accelerators using the reactions $^7$Li(p, n), T(p, n), and D(d, n) on solid targets of titanium hydride on molybdenum backings as the neutron sources. The energy resolution amounted to 50-200 keV.

The fission fragments were recorded with a double ionization chamber [7], in which layers of $^{249}$Cf and $^{239}$Pu were arranged. The use of an incomplete flight of the fragments allowed the pulses due to fission fragments and $\alpha$ particles to be reliably separated, despite the relatively high $\alpha$ activity of the nuclei being investigated. Owing to the high quality of the layers in the detector, the estimate of the recording efficiency of the fission fragments did not cause any difficulties and for the chambers with $^{239}$Pu and $^{249}$Cf amounted to 98 and 97%, respectively.

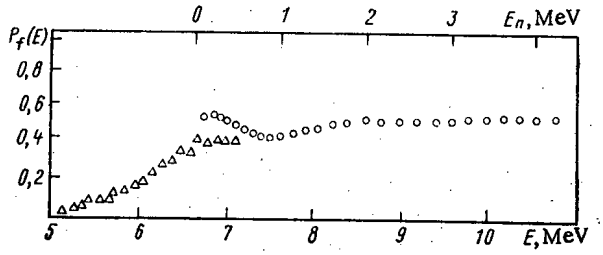


Fig. 2. Dependence of the fissility $P_f$ on the energy of excitation E for the compound nucleus $^{250}$Cf: ○) reaction $^{249}$Cf(n, f), present paper; Δ) reaction $^{249}$Cf(d, pf) [6].

A layer of $^{249}$Cf with a mass of ∿5.5 μg (diameter 8 mm) was used in the experiment, and these same dimensions for the layer of $^{239}$Pu with a mass of ∿175 μg (with 99.891% isotopic purity). The sample of $^{249}$Cf, obtained as the result of the β decay of $^{249}$Bk, was carefully purified from heavy isotopes of californium, which create an undesirable background of spontaneous fissions. The content of $^{252}$Cf did not exceed $3 \cdot 10^{-6}$%. The layer was located at a distance of 36 mm from the accelerator target. In these conditions the spontaneous fission background amounted to 5-8% in the major part of the energy range being studied and reached 30% of the total number of fissions for neutron energies of 0.22 and 3.6 MeV. Special attention was paid to the correct count of spontaneous fissions. The total duration of its measurement time during work on the accelerator amounted to more than 180 h. As a result of this, a measurement accuracy of 1.4% was achieved for the intensity of the spontaneous fission, determined from the spread of the results during the whole cycle of experiments.

The ratio of the number of nuclei fissioned in the layers was determined by a comparison of their α activity by means of a semiconductor detector in "good" geometry. The following values were used for the half-lives: $^{249}$Cf, (350.6 ±2.1) yrs [8], $^{239}$Pu, (24,119 ±26) yrs [9]. The error in determining the ratio of the number of fissioned nuclei, taking account of the indeterminacy of the decay constants, amounted to 1.4%. It also includes the error in determining the ratio of the fission chamber efficiencies (1%).

The background of neutrons scattered by the structure of the target holder was measured by increasing the effective thickness of the structure by a factor of two, with subsequent extrapolation to zero thickness. The maximum correction amounted to 2.2% ($E_n$ = 0.8 MeV). The background of neutrons accompanying (d, n) reactions in the target material was measured by replacing the target by an equivalent template not containing deuterium. The maximum correction amounted to 4% for $E_n$ = 7.4 MeV. The neutron background of the experimental room was not measured, in view of the smallness of the fissile material and the considerable spontaneous fission intensity; however, previous measurements in these same conditions [7] permit the assumption that it is negligibly small.

Corrections were introduced into the measurement results for the energy dependence of the fission chamber efficiency, taking account of the pulse contributed by the neutron, and the angular fission anisotropy (0.1-1.6%), for the difference in the neutron fluxes through the $^{249}$Cf and $^{239}$Pu layers (1.1%), and for the contribution of the induced fission of a small impurity of $^{240}$Pu in the $^{239}$Pu layer (0.109%).

The ratios of the fission cross sections of $^{249}$Cf and $^{239}$Pu, measured directly in this experiment, are given in Table 1. The total error of the results is shown, which is the mean-square sum of the following components:

the statistical error, determined from the spread of the results (1-2%);

the spontaneous fission counting error (0.1-0.5%);

the indeterminacy due to the neutron background count (0.4-1.2%);

errors, introduced by the corrections (0.7-0.9%);

calibration errors (1.4%).

For convenience of comparing the results with the data of other authors, Table 1 also shows the absolute values of the $^{249}$Cf cross section and the values used for the reference fission cross section of $^{239}$Pu [10].

In Fig. 1 the results of the present experiment, for which the total error is shown, are compared with the data of other authors. Because the other experiments were performed several years ago and constants were used in them which are obsolete at the present time, these experiments [4, 5] are scaled to the present-day values of $\sigma_f(^{235}U)$ [10], coincident within the scope of a single estimate with the values of $\sigma_f(^{239}Pu)$ which were used in the present experiment as reference values. In addition, the data of [4] are reduced on the whole by 1.8% because of the refinement of the thermal fission cross sections of $^{249}$Cf and $^{235}$U. Scaling of all data to the present-day constants has significantly improved the mutual agreement of the results of previous experiments [2, 4, 5] both between themselves and with the data of the present experiment. It can be seen from Fig. 1 that from the overall set of results, the results of [3] fall outside in absolute value and in shape of the energy dependence.

The fission of the compound nucleus $^{250}$Cf was studied in the reaction $^{249}$Cf(d, pf) [6], by means of which the range of the energy of excitation of the compound nucleus $E < B_n$ becomes accessible, where $B_n$ is the binding energy of the neutron. Figure 2 shows the experimental data on the fissility $P_f(E)$ in the reactions $^{249}$Cf (d, pf) and $^{249}$Cf (n, f). The fissility for excitation by neutrons was established from the results of the present experiment $\sigma_f(E_n)$ in accordance with the definition

$$P_f(E) = P_f(B_n + E_n) = \sigma_f(E_n)/\sigma_c(E_n), \tag{1}$$

and the cross section of formation of the compound nucleus $\sigma_c(E_n)$ was calculated by an optical model, with the parameters of the potential taken from [11]; the value of $B_n = 6.61$ MeV was assumed in accordance with [12]. Unfortunately, the section on which the energy dependences of $P_f(E)$ overlap for the compared modes of excitation of the compound nucleus $^{250}$Cf is very small. It may be thought that the difference in fissility on this section is a consequence not of the experimental errors, but of the differences in the input channel of the reactions, namely in the accessible quantum states $\sigma_c^{J,\pi}$ in accordance with the expression

$$\begin{gathered} P_f(E) = \frac{1}{\sigma_c} \Sigma \sigma_c^{J,\pi} \left(\frac{\Gamma_f}{\Gamma_t}\right)_{J,\pi}; \\ \sigma_c = \Sigma \sigma_c^{J,\pi}; \quad \Gamma_t = \Gamma_f + \Gamma_n + \Gamma_\gamma, \end{gathered} \tag{2}$$

where $\sigma_c^{J,\pi}$ is the partial cross section of formation of the compound nucleus; $\Gamma_t$, $\Gamma_f$, $\Gamma_n$, and $\Gamma_\gamma$ are the total, fission, neutron, and radiation widths, being functions of J and $\pi$ — the spin and parity of the excited states of the compound nucleus. The distributions of $J^\pi$ for the reactions compared differ strongly at low energy $E_n = E - B_n$, but with increase of $E_n$ they converge, by which obviously is also explained the reduction of the difference of the observed fissilities with energy in Fig. 2. The satisfactory agreement of the experimental results of measurement of the fissility of heavy nuclei in neutron and direct reactions was also noted earlier, e.g., in [13].

The authors thank V. I. Ivanov and B. F. Samylin for participation in the work.

LITERATURE CITED

1. M. Moore, J. McNally, and R. Baybarts, Phys. Rev., C4, 273 (1971).
2. B. I. Fursov, V. I. Ivanov, and G. N. Smirenkin, Yad. Fiz., 19, 50 (1974).
3. P. E. Vorotnikov et al., Yad. Fiz., 15, 34 (1972).
4. É. F. Fomushkin, E. K. Gutnikova, and G. F. Novoselov, Yad. Fiz., 22, 459 (1975).
5. M. Silbert, Nucl. Sci. Eng., 51, 376 (1973).
6. H. Britt et al., Phys. Rev. Lett., 15, 1010 (1978).
7. B. I. Forsov et al., At. Energ., 43, No. 3, 181 (1977); No. 4, 261; 44, No. 3, 236; 45, No. 6, 440; 46, No. 1, 35 (1979).
8. Transactinium Isotopes Nuclear Data, IAEA-TECDOC 232, Vienna, 137 (1980).
9. D. J. Adams, Appl. Rad. Isotopes, 29, No. 8, 479 (1978).
10. V. A. Kon'shin, E. Sh. Sukhovitskii, and V. F. Zharkov, "Estimation of the fission cross section of $^{239}$Pu," Preprint Institute of Heat and Mass Exchange, Academy of Sciences of the Belorussian SSR, Minsk (1978).
11. G. V. Anikin et al., Preprint FÉI-405, Obninsk (1973).

12. V. A. Kravtsov, Atomic Mass and Nuclear Binding Energy [in Russian], Atomizdat, Moscow (1974).
13. J. Cramer and H. Britt, Nucl. Sci. Eng., 41, 177 (1970).

# MULTILEVEL PARAMETRIZATION OF THE TOTAL CROSS SECTION AND FISSION CROSS SECTION OF $^{239}$Pu IN THE RESONANCE REGION OF NEUTRON ENERGIES

T. Bakalov, G. Ilchev,
S. Toshkov, V. F. Ukraintsev,
Mai Chan Khan', and N. Yaneva

UDC 539.170.013

The problem of the multilevel parametrization of resonance cross sections has been considered by many authors because of the necessity for analyzing not only the resonance, but also the interference features of the cross-section energy dependence.

For the parametrization of the energy dependence of the cross sections of fissile nuclei, the Breit—Wigner [1] and Reich—Moore [2] schemes are used in R-matrix theory, and Adler's [3] scheme in S-matrix theory. The advantage of the Reich—Moore and Breit—Wigner schemes is the simple physical meaning of the parameters, their direct relation with the nuclear models, and the possibility of extrapolating the parameters to the region of forbidden resonances, using the well-known distributions. However, in these schemes it is complicated to allow for the Doppler effect, and to use the method of least squares in order to obtain the parameters is a very time-consuming problem. Moreover, consideration of the interference of more than two levels and the introduction of more than three reaction channels also leads to large volumes of calculations.

Adler's scheme is more suitable for the reproduction of the cross sections in reactor calculations. When using this scheme, the Doppler effect is easily taken into account, the cross sections can be described with any number of reaction channels and interference levels, corrections can be introduced for the experimental resolution, and it is relatively simple to obtain the parameters by the method of least squares.

In the present paper the results are presented of the multilevel analysis of data on the transmission of neutrons through samples of $^{239}$Pu of different thickness, in the energy

TABLE 1. Total Cross Section (TCS) and Fission Cross Section (FCS) Resonance Parameters of $^{239}$Pu, MeV

| $\mu_k$, eV | TCS | | FCS | | $\nu_k$ |
|---|---|---|---|---|---|
| | $G_k^t$ | $H_k^t$ | $G_k^f$ | $H_k^f$ | |
| 7,810 | 0,4173 | —0,0092 | 0,2225 | 0,0041 | 42,94 |
| 10,924 | 0,8385 | 0,0511 | 0,5791 | 0,0702 | 88,88 |
| 11,880 | 0,4223 | —0,0324 | 0,1518 | —0,0283 | 33,05 |
| 14,300 | 0,2606 | —0,0324 | 0,1585 | —0,0315 | 53,20 |
| 14,642 | 0,7434 | 0,0507 | 0,3200 | 0,0361 | 36,45 |
| 15,423 | 0,2849 | —0,0131 | 0,2611 | —0,0969 | 404,56 |
| 17,634 | 0,6446 | 0,0018 | 0,2914 | —0,0119 | 38,20 |
| 22,230 | 0,8235 | 0,0229 | 0,4734 | 0,0224 | 52,43 |
| 23,800 | 0,0285 | —0,0053 | 0,01806 | —0,0048 | 45,75 |
| 26,233 | 0,4533 | 0,0016 | 0,2257 | —0,0065 | 42,96 |
| 27,240 | 0,0346 | 0,0022 | 0,0056 | —0,0005 | 24,50 |
| 32,285 | 0,0734 | 0,0021 | 0,0509 | 0,0041 | 82,95 |
| 35,430 | 0,0589 | 0,0001 | 0,0057 | 0,0001 | 19,40 |
| 41,378 | 0,8935 | 0,0342 | 0,0714 | 0,0066 | 22,50 |
| 44,444 | 1,3632 | —0,0382 | 0,1207 | —0,0027 | 25,80 |
| 47,550 | 0,3736 | 0,0267 | 0,3259 | 0,0157 | 140,6 |

Translated from Atomnaya Énergiya, Vol. 55, No. 1, pp. 34-37, July, 1983. Original article submitted July 22, 1982.

 0038-531X/83/5501-0476$07.50 

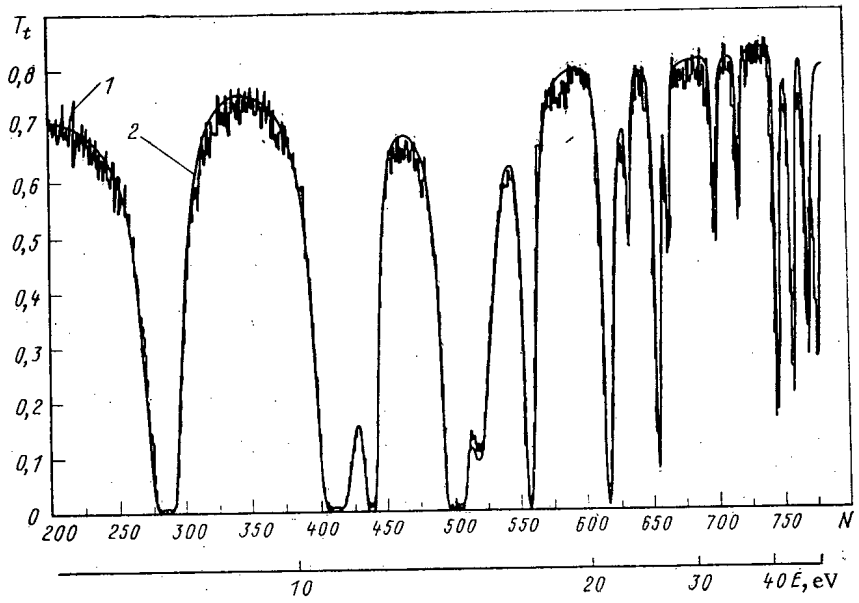


Fig. 1. Result of multilevel parametrization of the transmission as a function of the channel number N and the neutron energy E, for a sample thickness of 0.0165 nuclei/barn: 1) experiment; 2) transmission values, reconstructed from the parameters obtained.

range from 4 to 50 eV, which was carried out on the basis of Adler's scheme in S-matrix theory [3].

Procedure and Basic Formulas. The partial cross section of type $\alpha$, and also the total cross section after deduction of the potential scattering cross section, is represented in Adler's scheme in the form of a sum over the resonances k:

$$\sigma_\alpha(E) = \pi\lambda^2 \sum_k \left\{ \frac{1}{\nu_k} [G_k^\alpha \psi_k(x_k, \xi_k) + H_k^\alpha \chi_k^\alpha(x_k, \xi_k)] \right\}, \quad (1)$$

where $\lambda$ is the wavelength of the neutron; $\nu_k$, half-width of the level; and $G_k$, $H_k$, parameters defining the area of the levels and the interresonance interference.

The functions $\psi$ and $\chi$ are Doppler functions of $x_k$ and $\xi_k$. Here $x_k = (E - \mu_k)/\nu_k$; $\xi_k = \nu_k/\Delta$; $\Delta$ is the Doppler width; E, neutron energy; and $\mu_k$, position of the level.

The observed transmission is related with the total cross section by the relation

$$T_t(E, n) = \int_{\Delta E} R(E', E) \exp[-\sigma_t(E') n] dE', \quad (2)$$

and the fission cross section is described by the formula

$$\sigma_f(E) = \int_{\Delta E} R(E', E) \sigma_f(E') dE', \quad (3)$$

where R(E', E) is the resolution function; n, thickness of the samples being investigated: nucleus/b (1 b = $10^{-28}$ $m^2$); and $\Delta E$, averaging interval with respect to energy. The resolution function R(E' E) for the regime of the IBR-30 reactor has the form of a Gaussian distribution [4] with a neutron pulse width of 80 μsec. For the booster regime of the reactor, R(E' E) has a more complex form, and we have used the resolution function obtained by us by analogy with [5], taking into account that the width of the analyzer channel is comparable with the width of the neutron pulse.

After reproduction of the detailed energy dependence of the total cross section and the fission cross section by means of the S-matrix parameters obtained, the mean cross section and the factors of its resonance self-screening can be obtained in the energy interval $\Delta u$ as a function of the temperature and the dilution cross section [6]:

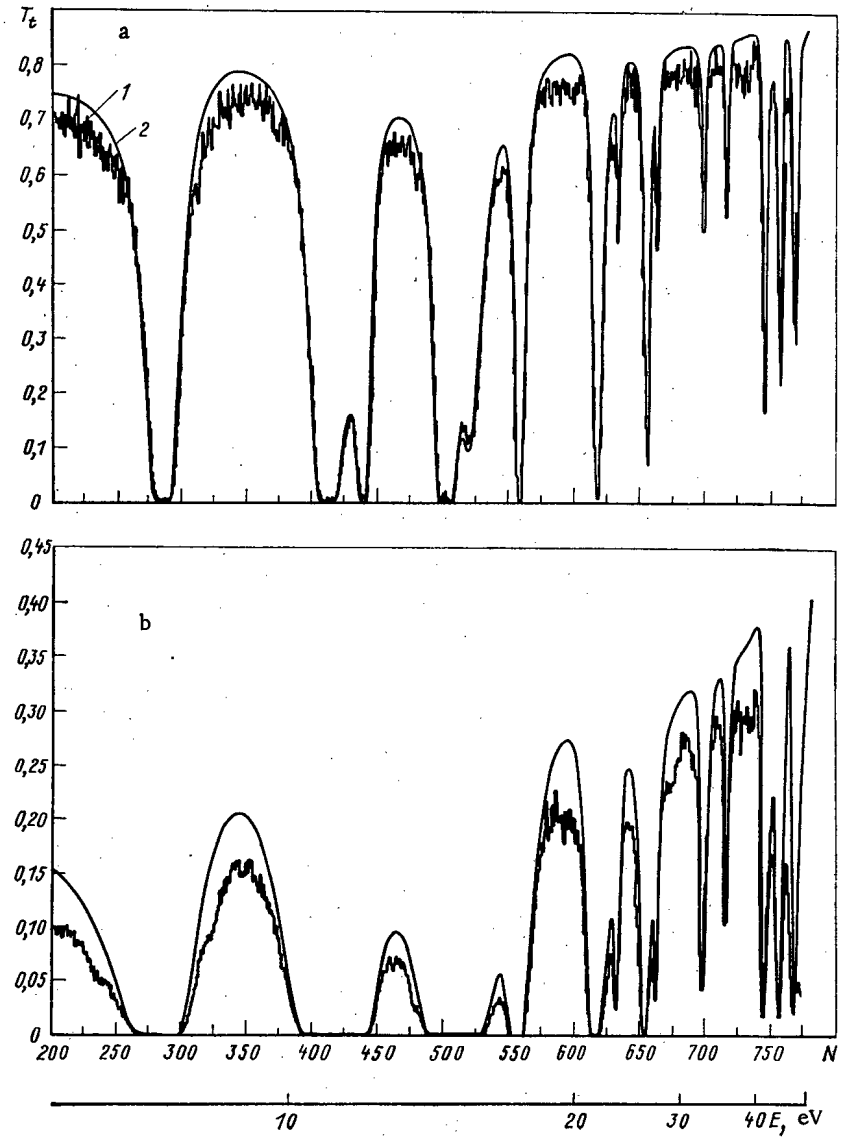


Fig. 2. Transmission function T (E, n) vs channel number N for $^{239}$Pu with E < 50 eV, n = 0.0165 (a) and 0.1085 nuclei/b (b): 1) experiment; 2) results of [9], scaled to the conditions of our experiment.

$$\langle\sigma\rangle = \frac{1}{\Delta u}\int_{\Delta u}\sigma(u)\,du; \tag{4}$$

$$\langle f_t(\sigma_0)\rangle = \frac{1}{\langle\sigma_t\rangle}\left[\frac{\langle 1/(\sigma_t+\sigma_0)\rangle}{\langle 1/(\sigma_t+\sigma_0)^2\rangle} - \sigma_0\right]; \tag{5}$$

$$\langle f_f(\sigma_0)\rangle = \frac{1}{\langle\sigma_f\rangle}\,\frac{\langle\sigma_f/(\sigma_f+\sigma_0)\rangle}{\langle 1/(\sigma_t+\sigma_0)\rangle}, \tag{6}$$

where $\sigma_0$ is the dilution cross section.

Analysis of the Experiment and Results. The values of the transmission $T_t(E, n)$ were obtained for a thickness of the $^{239}$Pu samples in the range 0.0165-0.1085 nuclei/b on the neutron spectrometer by the time of flight of the IBR-30 reactor. The flight base was 1000 m, resolution 90 nsec/m, and width of the analyzer 32 μsec. A battery of $^{3}$He counters with a low inherent background served as the detector. In addition, the self-indication function of the fission process was measured, using an ionization plutonium fission chamber on bases of 75 and 250 m for the booster regime of the reactor with a neutron pulse width of about 4 μsec. The time-variable background of the reactor was measured by the method of resonance filters and was subtracted from the equipment spectrum.

TABLE 2. Average Group Total Cross Sections, Fission Cross Sections, and Resonance Self-Screening Factors for $^{239}$Pu

| Expt. | E, eV | Variant | $\langle\sigma_t\rangle$, b | $\langle\sigma_f\rangle$, b | $f_t(\sigma_0)$ | | | | $f_f(\sigma_0)$ | | | |
|---|---|---|---|---|---|---|---|---|---|---|---|---|
| | | | | | 0 | 10 | $10^2$ | $10^3$ | 0 | 10 | $10^2$ | $10^3$ |
| 19 | 21,5—46,5 | A | 65,5±3,6 | | 0,162 | 1,184 | 0,304 | 0,660 | 0,235 | 0,260 | 0,399 | 0,778 |
| | | B | 65,8±2,7 | 23,3±0,9 | 0,214 | 0,231 | 0,306 | 0,574 | 0,258 | 0,291 | 0,427 | 0,740 |
| | | C | 62,4 | 22 | 0,235 | 0,249 | 0,359 | 0,632 | 0,132 | 0,176 | 0,363 | 0,718 |
| | | D | 62,59 | 22,03 | 0,25 | 0,27 | 0,38 | 0,74 | 0,19 | 0,23 | 0,44 | 0,87 |
| 20 | 10—21,5 | A | 179±8 | | 0,124 | 0,134 | 0,229 | 0,609 | 0,167 | 0,199 | 0,366 | 0,757 |
| | | B | 184±9 | 101,8±5 | 0,115 | 0,133 | 0,220 | 0,522 | 0,184 | 0,220 | 0,375 | 0,707 |
| | | C | 188,5 | 104,7 | 0,110 | 0,118 | 0,217 | 0,516 | 0,149 | 0,186 | 0,372 | 0,679 |
| | | D | 187,8 | 104,4 | 0,11 | 0,13 | 0,21 | 0,51 | 0,12 | 0,15 | 0,29 | 0,66 |
| 21 | 4,65—10 | A | 76±4 | | 0,224 | 0,233 | 0,303 | 0,605 | 0,198 | 0,225 | 0,367 | 0,736 |
| | | B | 69,1±2,7 | 32,5±1,4 | 0,312 | 0,320 | 0,363 | 0,565 | 0,266 | 0,283 | 0,378 | 0,673 |
| | | C | 72,1 | 34,1 | 0,276 | 0,281 | 0,334 | 0,536 | 0,268 | 0,286 | 0,393 | 0,648 |
| | | D | 71,96 | 34,06 | 0,28 | 0,29 | 0,33 | 0,54 | 0,17 | 0,19 | 0,30 | 0,63 |

*A) Measurements of present paper (see also [10]); B) results calculated from the parameters of the present paper; C) data of BNAB-88 [6]; D) data from [11].

The experimental errors are due to the statistical counts of the detectors and the error incurred in taking account of the variable background. The transmission errors can be obtained by the formula

$$\Delta T(x)=\sqrt{\frac{T(x)}{N_0^0 T+K(x-x_0)}}+\frac{T(x)}{\sqrt{N_n^0+K(x-x_0)}}+0.02\lg_2\left(\frac{n}{0.0862}\right)+0.01,$$

where $N_o^o$, $N_n^o$, $T_o$, and K are constants, the values of which are given in [7]; x is the channel number of the equipment spectrum; T is the transmission value. The experimental information obtained was transmitted in the EXFOR exchange format.

Figure 1 shows the experimental values of the transmission and the result of the multilevel fitting of the transmission by the method of least squares in the range 4-50 eV. The parameters of the total cross section and the fission cross section of 16 resonances in the range of energies considered are given in Table 1. The parameters of the total cross section are obtained with simultaneous fitting of the transmissions for a sample thickness of 0.0165, 0.0329, 0.0658, and 10.1085 nuclei/barn, and the resonance parameters of the fission cross section are obtained with fitting of the fission self-indication functions (columns 4 and 5). The parameters $\mu_k$, $G_k$, and $\nu_k$ are found to be in good agreement with the results of [3] and [8]. However, the estimate of the parameter $H_k$ differs from the estimate obtained by analysis of the detailed course of the cross sections by the authors of [3] and [8]. An analysis of our data was also carried out in [7], using the Breit—Wigner one-level approximation.

The experimental transmission function $T_t(E, n)$ for $^{239}$Pu with $E < 50$ eV and for a sample thickness of 0.0165 and 0.1085 nuclei/b, and the results of its calculation by means of the multilevel parameters obtained from an analysis of the data of Derrien [9] and Kolesov [8], taking account of the conditions of our experiment, are shown in Fig. 2. It can be seen that in the region of energies analyzed, experiment gives the total cross section of $^{239}$Pu between resonances as greater by approximately 1.5-2 b. Since the measurements of the neutron transmission at large thickness show the effect of interresonance interference well, it is possible that they give a more accurate cross section in the minima and, consequently, a more reliable estimate of the parameter $H_k$.

Table 2 shows the mean group total cross sections and fission cross sections and their resonance self-screening factors as a function of the dilution cross section $\sigma_o$[b] at a temperature of T = 300°K. The errors $f_t$ and $f_f$, obtained as a result of varying the parameters $G_k{}^t$, $G_k{}^f$, $H_k{}^t$, $H_k{}^f$, and $\nu_k$ within the limits of their errors, amount to 10%. The nuclear constants, calculated from our multilevel parameters, coincide satisfactorily with the experimental values [10] and do not differ significantly from the data of other authors [11].

## CONCLUSIONS

By means of Adler's multilevel formalism, the transmission and self-indication spectra of $^{239}$Pu are analyzed over a wide range of neutron energies below 50 eV. The resonance

parameters of the total and fission cross sections are obtained, which contain more-reliable information about the effects of resonance interference.

The procedure for the transmission analysis is applicable for estimating the resonance parameters of other heavy isotopes, where Adler's approximation is the most useful and effective. The experimental data on the transmission can be used for the compilation of evaluated files of $^{239}$Pu nuclear data, and the average group cross sections and resonance self-screening factors obtained on their basis can be used for the compilation of new systems of group constants.

The authors thank A. A. Luk'yanov, L. B. Pikel'ner, and A. A. Van'kov for constant interest in the work and for useful discussions.

LITERATURE CITED

1. A. Lane and R. Thomas, Theory of Nuclear Reaction at Low and Medium Energies [Russian translation], IL, Moscow (1960).
2. C. Reich and M. Moore, Phys. Rev., 3, 929 (1958).
3. F. Adler and D. Adler, in: Proceedings of a Conference on Neutron Cross Sections and Technology, Washington, March 4-7, 1978, p. 967.
4. É. N. Karzhavina et al., Yad. Fiz., 5, 471 (1967).
5. A. B. Popov et al., Report JINR 3-9742 [in Russian], Dubna (1976).
6. L. P. Abagyan et al., Group Constants for the Calculation of Nuclear Reactors and Shielding [in Russian], Énergoizdat, Moscow (1981).
7. V. A. Konshin and G. B. Morogovskii, INDC(NDS)-129/GJ, Vienna, 360 (1982).
8. V. V. Kolesov and A. A. Luk'yanov, in: Neutron Physics, Pt. 2 (Data of the Fifth All-Union Conference on Neutron Physics) [in Russian], TSNIIatominform, Kiev (1980), p. 187.
9. H. Derrien, in: Proceedings of an IAEA Symposium "Nuclear Data for Reactors — 1966," October 17-21, 1966, Paris, Vol. 11 (1966), p. 195.
10. T. Bakalov et al., Proceedings of an International Conference on Nuclear Cross Sections for Technology, NBS Special Publication No. 594, p. 692 (1980).
11. E. Monapace, M. Motta, and G. Panini, A 26-Group Library with Self-Shielding Factors for Fast Reactor Calculations from UK Nuclear Data File. CNEN-RT/FI(73) 15 (1973).

# THERMOPHYSICS OF THE FOCUSING MIRRORS FOR LASER THERMONUCLEAR REACTORS

V. I. Subbotin, P. A. Grishunin, and V. V. Kharitonov

UDC 621.039:621.375:621.3.038:533.92:539.3

It is thought that a thermonuclear reaction in a laser thermonuclear reactor should be realized in the form of a series of microexplosions, initiated by powerful pulses of laser radiation [1-5]. To focus several laser beams on the surface of a deuterium—tritium target, either focusing mirrors or lenses can be used. These mirrors or lenses will evidently be the last optical elements on the light path from the laser to the target.

Very strict requirements are imposed on the focusing system of laser thermonuclear reactors. First of all, the system must allow for passage of powerful laser radiation with the following parameters (in the ideal case) [1, 3]: radiation wavelength $\lambda = 0.2\text{-}2.0$ μm; pulse energy $E = 0.3\text{-}3.0$ MJ; pulse duration $\tau = 0.1\text{-}10$ nsec; and pulse repetition frequency $f = 1\text{-}100$ Hz. Second, the system must be reliably shielded from the destructive action of the thermonuclear microexplosion, whose energy is expected to be 100-1000 times greater than the energy of the laser pulse. About 70% of the energy of the explosion goes into neutrons, 1-5% of the energy goes into x-ray radiation, and the remaining energy goes into the charged products of the thermonuclear reaction and unburned fuel. Third, the focusing system must have stable geometric and optical parameters during the operation of the laser system (approximately $10^8$ pulses [1]). In particular, the roughness and thermal and other deformations of the mirrors should not exceed tenths-to-hundredths of the wavelength of the laser radiation.

Translated from Atomnaya Énergiya, Vol. 55, No. 1, pp. 37-42, July, 1983. Original article submitted August 6, 1982.

 0038-531X/83/5501-0480$07.50 

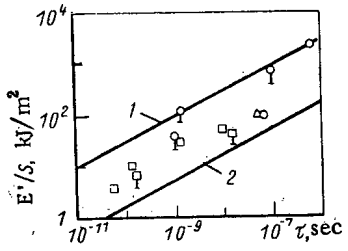


Fig. 1

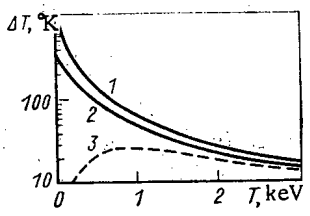


Fig. 2

Fig. 1. Influence of laser pulse duration on the damage threshold of copper mirrors. The experimental data are taken from [6, 7] with R = 98-99% for wavelengths 1.06 (□), 3 (Δ), and 10.6 μm (○). The calculation is performed for R = 99% using: 1) Eq. (1) with $\Delta T_{melt} = 1060°K$; 2) Eq. (3) with $[\sigma] = 10^8$ Pa.

Fig. 2. Dependence of the jump in the surface temperature of a copper mirror on the temperature of x-ray radiation with a black-body spectrum with pulse energy 0.3 kJ on 1 $m^2$ mirror and pulse durations $10^{-10}$ (1) and $10^{-9}$ sec (2, 3): ——) unshielded mirror; ———) shielding, consisting of a layer of neon gas with a thickness of 20 m at a pressure of 100 Pa.

These rigid and contradictory requirements on the focusing system of laser thermonuclear reactors raise the problem of developing it to the same level as the problem of the first wall of the reactor vessel. The purpose of this paper, which is primarily concerned with the thermophysical aspects of the problem, is to draw attention to the difficult and complex problem of the focusing system of these reactors.

Heating of a Mirror by a Single Laser Pulse. When a mirror is irradiated by a single pulse with energy E', part of this energy RE' is reflected from the mirror, while the remaining part (1 — R)E' is absorbed in the surface layer of the mirror and heats it (R is the coefficient of reflection of the mirror material at the given wavelength). In experiments on pulsed heating of mirrors, the threshold of their breakdown is usually determined from the appearance of visible damage on the surface of the mirrors, which, as a rule, is related with melting of the surface or separate parts of the surface (Fig. 1). However, in order to ensure prolonged operation of the mirrors, it is necessary that the thermal stresses not exceed the elastic limits [8, 9]. When a rectangular pulse with duration τ heats a mirror, the temperature of the mirror surface increases by

$$\Delta T = \frac{(1-R)E'\delta}{\tau S K}, \tag{1}$$

where S is the area of the mirror; K, coefficient of thermal conductivity of its material; $\delta = \sqrt{(4/\pi)a\tau}$, thickness of the thermal boundary layer; $a = K/\rho C_p$, thermal diffusivity of the mirror material; and $\rho C_p$, heat capacity per unit volume. The thermal stresses of compression, due to heating of the mirror, are

$$\sigma = \beta E \Delta T/(1-\nu), \tag{2}$$

where E is Young's modulus; ν, Poisson's coefficient; and β, coefficient of thermal expansion. Bounding the stresses (2) by the elastic limit (yield stress) [σ], we find the permissible light load on the mirror (see Fig. 1):

$$\frac{E'}{S} = \frac{2}{\sqrt{\pi}} \frac{D\sqrt{\tau}}{(1-R)}. \tag{3}$$

Here $D = [\sigma]K\sqrt{a}/\beta E$ is the dimensional complex, which depends only on the physical properties of the mirror material. It follows from expression (3) that a small light load or minimum mirror area with fixed pulse energy can be achieved when the mirror is made of a material with maximum thermoelastic Q-factor D and has a high coefficient of reflection. Increasing

the pulse duration with fixed energy likewise decreases the surface area of the mirror. Thus, when the surface of a copper mirror is heated up by only 20-30°K, the thermal stresses reach 60-90 MPa, which is close to the yield stress of copper. This limits the light load (absorbed) by the value 20-30 $J/m^2$ with a pulse duration of $10^{-9}$ sec. This is enough time for a layer of thickness $\sim$0.4 μm to be heated. In this case, for a laser pulse energy of 1 MJ and a coefficient of reflection of the mirror equal to 99%, a mirror with area >300 $m^2$ would be required. The first wall of a spherical reactor vessel with a diameter of 10 m has such an area.

The coefficient of absorption of the mirror can be decreased by an order of magnitude (and its area can be decreased by the same factor) by using multilayered dielectric coatings. Such materials as $ThF_4$, Na(F, Cl), KCl, (Ba, Sr)$F_2$, Zn(S, Se), and others [10] have proved to be effective for 10.6-μm $CO_2$ lasers. As a rule, $Th(IO_3)_4$, $SiO_2$, $ZrO_2$, $TiO_2$ coatings [11] are used for 1.06-μm neodymium glass lasers, while $TiO_2$, MgO, $ZrO_2$, $MgF_2$, and others are used in the ultraviolet region of the spectrum (0.25-0.35 μm). However, some of these materials may be incompatible with the requirement of optical stability of the mirrors ($10^8$ pulses) under conditions of neutron and x-ray irradiation and contact with hydrogen (deuterium and tritium) and lithium vapors. In addition, the thresholds for destruction of the coatings are often less than the thresholds for destruction of the metallic surfaces, worked by diamond sharpening, due to the fact that the technology for depositing multilayered coatings over large areas has not been perfected.

Permissible light loads with $\tau \leq 10^{-9}$-$10^{-10}$ sec must be estimated taking into account the dynamic effects, related with the finite value of the velocity of propagation of thermal and mechanical disturbances (expansion wave), as well as with overheating of the conduction electrons relative to the crystal lattice, and other effects [12]. It is shown in [12] that thermal stresses at the front of the expansion wave, propagating with a higher (approximately by a factor of 1.3) velocity than the temperature wave, can exceed the stress (2) at the surface of the mirror with pulse duration <0.1 nsec.

Overheating of the conduction electrons relative to the crystal lattice "softens" this effect to some extent. Laser radiation is absorbed in metals primarily by electrons. The transfer of energy from electrons to the lattice occurs comparatively slowly due to the large difference between the masses of the electrons and ions [12]. For this reason, as well as due to the low heat capacity of the electron gas, the temperature of the latter may greatly exceed the temperature of the lattice [12]. The time for equilibrating the electron and lattice temperatures in metals depends on the coefficient of heat exchange between them and on the heat capacity of the lattice and constitutes $\sim 10^{-11}$-$10^{-9}$ sec, so that the effect of electron overheating can be considerable in the case of heating by picosecond pulses. Thus, Agranat et al. [13], who irradiated metallic foils with 20-nsec laser pulses, observed heating of the electron gas to a temperature of $\sim$3500°K. The temperature of the overheated electrons was determined from their emission spectrum.

Overheating of electrons in mirrors can have several consequences: First, the delay in heating the lattice will decrease the thermal stresses; second, as the temperature of the electrons increases, the reflection of light decreases; and third, electron emission from the surface of the mirror increases with increasing temperature, which could be a reason for the breakdown of gas at the surface of the mirror.

Heating of the Mirror with a Pulse of X-Ray Radiation. X-ray radiation is liberated primarily in the process of thermonuclear burning of the target, which continues for approximately $10^{-11}$-$10^{-10}$ sec [4, 5, 14-16, 17], i.e., the x-ray pulse is 10-100 times shorter than the laser pulse. The energy of the x-ray pulse, reaching the surface of the mirror and almost completely absorbed in it, can exceed, by an order of magnitude, the energy from the laser absorbed in the mirror. Taking into account the small duration of the x-ray pulse, it may be concluded that its thermal effect on the focusing system of the laser thermonuclear reactor can be very dangerous.

For exponential attenuation of the radiation in the mirror with attenuation coefficient μ(ε), which depends on the energy of the photon [4, 5, 14, 17], the surface is heated by an amount

$$\Delta T = \frac{Q}{SK\mu\tau}\left[e^{u^2}\operatorname{Erfc}(u) + \frac{2}{\sqrt{\pi}} - 1\right], \qquad (4)$$

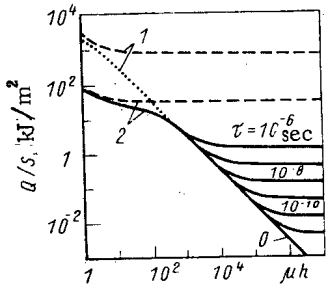


Fig. 3

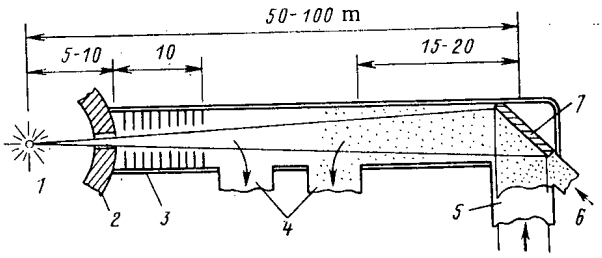


Fig. 4

Fig. 3. Limiting heat loads, which raise the surface temperature of a copper mirror by 50°K with periodic heating by pulses with different duration and penetrability with repetition frequency of 1 (1) and 25 Hz (2); ———, ....) calculations using Eq. (6); — — —) calculations using Eq. (8) with h = 20 mm and Bi → ∞.

Fig. 4. Diagram of the shielding of the focusing mirror: 1) target; 2) blanket; 3) damper (and simultaneously condenser of lithium vapor); 4) exhaust pipes; 5) inlet of laser beam; 6) inlet of shielding gas; 7) mirror.

where Q is the energy of the x-ray pulse absorbed by the mirror; $u = \mu\sqrt{a\tau}$ is a dimensionless parameter, characterizing the ratio of the diffusion length of heat $\sqrt{a\tau}$ to the attenuation length of heat liberation $1/\mu$. For radiation with low penetrability, when $u \gg 1$, expressions (4) and (1) give practically an identical result. For radiation with high penetrability or with very short duration, when $u \ll 1$, it follows from expression (4) that $\Delta T = (Q/S)\mu/\rho C_p$, i.e., the heating of the surface does not depend on the pulse duration (with fixed energy) and is much less than that calculated using the surface heating model (1). The x-ray radiation spectrum of structured targets can be approximated by the emission spectrum of a black body with a temperature ranging from fractions of keV to tens of keV; in addition, this temperature depends on the energy of the explosion, the mass, and the composition of the target [4, 5, 14, 15]. The heating of the surface of the mirror as a function of the x-ray radiation temperature can be determined by integrating expression (4) over the spectrum of x-ray photons. The results of such a calculation for a copper mirror are presented in Fig. 2. It is evident that radiation with a "softer" spectrum, due to its lower penetrability, gives rise to a larger jump in the surface temperature of the mirror. For the example examined, radiation with a temperature spectrum >2 keV is safe from the point of view of the temperature jump ($\Delta T < 30$°K). However, dynamic effects, which can make a significant contribution to the temperature jump in view of the short duration of the x-ray pulse, have not been included in the estimate presented.

Periodic Heating of the Mirror. Above we examined the heating of focusing mirrors by single pulses. In general, the thermal load on the mirrors includes a sequence of pulses from different heat sources differing in intensity and duration. The primary laser pulse, initiating the thermonuclear reaction in the target, is followed with a delay of ~100 nsec by the laser pulse reflected from the target and then by an x-ray pulse, fast thermonuclear neutrons, α particles and, finally, the slower products of the explosion and fragments from the target. All of this is repeated with the next laser pulse. After a large number of pulses, the temperature of the mirror will oscillate between the maximum and the minimum values around some average temperature, which depends on the time-averaged liberation of heat. The thermal deformations and stresses in the mirror, which should not exceed permissible values, will vary correspondingly. For this reason, to select safe operational regimes of the mirror, it is necessary to know the dependence of the amplitude of the oscillations of the mirror temperature as a function of the pulse repetition frequency f and duration τ, the range of any of the forms of radiation in the mirror material, the intensity of cooling of the mirror, and its dimensions. For this purpose, we shall examine the problem of heating of the mirror by periodic, rectangular (temporally) pulses of volume liberation of heat, decreasing exponentially with depth, with the energy of each pulse being Q. Due to the small thickness of the mirror h compared to its diameter, we shall represent the mirror as a flat layer, whose rear surface is cooled with a coolant with constant temperature $T_1$ and heat-transfer coefficient α. Prior to the first pulse, the temperature of the mirror equals the

temperature of the liquid. In this formulation, the nonstationary heat-conduction problem is solved analytically. The maximum temperature of the surface (immediately after the passage of the N-th pulse) is determined by the expression

$$\Theta_{\max}=\frac{4(\mu h)^2}{W}\sum_{n=1}^{\infty}\frac{1+(e^{-\mu h}/\mu h)(\varkappa_n\sin\varkappa_n-\mu h\cos\varkappa_n)}{\varkappa_n[(\mu h)^2+\varkappa_n^2](2\varkappa_n+\sin 2\varkappa_n)}\left\{1-\frac{[e^{\varkappa_n^2P}-e^{\varkappa_n^2W}+e^{-\varkappa_n^2NP}(e^{\varkappa_n^2W}-1)]\,e^{-\varkappa_n^2W}}{e^{\varkappa_n^2P}-1}\right\}, \tag{5}$$

while the minimum temperature (prior to the beginning of the (N +1)-st pulse) is determined by the expression

$$\Theta_{\min}=\frac{4(\mu h)^2}{W}\sum_{n=1}^{\infty}\frac{1+(e^{-\mu h}/\mu h)(\varkappa_n\sin\varkappa_n-\mu h\cos\varkappa_n)}{\varkappa_n[(\mu h)^2+\varkappa_n^2](2\varkappa_n+\sin 2\varkappa_n)}\frac{(e^{\varkappa_n^2W}-1)(e^{\varkappa_n^2P}-e^{-\varkappa_n^2NP})\,e^{-\varkappa_n^2P}}{e^{\varkappa_n^2P}-1}. \tag{6}$$

The following dimensionless variables enter into Eqs. (5) and (6): $\Theta=(T-T_l)/(Q/Sh\rho C_p)$ is the temperature; $W=a\tau/h^2$ and $P=a/h^2f$, duration and repetition period of the pulses, respectively; $\varkappa_n$, n-th root of the equation $\varkappa\tan\varkappa=Bi$, where $Bi=\alpha h/K$ is Biot's number (dimensionless heat-transfer coefficient); and N, number of pulses. For $N\gg1$, the temperature values [see expressions (5) and (6)] approach their quasistationary values.

The average dimensionless temperature of the mirror surface is determined by the expression

$$\overline{\Theta}=\frac{1}{P}\left[1-(1-e^{-\mu h})\left(\frac{1}{\mu h}-\frac{1}{Bi}\right)\right]. \tag{7}$$

As follows from data presented in Fig. 3, the thermal loads, which raise the surface temperature of the copper mirror by 50°K with heating both by single [see expression (4)] and periodic pulses [see expression (5)], are practically identical. Thus, for $\tau f\ll1$, neither the pulse repetition frequency nor the heat transfer affect the amplitude of the oscillations of the temperature in the mirror. However, taking into account the fact that the thermomechanical cycling greatly decreases the strength properties of metals, the permissible heat loads on the mirror must be decreased with periodic heating.

Heating with Neutrons. Heating of metallic mirrors made of copper, aluminum, steel, and molybdenum by neutrons with a neutron load of 0.8 MW/m$^2$ was calculated in [18]. The diameter of the mirrors was 3.5 m, and their total thickness was 0.35 m; the thickness of the metallic reflecting layer was 25 mm and the porous water-cooled structure contained 5% by volume of the same metal. According to these estimates, the average volume intensity of heat liberation $q_V$ from neutrons and secondary $\gamma$ quanta will be ~10 MW/m$^3$ in copper and molybdenum, 9 MW/m$^3$ in iron, and 3.3 MW/m$^3$ in aluminum. As a result of the volume heating, the temperature of the mirror surface will exceed the coolant temperature by

$$\Delta T=\frac{q_Vh^2}{2K}\left(1+\frac{2}{Bi}\right), \tag{8}$$

which for copper will be ~8°K with h =25 mm and $Bi\to\infty$. The pulsations in the temperature of the mirror, equal to $q_V/f\rho C_p$, arising with the passage of neutron pulses, are not large. Thus, for a pulse repetition frequency of 20 Hz, they constitute ~0.15°K for copper.

Methods for Shielding the Focusing Mirrors. The products of the thermonuclear explosion, as well as the products of reactions occurring in the blanket, can give rise to different types of damage in the focusing system of laser thermonuclear reactors: X-ray radiation and ions, in addition, atomize the surface; neutrons are more dangerous due to the reactions (n, $\alpha$) and (n, p), causing swelling of the materials and, as a result, distortion of the optical surfaces; impact loading gives rise to vibration and misalignment of the optical system. Thus, according to estimates in [18], neutrons give rise to the largest number of atomic displacements in copper and gas liberation in iron (hydrogen) and aluminum (helium). Of the metals examined in [18] (Al, Cu, Fe, Mo, and Ti), molybdenum is subjected most to destructive action.

Conn et al. [16] note that almost all materials of dielectric coatings are very susceptible to the formation of color centers which absorb laser radiation (F centers, etc.) and to a change in the index of refraction induced by neutrons, $\gamma$ quanta, and ions. It is very probable that the decisive mechanism of destruction of dielectric coatings is the formation of a cascade of displacements in the crystal lattice induced by 14-MeV neutrons [16]. It is

especially important to provide radiation shielding for the mirrors when using short-wavelength lasers (0.2-0.5 μm), since their radiation is intensively absorbed by metals. The mirrors must therefore have dielectric coatings, which will greatly increase the costs of constructing the mirrors.

An atmosphere consisting of gas with a high nuclear charge (neon, xenon) effectively shields the focusing system, as well as the first wall of the target chamber, from x-ray radiation and plasma. The gas not only absorbs the "soft" x-ray radiation, which is most dangerous for the output optics, but can also brake the ions forming in the explosion. For this it is sufficient that the path of x-ray photons and ions be several times shorter than the distance from the target to the focusing system. At the same time, the gas present in the explosion chamber must be low enough so as not to hinder the propagation of laser radiation and its focusing on the target. Helium and neon have the highest laser breakdown threshold. For this reason, these gases can be used at the highest pressures [15]. However, for a neon pressure of 100 Pa and a distance of less than 20 m between the mirror and the target, the shielding provided by this gas from x-ray radiation with temperature exceeding 1 keV is ineffective (see Fig. 2).

The simplest method for decreasing the destructive action of radiation on the focusing system is, apparently, increasing its distance from the center of the explosion chamber to the maximum possible distance. According to estimates in [19], for an explosion energy of 500 MJ and repetition frequency of 2 Hz, the deformation of the copper mirror, placed at a distance of 100 m, reaches an inadmissible value of $\lambda/8$ after approximately 5 yrs as a result of swelling. Decreasing the focal distance to 50 m will decrease the lifetime of the mirror by 1 yr.

Figure 4 shows a diagram of the shielding of the focusing mirror [19]. It is proposed that the laser system be placed in a special building separate from the reactor building. Different beams are directed through underground vacuum chambers to the focusing mirrors, situated in the reactor building. The focused beams are extracted onto the target along a tube of length $\sim$100 m. The gaseous products of the explosion are decelerated in the sectioned part of the tube, cooled with a special coolant, and partially removed by vacuum pumps. This section, which is next to the blanket, acts like a damper and a condenser. A zone in which the ionized products of the explosion and the x-ray radiation are absorbed is situated at the other end of the tube near the mirror. Here the shielding gas circulates away from the mirror, enters the pumping system, and returns to the mirror. Essentially, only neutrons reach the focusing mirrors.

## CONCLUSIONS

In this paper we examined several problems involved in the development of focusing systems of laser thermonuclear reactors. We analyzed the heating of mirrors by single and periodically repeating pulses of laser, x-ray, and neutron radiation. We estimated the permissible light loads on the mirror. The relations presented can be used to analyze the thermal state of the focusing mirrors of these reactors. We discussed methods for shielding the output optics from the products of the thermonuclear microexplosion. The greatest difficulties in preparing focusing mirrors and ensuring a long operational lifetime arise with the use of short-wavelength lasers and thermonuclear targets with large energy gain.

To make a more definite selection of the construction and materials of the focusing systems, further investigations are required in at least three interrelated directions:

determination of permissible light and thermal loads on the focusing system and its minimum dimensions;

investigation of the effect of the products of the thermonuclear explosion on the optical properties of the focusing system and selection of a method for shielding it, matched with the method for shielding the first wall;

optimization of the construction, manufacturing technology, and operational lifetime of focusing mirrors of laser thermonuclear reactors.

## LITERATURE CITED

1. N. G. Basov et al., Izv. Akad. Nauk SSSR, Energ. Transport, No. 2, 3 (1979).
2. L. S. Kokorev and V. V. Kharitonov, in: Direct Conversion of Energy and Nuclear Power Installations [in Russian], V. I. Subbotin (ed.), Atomizdat, Moscow (1980), p. 179.

3. J. Maniscalo, in: Technical Paper Topical Meeting, San Diego (1978), WC-3, p. 1.
4. L. S. Kokorev et al., "Heat liberation and temperature field in elements of laser thermonuclear reactors," Report of MIFI, B827559, February 21, 1980, p. 5.
5. J. Hoving, in: Proc. Thirteenth Intersoc. Conversion Eng. Conf., San Diego (1978), No. 2, p. 1353.
6. R. Pierce and W. Spawr, Optics and Laser Technology, No. 2, 25 (1976).
7. Laser Induced Damage in Optical Materials: NBS, Boulder, Colorado (1976), pp. 29, 173, 181.
8. V. V. Apollonov et al., Radiotekh. Elektron., 19, No. 1, 204 (1974).
9. V. S. Kolesov and S. Ya. Gicheva, Fiz.-Khim. Obrab. Mater., No. 6, 15 (1980).
10. M. Sparks, [7], 3.1, p. 203.
11. S. Glaros et al., [7], 4.10, p. 331.
12. P. A. Grishunin et al., in: Problems of the Thermophysics of Nuclear Reactors [in Russian], No. 10, V. I. Subbotin (ed.), Énergoatomizdat, Moscow (1981), p. 48.
13. M. B. Agranat et al., Zh. Eksp. Teor. Fiz., 1, (7), 55 (1980).
14. T. Frank, AIChE T., Symp. Ser., 73, No. 168, 77 (1977).
15. S. A. Abdel'-Kalik and T. O. Khanter, Teploperedacha, 100, No. 2, 159 (1978).
16. R. Conn et al., in: SOLACE, A Conceptual Laser Fusion Reactor Design. UWFDM-220, Univ. Wisconsin (1978).
17. L. S. Kokorev, V. V. Ignat'ev, and V. V. Kharitonov, in: Problems of the Thermophysics of Nuclear Reactors [in Russian], No. 6, V. I. Subbotin (ed.), Atomizdat, Moscow (1977), p. 15.
18. M. Ragheb and C. Maynard, Atomkernenergie, 34, No. 3, 188 (1979).
19. M. Monsler and J. Maniscalo, [3], WC-5, p. 1.

## LETTERS TO THE EDITOR

# ELECTRICAL CONDUCTIVITY OF BINARY MELTED MIXTURES OF POTASSIUM, RUBIDIUM, AND CESIUM FLUORIDES WITH THORIUM TETRAFLUORIDE

V. N. Desyatnik, A. P. Koverda, and N. N. Kurbatov

UDC 621.3:035.431:437.311:546.16

The experimental values of the electrical conductivity of different melted compositions containing uranium and thorium salts are required to select the optimum technology for regenerating irradiated nuclear fuel by electrochemical methods [1, 2]. The systematic study of charge transfer in melted salt mixtures plays an important role in establishing the ionic nature of the melts and helps in judging the structure of the melts and their change under the action of different factors [3-5].

We obtained potassium, rubidium, and cesium fluorides free of water from their crystalline hydrates following the recommendations in [6] with subsequent remelting in an argon atmosphere and cleaning of traces of impurities by two- and threefold zone remelting. The preparation of the starting thorium tetrafluoride and the method for studying the electrical conductivity were described previously [5]. The melting temperature of the salts studied, measured by the method of differential-thermal analysis, agreed well with the handbook data

TABLE 1. Electrical Conductivity of Binary Melted Mixtures

| $ThF_4$ content, mol.% | $\varkappa = a + bT + cT^2$, $S \cdot m^{-1}$ | | | $\pm S$ | $T$, °K |
|---|---|---|---|---|---|
| | $-a \cdot 10^2$ | $b$ | $-c \cdot 10^3$ | | |
| | | | $KF-ThF_4$ | | |
| 10,0 | 5,0655 | 0,9346 | 0,2357 | 0,544 | 1050—1400 |
| 20,0 | 5,7883 | 0,9606 | 0,2680 | 0,562 | 1150—1400 |
| 30,0 | 3,8586 | 0,6194 | 0,1503 | 0,499 | 1050—1400 |
| 40,0 | 4,8899 | 0,7749 | 0,2214 | 1,0241 | 1150—1400 |
| 50,0 | 5,0448 | 0,7706 | 0,2119 | 0,448 | 1190—1400 |
| 60,0 | 4,8080 | 0,6547 | 0,1357 | 0,518 | 1200—1400 |
| 70,0 | 8,5960 | 1,1299 | 0,2786 | 0,571 | 1280—1400 |
| 80,0 | 17,4340 | 2,4840 | 0,8003 | 0,533 | 1280—1420 |
| 90,0 | 12,4930 | 1,5720 | 0,3997 | 0,447 | 1320—1440 |
| 100,0 | 1,8653 | —0,1064 | —0,2634 | 1,515 | 1380—1480 |
| | | | $RbF-ThF_4$ | | |
| 9,3 | 1,9437 | 0,4038 | 0.0736 | 1,047 | 1140—1300 |
| 20,0 | —0,3463 | —0,0329 | —0,0859 | 0,352 | 1140—1300 |
| 30,0 | 1,5600 | 0,2671 | 0,0524 | 0,471 | 1140—1300 |
| 40,0 | 2,4272 | 0,3858 | 0,0949 | 0,397 | 1200—1300 |
| 45,0 | 2,6623 | 0,4262 | 0,1117 | 0,420 | 1200—1350 |
| 53,0 | 3,2023 | 0,5054 | 0,1316 | 1,030 | 1250—1350 |
| 60,0 | 0,6904 | 0,0313 | —0,0882 | 0,283 | 1250—1350 |
| 70,0 | —0,4559 | —0,2239 | —0,2244 | 0,427 | 1280—1350 |
| 80,0 | 1,3211 | 0,0233 | —0,1377 | 0,466 | 1280—1350 |
| 90,0 | —15,4082 | —2,4619 | —1,0571 | 0,231 | 1300—1400 |
| | | | $CsF-ThF_4$ | | |
| 10,0 | 4,8925 | 0,8639 | 0,2691 | 0,562 | 1150—1300 |
| 20,0 | 4,8601 | 0,7821 | 0,2524 | 0,636 | 1150—1300 |
| 30,0 | 4,3366 | 6,7199 | 0,2547 | 0,718 | 1150—1300 |
| 40,0 | 5,0850 | 0,8574 | 0,3190 | 1,142 | 1150—1300 |
| 50,0 | 5,8952 | 1,0242 | 0,3905 | 1,877 | 1100—1350 |
| 60,0 | 5,5861 | 0,8915 | 0,2952 | 0,645 | 1190—1350 |
| 70,0 | 9,3200 | 1,3257 | 0,4003 | 0,436 | 1250—1350 |
| 80,0 | 8,3805 | 0,9980 | 0,1995 | 0,447 | 1280—1350 |
| 90,0 | 9,3292 | 1,0660 | 0,2011 | 1,342 | 1300—1400 |

Translated from Atomnaya Énergiya, Vol. 55, No. 1, pp. 43-44, July, 1983. Original article submitted April 16, 1982.

0038-531X/83/5501-0487$07.50 

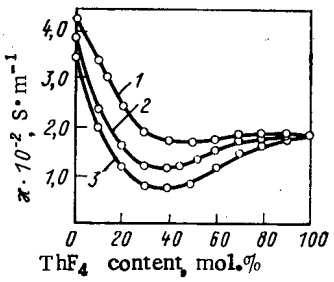


Fig. 1. Isotherms of the electrical resistivity of melted binary systems KF—$ThF_4$ (1); RbF—$ThF_4$ (2); CsF—$ThF_4$ (3) at 1400°K.

[7], while the values of the electrical conductivity agreed with the most reliable published value [8].

We measured the electrical conductivity using a relative capillary method at a frequency of 50 kHz in an argon medium. The electrical conductivity of 9-10 different salt compositions was measured in each of the binary mixtures KF—ThF, RbF—$ThF_4$, and CsF—$ThF_4$ studied (see Fig. 1).

The presence of a deep minimum in the electrical conductivity at concentrations of 30-50 mol.% $ThF_4$ is characteristic for mixtures of the melted salts studied. This contrasts with the previously studied mixtures of binary systems of this series LiF—$ThF_4$ and NaF—$ThF_4$ [5], in which the electrical conductivity was observed to decrease monotonically with increasing concentration of thorium tetrafluoride. The deviations of the electrical conductivity from the values calculated using the additivity rule increase successively from mixtures containing LiF to mixtures containing CsF, which indicates an intensification of the interaction of the starting components in the series of these melted systems.

Table 1 presents the coefficients $a$, b, and c in the equation describing the temperature dependence of the electrical conductivity $\varkappa = a + bT + cT^2$ of all salt mixtures studied, obtained by analyzing the polytherms of the electrical conductivity by the method of least squares, as well as the values of the standard deviations S and the temperature intervals of the measurements.

LITERATURE CITED

1. M. Rosental, P. Kasten, and R. Briggs, Nucl. Appl. Tech., 8, No. 2, 107 (1967).
2. V. L. Blinkin and V. M. Novikov, Liquid-Salt Nuclear Reactors [in Russian], Atomizdat, Moscow (1978).
3. H. Blume and J. O. Bokris, in: Structure of Fused Salts [Russian translation], Mir, Moscow (1976), p. 70.
4. Yu. K. Delimarskii, Chemistry of Melts [in Russian], Naukova Dumka, Kiev (1980), p. 72.
5. V. N. Desyatnik et al., At. Energ., 49, No. 2, 129 (1980).
6. Yu. V. Karyakin and I. I. Angelov, Pure Chemical Substances [in Russian], Khimiya, Moscow (1974).
7. Basic Properties of Inorganic Fluorides (Handbook) [in Russian], Atomizdat, Moscow (1976).
8. M. V. Smirnov, Yu. A. Shumov, and V. A. Khokhlov, in: Electrochemistry of Fused Salts and Solid Electrolytes [in Russian], No. 18, Inst. Electrochemistry, Ural Science Center, Academy of Sciences of the USSR (1972), p. 3.

# RADIATION-INDUCED CHANGE IN THE PROPERTIES OF UNGRAPHITIZED MATERIAL

Yu. S. Virgil'ev, V. G. Makarchenko, and R. G. Pikulik

UDC 621.039.532.21

As is well known, the properties of structural graphite can change considerably under neutron irradiation. Thus, above 520-570°K, specimens of almost isotropic reactor graphite at first settle on both sides of a cutout in the specimens relative to the axis of the part, which, in the fluence range of $\sim 10^{22}$ neutrons/cm$^2$ ($E > 0.18$ MeV), is then replaced by secondary swelling, caused by an irreversible (not restored by thermal annealing) change in the supercrystalline structure [1]. Secondary swelling is likewise accompanied by a change in physical properties: new large increase in the electrical and thermal resistance and drop in the modulus of elasticity [2], which must finally lead to breakdown of the material.

The experimental study of the effects accompanying secondary swelling is very laborious, since prolonged high-temperature irradiation is required. We can attempt to model this process, in order to study its characteristics, by using semifinished products, i.e., specimens of ungraphitized material, which were not graphitized after annealing at 1600°K. In this case the settling rate increases sharply, while the transition to secondary swelling begins

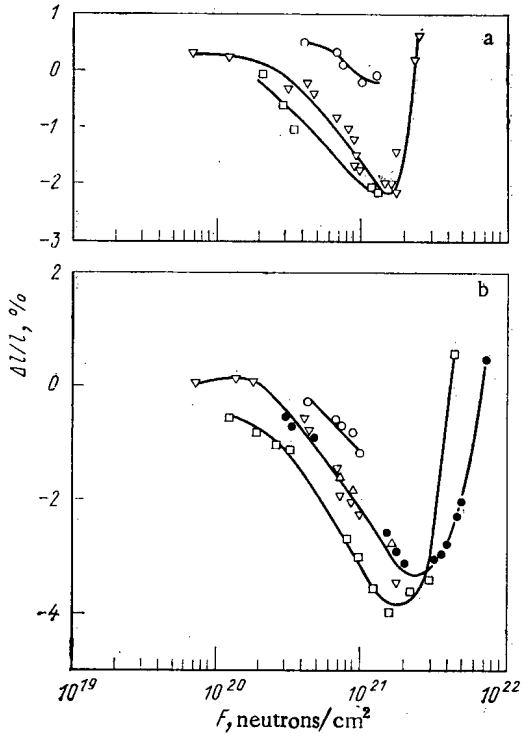


Fig. 1

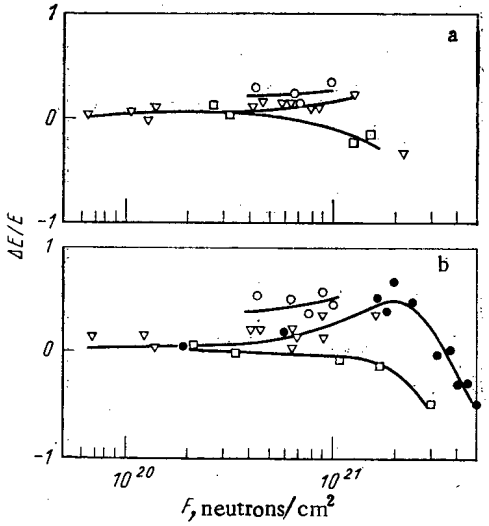


Fig. 2

Fig. 1. Dependence of the relative change in length of specimens irradiated at 400-450 (○), 770 (•) (from data in [4]), 770-870 (▽, △), and 1000-1150°K (□) on the neutron fluence. The specimens were cut out perpendicular (a) and parallel (b) to the axis of the part.

Fig. 2. Dependence of the relative change in the modulus of elasticity of specimens studied on the neutron fluence (notation same as in Fig. 1).

Translated from Atomnaya Énergiya, Vol. 55, No. 1, pp. 44-46, July, 1983. Original article submitted July 9, 1982.

0038-531X/83/5501-0489$07.50  

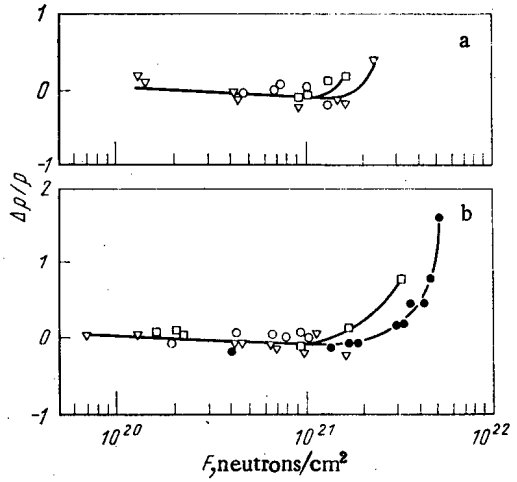


Fig. 3

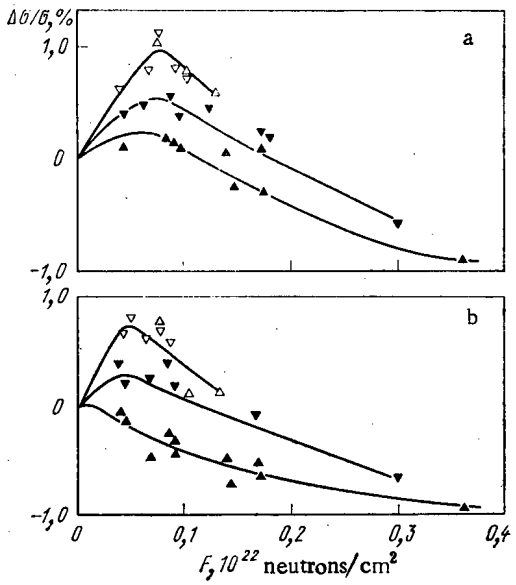


Fig. 4

Fig. 3. Dependence of the relative change in the electrical resistivity of specimens studied on the neutron fluence (notation same as in Fig. 1).

Fig. 4. Dependence of the relative change in the compression (a) and bending (b) strengths on neutron fluence at irradiation temperatures of 400-450 (▽, △) and 1000-1150°K (▼, ▲). The specimens are cut out parallel (▽, ▼) and perpendicular (△, ▲) to the axis of the part.

at a fluence that is 10 times lower (i.e., $\sim 10^{21}$ neutrons/cm$^2$) than in the case of reactor graphite [3, 4]. When specimens of parallel-oriented semifinished product of reactor graphite are irradiated (770°K), secondary swelling is accompanied by a sharp decrease in the modulus of elasticity and an increase in the electrical resistance [4].

In this paper we examine the radiation-induced changes in length, modulus of elasticity, electrical resistance, and bending and compression strengths of specimens of a semifinished product of reactor graphite, cut out parallel and perpendicular to the axis of the part.

We present below the properties of the specimens prior to irradiation (in the numerator, for specimens cut out parallel to the axis of the part, and in the denominator, for specimens cut out perpendicular to the axis):

| | |
|---|---|
| Density, g/cm$^3$ | 1.55 ±0.05 |
| Electrical resistance, $10^{-6}\Omega\cdot$m | 43.1 ±1.5 / 58.6 ±4.0 |
| Modulus of elasticity, 10GPa | 1.15 ±0.11 / 0.78 ±0.10 |
| Strength, MPa: | |
| under compression | 53.0 ±7.0 |
| under bending | 22.0 ±4.0 |

We irradiated the specimens at temperatures ranging from 400-450 to 1000-1150°K, using an ampoule setup [5]. We measured the temperature with the help of diamond indicators (to within ±10-15°K) and indicators made of pyrolytic graphite. The maximum temperature (1000-1150°K) was obtained in holders with specimens containing graphite tubes with tungsten rods. The fluence of fast neutrons ($E \geq 0.18$ MeV) was determined from the duration of irradiation (taking into account the power of the reactor). In this case the neutron flux density was $(5\text{-}9)\cdot 10^{13}$ neutrons/(cm$^2\cdot$sec).

Irradiation at 400-500°K induced settling parallel to the oriented specimens. For perpendicularly oriented specimens, the initial growth to 0.2% was replaced by settling, which with a fluence of $\sim 10^{21}$ neutrons/cm$^2$, evidently, stabilizes at a level of 0.2% (Fig. 1). The relative increment of the modulus of elasticity was 20-40%, while the electrical resistance did not increase (Figs. 2, 3).

For the case of irradiation at 770-870°K, settling develops intensively in both directions with increasing fluence. This corresponds to some growth $\Delta E/E$ in the range 0-60% for parallel and 0-20% for perpendicularly oriented specimens. The relative change in the electrical resistance, as before, is nearly zero. After settling stopped and restoration of the specimens started, the relative change in the modulus of elasticity began to decrease, while the relative change in the electrical resistance began to increase. As the irradiation temperature is increased to 1000-1150°K, the settling and subsequent restoration of the dimensions are observed at lower fluences. The onset of secondary changes in the modulus of elasticity and electrical resistance is also displaced correspondingly.

The bending and compression strength of the irradiated graphite at first, as is well known, increase and then rapidly stabilize. The level of strength reached decreases with increasing irradiation temperature. For the specimens of semifinished product investigated, the increase in strength during irradiation at a temperature above 400-450°K is rapidly replaced by a decrease in strength and even destruction of the specimens (Fig. 4). The position of the maximum on the curves of the relative change in the bending and compression strengths (see Fig. 4) is reached with a lower neutron fluence than the position of the minimum on the curve showing the change in length (Fig. 1), i.e., processes leading to a decrease in strength, which still have no effect on the modulus of elasticity and the electrical resistance, already begin to occur during the settling process in such ungraphitized material.

The increase of the ratio of the compression and bending strengths with increasing fluence, measured on one specimen, from 2.5 to 3.0-5.0 must be explained by the more rapid drop in the resistance of the material to bending loads at which the effect of radiation-induced cracks, acting as concentrators of stress, is more strongly manifested.

Investigations of the macrostructure of the specimens established that the number of cracks, pulverizing grains in the coke-filler, increase with increasing fluence. At the same time, the strength of the undamaged sections of the macrograins remains high. Measurements of microhardness established that for fluence values of 0, $1.2 \cdot 10^{21}$, and $4.4 \cdot 10^{21}$ neutrons/cm$^2$, the microhardness of the specimens is 108, 202, and 228 relative units, respectively. For this reason it may be assumed that the decrease in strength accompanying crumbling of the material and fracturing of the specimens is due to fragmentation of the macrostructure.

LITERATURE CITED

1. Yu. S. Virgil'ev, E. I. Kurolenkin, and T. N. Shurshakova, Izv. Akad. Nauk SSSR, Ser. Neorg. Mater., 13, No. 4, 752 (1977).
2. Yu. S. Virgil'ev, I. P. Kalyagina, and V. G. Makarchenko, in: Structural Materials Based on Carbon [in Russian], No. XV, Metallurgiya, Moscow (1980), p. 60.
3. Yu. S. Virgil'ev, I. P. Kalyagina, and V. G. Makarchenko, At. Energ., 36, No. 4, 310 (1974).
4. P. A. Platonov et al., ibid., 46, No. 4, 248 (1979).
5. Yu. S. Virgil'ev et al., ibid., 40, 423 (1976).

# DETECTION OF RADIONUCLIDES WITH THE AID OF AN AUTOMATIC LEARNING CLASSIFIER

B. V. Sazykin

UDC 550.835.08

It has been shown earlier [1] that sources of radiation with a known spectral distribution of the emitted particles on an unknown background can be automatically detected with radiometric equipment making use of a learning classifier. We describe in the present article a method of building a logic detector in which the decision rule is developed during a learning process on the basis of a stochastic approximation method and the clustering principle of the theory of sample recognition.

Formulation of the Problem. Assume that the medium to be examined contains a mixture of radionuclides, the radiation field of which is assumed to be stationary and homogeneous in space. A stationary sequence of pulses then will be observed at the output of some proportional pulse detector. Each of the pulses is generated by the useful radiation or by the background. The useful radiation corresponds to the L most intensive lines of the spectrum of the radionuclide to be detected. All the other radiation is related to the background. The background flux is initially unknown, but it is assumed that the form of the amplitude spectra of both signal and background are known. It is assumed that the detector output pulses are recorded by a measuring instrument without counting losses. The problem is to determine a criterion which at a fixed time of measurements provides a classification of the radionuclide to be detected with a certain reliability.

We disregard the problems which are associated with the instruments of pulse-flux processing in the detection unit selected. The problems have been considered in detail in the literature (see, e.g., [2, 3]). Let us note only that the pulse filter in the processing unit has a linear structure and that, if $n_1^l$ and $n_2^l$ denote the number of counts in the suboptimal division of the amplitude-measurement range into two groups (1 refers to channels in which the signal spectrum dominates over the background spectrum; 2 refers to the other channels), the most likely estimates of the recurrence frequencies $\lambda_1^l$ of the useful pulses and $\lambda_2^l$ of the background pulses of the $l$-th component of the radiation field can be obtained with the formulas

$$\lambda_1^l = \frac{F_{22}^l n_1^l - F_{21}^l n_2^l}{t(F_{11}^l - F_{21}^l)}; \quad \lambda_2^l = \frac{F_{11}^l n_2^l - F_{12}^l n_1^l}{t(F_{11}^l - F_{21}^l)};$$
$$l = 1, 2, \ldots, L,$$

where $F_{ij}^l$ $(i = j = 1, 2)$ denotes the probabilities of belonging to group 1 or group 2, respectively, and t denotes the time of measurement. The decision rule of detecting the $l$-th characteristic line with the probability $\alpha$ of incorrect classification is given by the formula (see [2], p. 183, Eq. (5.51)):

$$r_1 n_1 - r_2 n_2 > u_{1-\alpha}\{r_1 r_2[(1-r_1)\, n_1 + (1+r_2)\, n_2]\}^{1/2}, \tag{1}$$

where $r_1 = F_{22}/(F_{11} - F_{21})$; $r_2 = F_{21}/(F_{11} - F_{21})$; and $u_{1-\alpha}$ denotes the quantized fraction of the order $(1 - \alpha)$ of the standardized normal distribution. The subscript $l$ has been omitted in all the terms of Eq. (1) in order to simplify the notation.

Construction of a Learning Classifier and Its Use in the Detection Problem. A radionuclide is detected through L indicators, each of which is obtained from assessing a signal present in L channel groups: 1) signal present; 0) no signal. Thus, after N trials and NL times using the decision rule (1), we obtain a sequence $\{\mathbf{x}_N\}$ of double samples $\mathbf{x}_n$ $(n = 1, 2, \ldots, N)$ consisting of zeros and ones with the dimension L. It must be established whether a sample $\mathbf{x}$ belongs to one of the two classes, namely $\omega_1$, i.e., the radionuclide of interest is not present, or $\omega_2$, i.e., the radionuclide is present.

Translated from Atomnaya Énergiya, Vol. 55, No. 1, pp. 46-48, July, 1983. Original article submitted August 20, 1982.

 0038-531X/83/5501-0492$07.50 

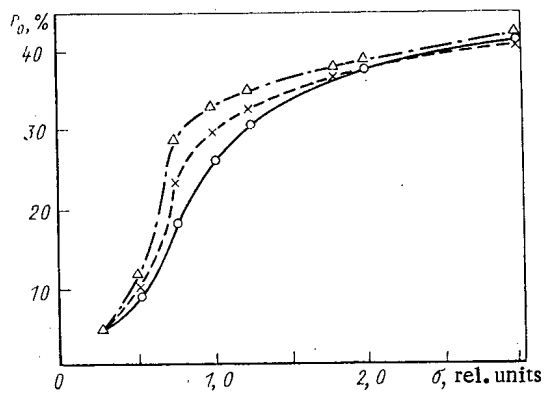


Fig. 1

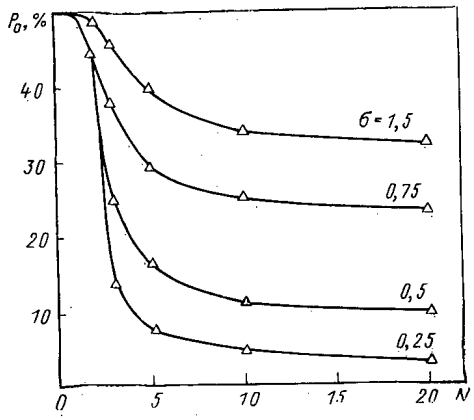


Fig. 2

Fig. 1. Dependence of the probability of a classification error upon the mean-square deviation of the pulse amplitude for m = 4 (×), 7 (Δ), and 8 (○); m is the number of terms in the expansion of the density of the relative distribution $p(\omega_1|\mathbf{x})$; N = 10 (number of terms of the learning sample set).

Fig. 2. Dependence of the probability of the classification error upon the number of terms of the learning sample set for various σ values.

It has been shown in [4] on the basis of a statistical approach to constructing a learning classifier that the dividing boundary $d(\mathbf{x})$ of the two classes is given by the formula

$$d(\mathbf{x}) = 2p(\omega_1|\mathbf{x}) - 1,$$

where $p(\omega_1|\mathbf{x})$ denotes the density of the distribution of the $\omega_1$ class. In this case the classification rule is formulated as follows:

$$\begin{aligned} \mathbf{x} &\in \omega_1, \quad \text{if} \quad p(\omega_1|\mathbf{x}) > 1/2; \\ \mathbf{x} &\in \omega_2, \quad \text{if} \quad p(\omega_1|\mathbf{x}) < 1/2. \end{aligned} \tag{2}$$

We represent the decision function in the form of an expansion of basis functions $\varphi_j(\mathbf{x})$, for which we choose the Rademacher—Walsh functions. Then

$$p(\omega_1|\mathbf{x}) \approx \sum_{j=1}^{m} W_j \varphi_j(\mathbf{x}) = \mathbf{W}^t \Phi(\mathbf{x}), \tag{3}$$

where $\mathbf{W} = (W_1, W_2, \ldots, W_m)^t$ denotes the weight vector for the class $\omega_1$, which must be determined through the learning process; and $\Phi(\mathbf{x}) = [\varphi_1(\mathbf{x}), \ldots, \varphi_m(\mathbf{x})]^t$ denotes the vector of the basis functions.

In order to construct the algorithm of the learning process and to determine the weight vector $\mathbf{W}$, we use an approximation based on the least mean-square error condition. We consider the function

$$J(\mathbf{W}, \mathbf{x}) = \frac{1}{2} E\{[r(x) - \mathbf{W}^t \Phi(\mathbf{x})]^2\},$$

of the criterion, where E is the mathematical expectation of some function;

$$r(\mathbf{x}) = \begin{cases} 1, & \text{if} \quad \mathbf{x} \in \omega_1; \\ 0 - & \text{otherwise}. \end{cases}$$

The minimum of the criterion can be found by taking the partial derivative of $J(\mathbf{W}, \mathbf{x})$ with respect to $\mathbf{W}$

$$\frac{\partial J(\mathbf{W}, \mathbf{x})}{\partial \mathbf{W}} = E\{-\Phi(\mathbf{x})[r(\mathbf{x}) - \mathbf{W}^t \Phi(\mathbf{x})]\}. \tag{4}$$

In order to calculate the root of the function of Eq. (4), we use the Robbins—Monroe algorithm [4]:

$$\mathbf{W}(k+1) = \mathbf{W}(k) - \alpha_k \left[\frac{\partial J(\mathbf{W}, \mathbf{x})}{\partial \mathbf{W}}\right]\Big|_{\mathbf{W}=\mathbf{W}(k)}, \tag{5}$$

where the value of the weight vector $\mathbf{W}(1)$ is arbitrarily chosen; the coefficients $\alpha_k$ are defined by the formula $\alpha_k = 1/k$; $k := k + 1$.

We obtain with Eqs. (4) and (5)

$$W(k+1) = \mathbf{W}(k) + \alpha_k \Phi(x_k)\,[r(x_k) - \mathbf{W}^t(k)\,\Phi(x_k)]. \tag{6}$$

The iteration procedure which is given by Eq. (6) terminates if all samples of the learning set which belong to the classes $\omega_i$, $(i = 1, 2)$ have been correctly classified, i.e., if they satisfy the rule

$$\begin{aligned} &\mathbf{W}^t\Phi(x) > 1/2 \quad \text{for} \quad x \in \omega_1; \\ &\mathbf{W}^t\Phi(x) < 1/2 \quad \text{for} \quad x \in \omega_2. \end{aligned} \tag{7}$$

Once the weight vector $\mathbf{W}$ and, hence, the coefficients of the decision function have been determined, the learning process ends. We can classify an unknown sample $\mathbf{x}$ by using the decision rule of Eq. (7) with a weight vector $\mathbf{W}$ obtained as a result of a learning process.

In order to assess the probability of the classification error $P_o$, we modeled on a computer the detection of a radionuclide from $L = 3$ indicators (the three spectral lines of highest intensity). Models of a quasioptimal pulse filter and a data processing unit (classifier) executing the decision rules defined by Eqs. (1) and (7) were used. The principle of the modeling is as follows. For a given ratio of the average recurrence frequencies of useful pulses and background pulses ($\beta = \lambda_1/\lambda_2$), a random-number generator was used to produce numerical sequences $\{a_l\}$, $(l = 1, 2, 3)$ corresponding to stationary fluxes of pulses for the three detection indicators. In each sequence $\{a_l\}$ generated, the distribution $f_1(a)$ of the useful pulses and $f_2(a)$ of the background pulses with respect to the amplitude $a$ were assumed to be normal with $\sigma_2^1 = \sigma_2^2 = \sigma^2$ and with a fixed distance $R = 1$ between the centers of the distribution. The random values $a_j$ of the amplitudes were obtained from the formulas

$$\sum_{k=1}^{j-1} f_{i,k}(a_k) \leqslant \gamma < \sum_{k=1}^{j} f_{i,k}(a_k), \quad i = 1, 2;$$

$$\sum_{k=1}^{K} f_{i,k}(a_k) = 1,$$

where $\gamma$ are random numbers of the interval between 0 and 1; and K is the number of intervals in the variability range of the amplitudes. When we constructed a statistical model of multichannel amplitude measurements, we assumed that each pulse is recorded with the probability 1 in the channel to which its amplitude belongs and that two channels are required for determining $\lambda_i^l$ from each $l$-th indicator of detection. According to [3], the boundary between two channels was taken at the point $a = a_o^l$. For this point $r_k^l(\beta, a) = 0$ $(k = 1, \ldots, K)$, where $r_k^l$ denotes the reduction coefficients of the quasioptimal filter, which were determined in the case $K = 10$ from the empirical $\lambda_1$ value and the minimization of the dispersion $D(\lambda_1)$ (see [2], p. 140, Eqs. (4.44) and (4.45)). Results of the $\lambda_1^l$ and $\lambda_2^l$ filtering were entered into the models of the decision blocks, which derived rules given by the formulas of the type of Eq. (1). When a useful signal was present, a detection indicator $x_l = 1$ was generated, whereas $x_l = 0$ when no such signal is present. Thus, a double sample $\mathbf{x} = (x_1, x_2, x_3)$ consisting of zeros and ones arrived at the input of the automatic classifier. The classification was made with the decision rule of Eq. (7). By generating sequences $\{a_l\}$ of random pulses with initially known parameters and classifying these sequences thereafter with the method outlined above, it is possible to calculate the probability of a classification error ($P_o = N_o/N_X$, where $N_o$ denotes the incorrectly classified part of sets out of $N_X$ independent, randomly chosen control sets of samples); the quality of the detection can be studied in this way.

Figures 1, 2 show the results of modeling for $\beta = 1$. There is a particular feature in the construction of the classifier. As could be expected, the error minimum is reached when the greatest possible number m of terms in the expansion given by Eq. (3) is taken into account. In the case of a three-dimensional double sample $\mathbf{x}$, the maximum value is $m = 2^3$ and at this m the probability $P_o$ of the classification error is minimal (see lower part of the curve of Fig. 1). However, when the number of expansion terms is odd ($m = 7$), the error curve increases and even exceeds the curve for $m = 4$. Calculations show that an even number of terms in the expansion in Rademacher—Walsh functions must be used in the construction of the classifier, because an odd number leads to an increase in the classification errors. The reasons for this feature stem from the normalization conditions of the basis functions selected. Figure 2 shows the dependence of the probability $P_o$ of the classification error upon

the number N of terms of the learning sample selection $\mathbf{x}$. Obviously, we obtain satisfactory results for $N = 10$, whereas for $N > 20$ the error curves reach "saturation" and a further increase in the number of terms of the learning sample is not advantageous.

The results of the modeling give reason to the assumption that the classification algorithms which we developed are operative and, in combination with algorithms of suboptimal filtering, provide a probability of a classification error of less than 10% when the number of terms of the learning sample is $N \geq 10$ and $D(\lambda_1) < R^2/4$, where $D(\lambda_1)$ denotes the dispersion of the estimate of the useful signal behind the pulse filter in the case of a normal distribution of both signal and background amplitudes.

The results of our investigation can be employed in the practice of mineral prospecting with the aid of radiometric techniques, radiation monitoring of media, and the detection of sources of cosmic radiation.

LITERATURE CITED

1. B. V. Sazykin, N. V. Nikitin, and L. P. Gorbachev, in: Abstracts of the Reports of the Second All-Union Symposium on the Joint Investigation of Hydrophysical Fields of the Ocean with the Aid of Isotope Techniques [in Russian], Vladivostok (1981), p. 19.
2. V. I. Bur'yan, V. I. Glagolev, and V. V. Matveev, Principles of the Theory of Measurements [in Russian], Atomizdat, Moscow (1977).
3. L. S. Gorn, M. V. Iovlev, and B. I. Khazanov, in: Nuclear Instrument Construction [in Russian], No. 19, Atomizdat, Moscow (1972), p. 39.
4. J. Tu and R. Gonzalez, Principles of Sample Recognition [Russian translation], Mir, Moscow (1978).

# OPTIMIZING HETEROGENEOUS SHIELDING COMPOSITIONS BY A SEQUENTIAL SIMPLEX METHOD

N. V. Nikitin and B. V. Sazykin

UDC 621.039.538

For a nuclear reactor, the designer must solve various optimization problems, of which optimization of a heterogeneous shield is typical. To find the optimum forms of shield composition, one usually employs the gradient method in various forms [1, 2]. Algorithms based on gradient methods have been found to be of good performance when the number of variables is small and simplified models are used for calculating the radiation-field functionals. However, a major disadvantage of these algorithms is the long run time along with the poor convergence if the target function is not unimodal. This leads one to abandon gradient methods and to use one of the direct search methods in optimization.

Here a simplex planning method is used in optimization, namely a sequential simplex method (SSM) [3]. The method has two substantial advantages: The search for the turning point by the SSM does not require complicated calculations, and the SSM algorithm combines test and working steps, which enables one to move toward the target with each change in the target function.

We consider the problem of minimizing the weight function for a one-dimensional shield

$$\min_{\mathbf{x} \in X} P(\mathbf{x}) \tag{1}$$

for given sources of neutron and $\gamma$ radiation subject to the constraints

$$D(\mathbf{x}) - D_0 = 0; \tag{2}$$

$$x_{i-} \leqslant x_i \leqslant x_{i+}; \quad i = 1, \ldots, n-1, \tag{3}$$

where $\mathbf{x} = [x_1, \ldots, x_n]^T$ is the parameter vector for the shield composition; $x_{i-}$ and $x_{i+}$, permissible limits to the parameter variation; X, region of acceptable solutions; and $D(\mathbf{x})$, $D_0$, overall dose rate defined by the parameter vector and the a priori specified neutron and

Translated from Atomnaya Énergiya, Vol. 55, No. 1, pp. 48-49, July, 1983. Original article submitted August 20, 1982.

0038-531X/83/5501-0495$07.50  

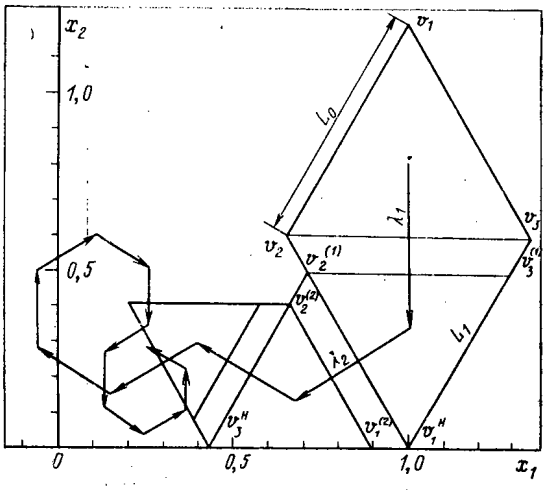


Fig. 1

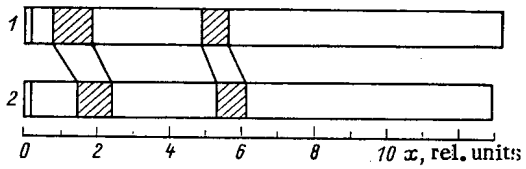


Fig. 2

Fig. 1. Example of the path followed by the center of the simplexes toward the minimum in the function $f = 4(x_1 - 0.25)^2 + (x_2 - 0.2)^2$ for $-1 \leq x_i \leq 1$; $i = 1, 2$.

Fig. 2. Parameters of the initial shielding composition (1) and the optimal one (2) made of lead and titanium hydride (lead layers hatched).

γ-ray dose rates behind the shield. The derivation of the minimum overall dose rate is handled similarly.

The nonlinear-programming problem of (1)-(3) was transformed into a sequence of problems without constraint of (2) in accordance with the sequential unconditional minimization method (SUMM) [4] by constructing a penalty function of the following form:

$$Q(\mathbf{x}^{(k)}, r^{(k)}) = f(\mathbf{x}^{(k)}) + \frac{1}{r^{(k)}} h(\mathbf{x}^{(k)}), \tag{4}$$

where

$$f(\mathbf{x}^{(k)}) = P(\mathbf{x}^{(k)})/P(\mathbf{x}^{(0)});$$
$$h = |D(\mathbf{x}^{(k)}) - D_0|/D(\mathbf{x}^0).$$

The values of the weighting coefficients r are positive and form a monotonically decreasing sequence, which can be induced by the relation

$$r^{(k)} = r^{(k-1)}/c, \tag{5}$$

where c is a positive constant and the initial value is $r^{(0)} = 1$.

To accelerate the convergence of the SUMM toward the conditional turning point, the solution to the problem $\mathbf{x}_* = \mathbf{x}(r^{(k)} \to 0)$ was found by an extrapolation procedure, in which the value of the vector $\mathbf{x}_*$ is represented as a polynomial in powers of $r^{1/2}$ [4]. The extrapolation estimate for $\mathbf{x}_*$ in the first approximation is

$$\mathbf{x}_* \simeq \frac{c^{1/2}\mathbf{x}(r^{(k)}/c) - \mathbf{x}(r^{(k)})}{c^{1/2} - 1}. \tag{6}$$

We now briefly describe how one searches for the minimum in $Q(\mathbf{x}^{(k)}, r^{(k)})$ by the simplex search method [3, 5], which is based on the construction and successive displacement of the simplex in n-dimensional space of the variable $\mathbf{x} = [x_1, \ldots, x_n]^{(T)}$. By simplex in n-dimensional space we mean a convex regular figure defined by a system of n+1 points; in two-dimensional space, the simplex is a triangle, while in three-dimensional space it is a tetrahedron, etc. The simplex-planning algorithm is as follows. We specify a system of n+1 points $\{x_1^0, \ldots, x_n\}$ forming the initial simplex $S^{(0)}$ (Fig. 1) and at all vertices of the simplex $v_j$, $j = 1, \ldots, n+1$ we calculate the values of the target function $Q_j$. A search step (first step $m = 1$) is performed by passing from the initial simplex to the new simplex $S^{(m)}$ by eliminating the worst vertex (at that vertex $Q_s^{(m)} = \max\{Q_j^{(m)}\}$) and constructing the mirror representation $v_s^m$ with respect to the face common to the two simplexes. Repeated reflection of the

worst vertices results in stepping motion of the center of the simplex toward the target along a certain kinked line. The length $\lambda_m$ of a step is defined by

$$\lambda_m = L_{m-1}\sqrt{\frac{2}{n(n+1)}},$$

where $L_m = L_0/(dm+1)$ is the length of a face of the simplex $S^{(m)}$, with d a positive constant. To choose the dimension $L_0$ we use the condition

$$L_0 \leqslant \frac{b}{2+n}\sqrt{\frac{(n+1)n}{2}},$$

where $b = \min\{x_{i+} - x_{i-}\}$ is the minimal range of variation in one of the parameters.

Note that a given accuracy in searching for the turning point is provided by the corresponding size $L_M$ of the last simplex $S^{(M)}$; if the maximum discrepancy is $\theta_0$, then $L_M = \theta_0[2m/(m+1)]^{1/2}$.

We would point out the simplicity of the SSM algorithm and the absence of complicated calculations. We leave aside the experiments in the vertices of the initial simplex $S^{(0)}$, and then at each search step one requires only one calculation of the target function at the vertex $v_j^m$ (Fig. 1). For the other vertices $v_j^{(m)}$ we use the values of the target function in the corresponding vertices $v_j$ or $v_j^m$. In the SSM algorithm, the direction of motion is dependent on the relation between the values of the target function at the vertices of the simplex, and therefore to choose the step direction it is sufficient to rank the target-function values. Also, all the constraints are very simply incorporated in the SSM: A vertex that does not satisfy the constraints is discarded.

We now describe a detailed example of optimizing a shielding composition for a water—water reactor. The initial form was a six-layer composition consisting of layers of steel, lead, and titanium hydride (Fig. 2), which initially was considered as optimal. The two boundaries of the first layer (steel thickness 1 cm) were taken as rigidly fixed and these parameters were not varied during the optimization. Apart from the constraints of (2) and (3), the following additional constraints were imposed on the coordinates of the zone boundaries:

$$x_0^0 < x_i < x_3^0; \quad x_2^0 < x_l < x_5^0; \quad i = 1, 2; \; l = i+2,$$

where $x_j^0$; $j = 0, \ldots, 5$ are the coordinates of the zones in the initial composition. In accordance with the recommendations of [4], the value of parameter c in Eqs. (5), (6) was taken as 4.

In search optimization by the SSM it was found that the weight characteristics of the shield can be reduced from $P = 7.482 \cdot 10^4$ g/cm in the initial form to $P = 7.391 \cdot 10^4$ g/cm. The zone coordinates of the optimal composition are shown in Fig. 2. To obtain these results required only 14 steps in SSM search. The values of the dose rate at the outer surface of the optimal multilayer shield and the components in relative terms were $D_0 = D_n + D_{n\gamma} + D_\gamma = 2$; $D_n = 0.82$; $D_{n\gamma} = 1.17$.

To optimize the shielding by the SSM, we wrote a program used with an EC-1033 computer. The optimization program included modules enabling one to calculate the characteristics of the neutron and $\gamma$-ray fields. The calculations on the neutron flux density were performed in a five-group diffusion-age approximation, while the neutron dose rate $D_n$ and the dose rate due to captured $\gamma$ radiation from the materials of the shield composition $D_{n\gamma}$ were calculated by means of the MGRZ program [6]. The group $\gamma$-ray flux densities from the core and the corresponding dose rate $D_\gamma$ were calculated by means of the modified CYLINDER program [6], in which the numerical integration is performed by the use of optimal Korobov coefficients. The optimization program was written in FORTRAN IV and enables one to perform calculations with $n \leq 20$ variables. The run time with $n = 4$-6 was about 15-20 min. This time, in the main, is determined by the time needed to calculate the multidimensional integral by Korobov's method. For example, the computing time with about 180 integration nodes is about 50 sec.

In conclusion, we are indebted to L. V. Ershova for assistance in writing and debugging the programs.

LITERATURE CITED

1. A. P. Suvorov and R. P. Fedorenko, in: Aspects of Reactor Shielding Physics [in Russian], Issue 3, Atomizdat, Moscow (1969), p. 6.

2. G. A. Germogenova et al., ibid, Issue 4, p. 89.
3. W. Spendly, G. Hext, and F. Himsworth, Technometrics, 4, 441 (1962).
4. D. M. Himmelblau, Applied Nonlinear Programming, McGraw-Hill (1972).
5. A. P. Dambrauskas, Simplex Search [in Russian], Énergiya, Moscow (1976).
6. Engineering Calculation of Nuclear Power Station Shielding [in Russian], Atomizdat, Moscow (1976).

# A MEDICAL INSTALLATION BASED ON AN IRON-FREE BETATRON

V. N. Amelichkin, V. V. Artemov,
V. B. Veselovskii, B. G. Kudasov,
V. O. Kuznetsov, Yu. P. Kuropatkin,
A. I. Pavlovskii, and V. N. Suvorov

UDC 621.384.643.3:615.849

High-current betatrons provide very simple compact and reliable pulsed high-energy x-ray and electron-beam sources [1].

High pulse currents in the windings of the electromagnet in an iron-free betatron do not rule out frequent repetition. However, such devices are comparatively uncommon at present, mainly because of difficulties in building the electromagnet power supply, in which a major element is the high-voltage rectifier switch, which carries current pulses of some tens of kiloamperes. Developments in thyristor engineering have resolved this problem [2] and should provide for substantial progress in the near future.

The energy of the accelerated electrons in an iron-free betatron is determined by the parameters of the electromagnet power supply and within certain limits does not influence the dimensions and mass of the radiator. For example, a betatron for an energy of 50-70 MeV has a diameter of 0.5 m and a mass of some tens of kilograms, which are substantially less than the size and mass of any other accelerator for this energy. This feature is particularly important in designing a system with a mobile radiator, particularly medical radiation systems with rotating stands.

Other attractive features are the relatively low cost and the constancy in time of the magnetic-field characteristics, which along with other advantages of iron-free accelerators determine the prospect for using them in routine radiotherapy.

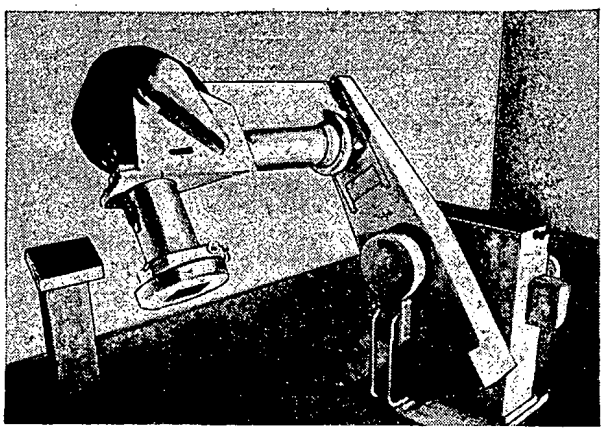

Fig. 1

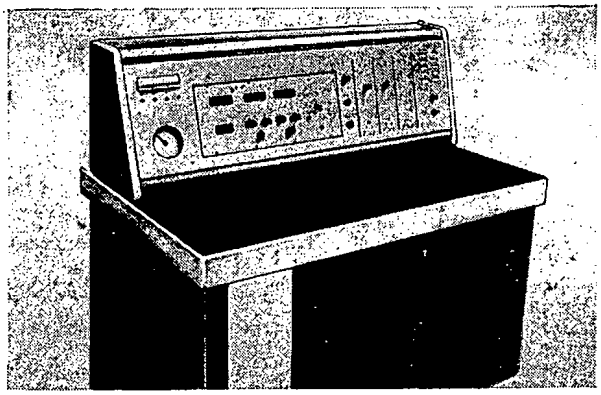

Fig. 2

Fig. 1. General view of the prototype medical betatron system.

Fig. 2. The control panel.

Translated from Atomnaya Énergiya, Vol. 55, No. 1, pp. 50-51, July, 1983. Original article submitted September 3, 1982.

 0038-531X/83/5501-0498$07.50 

Figure 1 shows a prototype medical betatron unit in which the electron beam is extracted in accordance with medical-engineering requirements and which was developed by the Oncology and Medical Radiology Research Institute (NIIOMR) of the Ministry of Health Care of the Belorussian SSR in accordance with the specifications laid down by the International Electrotechnical Commission. The initiative for the development came from the Director of the institute, Associate Member of the Academy of Medical Sciences of the USSR, Professor N. N. Aleksandrov.* Figure 1 shows the rotation stand with the radiating head fixed to a cantilever, the electromagnet power supply, the pulse-generator rack, and the auxiliary panel. The control panel is shown in Fig. 2. The following are the technical characteristics:

| | |
|---|---|
| Electron energies, MeV | 5, 8, 11, 14, 17, 20 |
| Energy spread, MeV | 0.5 |
| Intensity in radiation field, Gy/min | 1 |
| Dimensions of rectangular radiation field, cm | (2 × 2) — (20 × 20) |
| Inhomogeneity of radiation in field, % | ±5 |
| Penumbra dimensions, cm: | |
| along axes | 2 |
| along diagonals | 4 |
| Radiator oscillation limits, deg | ±120 |
| Oscillation rate, rpm | 0.33 |
| Accuracy in setting oscillation angle, deg | 1 |
| Radiation pulse repetition frequency, Hz | 3 |
| Power drawn, kW | 15 |

The apparatus is fitted with a sealed accelerator chamber having an autoemission injector with an energy of 250-300 keV. The chamber includes a channel for extracting the electron beam, and a beam of essentially circular cross section is then obtained at the output. This substantially simplifies the formation of the irradiation field by means of interchangeable scattering foils and a special toroidal magnetic lens [3], which focuses the peripheral part of the beam. The resulting shaped beam of circular cross section is then restricted to working dimensions by an adjustable diaphragm placed as close as possible to the irradiated object, which enables one to obtain acceptable dimensions for the penumbra. The autoemission nanosecond injector was described in prototype in [4], and this simplifies the design of the accelerator chamber and provides high-voltage injection into the acceleration region without special beam-transport devices.

The electromagnet is made separable in the median plane and has a device for adjusting the acceleration chamber. The high-voltage part of the injection-pulse generator is fixed on the cantilever and is connected to the injector by a flexible junction. To reduce the noise level, the betatron is surrounded by a sound-absorbing jacket, which is enclosed in a soft case. The mass of the radiator with the injection unit and shaper is not more than 120 kg. The electromagnet is supplied with half-sine waves of amplitude 20 kA and duration 600 μsec, which are produced by a push—pull generator as described in [5]. A feature of the generator is that there is transformer-free step-up from the line voltage of 3 × 380 V to the working voltage of 10 kV, which is attained by recuperating the energy of the shaping capacitor and resonant pumping. The controlled switch described in detail in [6] is a device consisting of five parallel columns, each consisting of ten series-connected thyristors type T16-320-12 together with equalizing circuits.

The equipment is fitted with a digital dosimetric monitoring system. The rapid monitoring device in 30-40 sec provides the intensity distribution along the axes or diagonals of the rectangular field. The beam is adjusted by means of a light field indicator. The control of the equipment is very simple: After the thyratrons in the pulse generators have warmed up for 5 min, the dose for the session is set together with the radiation energy (the latter is adjusted by switching the output phase), and the equipment is ready for use. During the session, the injection phase is adjusted either manually or by means of an automatic optimum-phase system. The radiation is switched off automatically when the given dose has been reached in any dosimetric channel. The interlock system makes it impossible to switch on the radiation if there is a discrepancy between any of the accelerator parameters from the given value, while there is emergency switch-off if any discrepancy arises during the irradiation. The dosimeter readings are then preserved.

*Deceased.

At present the apparatus is undergoing clinical tests at NIIOMR in Minsk, and when these are completed it is proposed to manufacture several experimental specimens. These will be tested at leading oncological clinics to provide a final conclusion on the applicability in oncology. The equipment is fitted with a radiator working with an extracted electron beam. There are no essential obstacles to operating with an x-ray source with appropriate radiation characteristics. For example, one can increase the pulse repetition frequency and/or increase the limiting acceleration energy. However, this would increase the power drawn from the line considerably and would increase the mass (on account of the shaping device for the x rays), and this would reduce the reliability of the power supply and also make the equipment much more expensive. On the other hand, an accelerator with an electron beam alone appears to be capable of handling a considerable number of tasks in radiation therapy, particularly in combination with standard tele-gamma equipment. An additional extension of the application may come from raising the electron energy to 30-35 MeV, which is possible without substantial change in the design. The dimensions and radiation characteristics also enable one to place the equipment in a typical gamma-equipment shielded room.

In Soviet oncology there are substantial difficulties on account of deficiencies in radiation technique for therapeutic purposes. Accelerators of a high class can be provided only for a few leading oncological centers. To provide maximum coverage of patients acutely needing therapy, methods of electron-beam therapy should be extended (as far as equipping regional clinics with accelerators). The problem can be solved by routine production of medical equipment suitable for mass use. We consider that such equipment can be based on this prototype medical betatron.

LITERATURE CITED

1. A. I. Pavlovskii et al., Dokl. Akad. Nauk SSSR, 160, No. 1, 68 (1965).
2. A. M. Kozodaev, Electrically Controlled Rectifiers for Shaping High-Power Current Pulses [in Russian], Atomizdat, Moscow (1975).
3. R. Wideroe, Patent Specification No. 1268714, Patent Office, London (1972).
4. V. O. Kuznetsov et al., Prib. Tekh. Eksp., No. 6, 30 (1976).
5. V. I. Amelichkin, B. G. Kudasov, and Yu. P. Kuropatkin, ibid., No. 4, 97 (1982).
6. V. I. Amelichkin and B. G. Kudasov, ibid., p. 98.

# INFLUENCE OF THE EFFICIENCY OF RECORDING FISSION EVENTS ON THE MEAN NUMBER OF INSTANTANEOUS FISSION NEUTRONS MEASURED

V. V. Malinovskii, V. G. Vorob'eva,
B. D. Kuz'minov, V. M. Piksaikin,
N. N. Semenova, V. S. Valyavkin,
S. M. Solov'ev, and P. S. Soloshenkov

UDC 539.173

The requirement on the accuracy of determining the mean number of instantaneous fission neutrons $\bar{\nu}_p$ (0.5-1.0%) [1], following from the requirements of nuclear energetics, entails the need for careful analysis of the methods and results of measurement. One possible experimental error is the incomplete recording of events of nuclear fission.

In most measurements of $\bar{\nu}_p$, an ionization chamber is used. In this case the probability of recording a fission event depends on the thickness of the fissile layer, on the type and operating conditions of the chamber, and also on the mass, kinetic energy, and angular distribution of the fragments. Earlier [2, 3], the influence of the layer thickness of the fissile material on the results of measuring $\bar{\nu}_p$ were investigated. In the present work, the more general dependence of the value measured for $\bar{\nu}_p$ on the efficiency of recording fission events is investigated.

The neutron detector consisted of 16 $^3$He counters in a polyethylene moderator. The detector characteristics, the electronic neutron-recording circuit, and the method of analyzing the experimental results were described in [4]. Fission events were recorded by a plane-parallel ionization chamber filled with argon containing 10% $CO_2$ to a pressure of 1.5 atm (0.152 MPa). The gap between the electrodes was 50 mm. A layer of a homogeneous mixture of the mixed oxide of natural uranium and $^{252}$Cf of thickness 0.1-1.95 mg·cm$^{-2}$ was used in the experiment. The "infinitely thin" layer was taken in the form of a $^{252}$Cf layer prepared by the self-transfer method in an electric field.

For six layers of fissile material, $\bar{\nu}_p$ was measured at several values of the amplitude-discrimination level of the fission-chamber pulses. The total number of fission events in each layer was determined from the $\alpha$ activity and from the intensity of the neutron radiation. The agreement between the level of discrimination of the fission-chamber pulses and the efficiency of recording fission events was established with an accuracy of no worse than 2%. The

TABLE 1. Decrease in $\bar{\nu}_p$ on Account of the Layer Thickness of the Fissile Material

| Composition of the fissile-material layer | Present work | | | δ for layer thickness 1 mg·cm$^{-2}$ [3],* % |
|---|---|---|---|---|
| | δ for layer thickness 1 mg·cm$^{-2}$, % | statistical error | error of approximation | |
| Homogeneous $^{252}$Cf impurity in the layer | | | | |
| $U_3O_8$ | 0,315 | 0,046 | | |
| $^{235}$U | 0,195 | 0,028 | 0,010 | 0,169 |
| $^{235}U_3O_8$ | 0,350 | 0,051 | 0,010 | 0,282 |
| $^{239}$Pu | 0,186 | 0,027 | 0,012 | 0,165 |
| $^{239}PuO_2$ | 0,314 | 0,046 | 0,020 | 0,251 |

*The accuracy of the results of [3] is about 20%.

Translated from Atomnaya Énergiya, Vol. 55, No. 1, pp. 51-52, July, 1983. Original article submitted September 13, 1982; revision submitted January 17, 1983.

0038-531X/83/5501-0501$07.50  

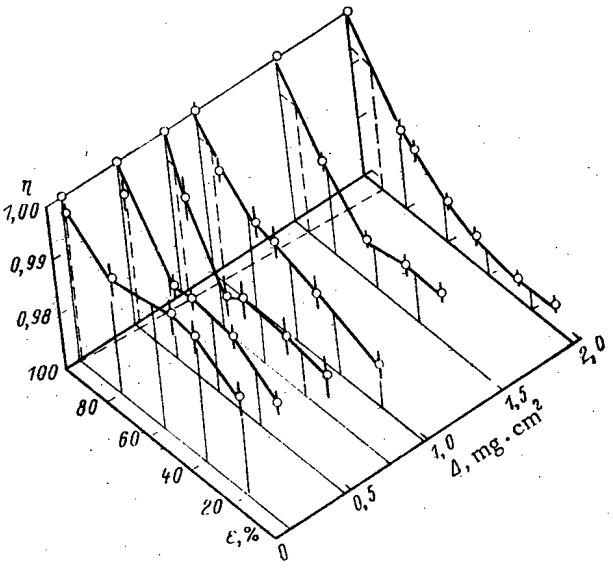


Fig. 1

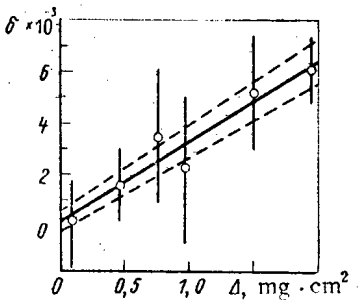


Fig. 2

Fig. 1. Dependence of $\eta = \bar{\nu}_p/\bar{\nu}_p^0$ on the efficiency of recording fission events $\varepsilon$ for various layer thicknesses of the fissile material $\Delta$ (the statistical error is indicated); the dashed lines indicate values corresponding to zero discrimination level of the fission-chamber pulses.

Fig. 2. Dependence of $\delta = (1 - \eta)$ on the layer thickness of the fissile material $\Delta$; the continuous curve corresponds to description by the least-squares method, the dashed curves to the level of statistical accuracy of the description obtained, and the points to experiment.

value obtained in measurements with an "infinitely thin" layer of $^{252}Cf$ was taken as the "true" value of $\bar{\nu}_p^0$, corresponding to 100% recording of the fission events. Analysis of the amplitude spectra of the pulses from spontaneous-fission fragments of $^{252}Cf$ for different thicknesses of the fissile material allows the efficiency of recording the fragments to be extrapolated to zero discrimination level (Fig. 1).

The results in Fig. 1 indicate that the greatest change in $\eta$ occurs when $\varepsilon$ is reduced from 100% to 70%; in this range, evidently, it is mainly fission events with a small kinetic energy, and correspondingly with a high value of $\nu$, that are lost. With 40-50% efficiency of recording fission events, the pulse amplitude is determined mainly by the geometric characteristics of the chamber, and not by the kinetic energy of the fragments. A "plateau" is then observed in the dependence $\eta = f(\varepsilon)$.

The results obtained indicate that the value of $\eta$ varies on account of the loss of fission events with total retardation of the fragments in the layer and on account of the amplitude discrimination of the chamber pulses. The dependence of $\delta = (1 - \eta)$ (zero discrimination level) on the layer thickness is shown in Fig. 2. The statistical error is given. Description by the least-squares method gives $\delta = [(0.113 \pm 0.524) + (3.154 \pm 0.459)\Delta] \cdot 10^{-3}$, where $\Delta$ is the layer thickness of the fissile material, $mg \cdot cm^{-2}$.

On the basis of the present results for a homogeneous mixture of $^{252}Cf$ and $^{238}U_3O_8$ and data on the kinetic energy, mass, and path lengths of the fragments [5, 6], the value of $\delta$ for the fission of $^{235}U$ and $^{239}Pu$ by thermal neutrons was calculated. A linear dependence of the effect on the path lengths of light and heavy fragments was assumed. The results of the calculation are shown in Table 1. Two components of the error are indicated: the statistical error and an estimate of the accuracy of the conversion from californium to uranium and plutonium. The results of [3] are given for comparison. Note that the data in Table 1 are strictly valid only for an isotropic angular distribution of the fragments. With fission by fast neutrons, the value of $\delta$ is different, generally speaking, since the proportion of fragments absorbed in the layer depends on their angular distribution. The value of $\delta$ obtained here is higher than in [3], although the difference does not exceed the measurement

error. One reason for this discrepancy is the use of neutron detectors which have, e.g., a different dependence of the efficiency on the direction of motion and energy of the neutrons.

As a result of the investigation it may be concluded that the correction to $\bar{\nu}_p$ taking account of incomplete recording of the fission events may reach a few percent. With a fixed level of amplitude discrimination of the fragment pulses, this correction depends on the layer thickness of the fissile material. In the general case it is also determined by the chosen methods of recording the neutrons and the fission events.

LITERATURE CITED

1. WRENDA 79/80 INDC (SEC), 73/URSF, IAEA, Vienna (1979).
2. H. Condé and M. Holmberg, Arkiv. Fys., 29, 33 (1965).
3. J. Boldeman and J. Frehaut, Nucl. Sci. Eng., 76, 49 (1980).
4. V. G. Vorob'eva et al., Vopr. At. Nauk. Tekh., Ser. Yad. Konst., No. 3 (38), 44 (1980).
5. L. Northcliff and R. Shilling, Nucl. Data Tables, A7, 233 (1970).
6. J. Unik et al., in: Proceedings of Third IAEA Symposium on the Physics and Chemistry of Fission, Rochester, August 13-17, 1973, Vol. 2 (1973), p. 19.

# GAMMA EQUIVALENT OF SOURCES OF IONIZING RADIATIONS*

V. V. Bochkarev, I. B. Keirim-Markus, and U. Ya. Margulis

UDC 389:553.76

In the practical work with radioactive sources, the physics quantity "γ equivalent" is widely used. Particularly in γ defectoscopy, γ therapy, and radiation technology, the γ equivalent is the basic radiation characteristic of radionuclides used as sources of γ radiation. The quantity is also necessary for evaluating the radiation hazard produced by technological solutions of radioactive materials with a complicated or undefined composition, and for calculating the shielding of communication parts and containers with such solutions. The γ equivalent can be used to assess the load of storage areas of radioactive waste or of transport media used for shipping radioactive materials, etc.; the γ equivalent is used to standardize γ radiation sources (Basic Health Regulation OSP-72/80, paragraph 1.2c, etc. [1]).

In the Radiation Safety Standards NRB-76 [1] the γ equivalent is defined as the relative mass of a $^{226}$Ra point source creating at a certain distance the same exposure dose rate as a particular source. The γ equivalent is therefore one of the most important radiation characteristics of photon-radiation sources.

The γ equivalent is defined through the exposure dose. However, there exists an international tendency to abandon the exposure dose as a dosimetric quantity in the international (SI) system of units. The use of radium as a standard radionuclide is also a matter of the past and radium is nowadays of very little importance in practice. Therefore, there arises the problem of a quantity replacing the γ equivalent in the SI system.

In view of the details outlined above, it is suggested to give up the use not only of radium, but of any other radionuclide source, and to define the γ equivalent in the SI system as the rate of the water kerma $\dot{K}$ of photon radiation (with a photon energy exceeding a certain threshold value Δ, keV) of a given isotropic point source in vacuum at the distance $l$ = 1 m from the source. In analogy to the γ equivalent, it is suggested to call this quantity the "photon equivalent of the source" and to denote it by $F_\Delta = \dot{K} l^2$. The photon equivalent of a volume source is, accordingly, equal to the sum of the photon equivalents of the component point sources. The unit of the photon equivalent in the SI system is $Gy \cdot m^2 \cdot sec^{-1}$ (Gray·meter$^2$ per second). This quantity should receive a special name and we suggest the term

*Published as a discussion — Remark of the editors.

Translated from Atomnaya Énergiya, Vol. 55, No. 1, p. 53, July, 1983. Original article submitted October 4, 1982.

0038-531X/83/5501-0503$07.50  

"photek" for it: 1 photek = 1 $Gy \cdot m^2 \cdot sec^{-1}$. The photek is defined as the photon equivalent of a point source creating at a distance of 1 m a water kerma rate of 1 $Gy \cdot sec^{-1}$. Fractions of the unit are conveniently used in practice, namely nphotek, μphotek, and mphotek. In these units, the photon equivalent of 1 mg of $^{226}Ra$ amounts to ∿2.2 nphotek. The existing unit of the γ equivalent of 1 kg-eq radium is 2.2 mphotek, and 1 photek is ≈ 460 kg-eq radium.

The proposed definition needs some explanation. The kerma in air is the energy equivalent of the exposure dose of a photon radiation. By contrast to the exposure dose, the use of the kerma is not restricted to values above some photon energy, and this is important when new sources of high-energy photons appear. The kerma renders the dosimetric characteristic of a field of ionizing radiation and is numerically close to the absorbed dose when the conditions of electron equilibrium develop.

Isaev and Tsenter [2] have previously shown that it is necessary to introduce a quantity replacing the γ equivalent in the SI system. They suggested for this purpose a quantity which is based upon the absorbed dose; the definition of this quantity did not require the use of radium as a standard source. However, the absorbed dose does not characterize a field of ionizing radiation. In a particular radiation field, the absorbed dose can assume various values, and only in the case of electron equilibrium can the absorbed dose serve as a measure of a photon radiation field. But under these conditions the absorbed dose is almost equal to the kerma [3]. It is therefore suggested to express the photon equivalent through the kerma.

For historical reasons, the exposure dose was defined for air. Air is close to biological tissue in regard to the interactions with photon radiation: the ratio rad/roentgen for soft biological tissue is 0.945 ±0.025 in the photon energy range of 10 keV to 3 MeV. However, for other types of radiation (particularly for neutrons), air cannot be used as a standard substance. It is therefore convenient to review the quantities in the transition to the SI system when a new universal standard substance with properties close to those of biological tissue is to be selected, since the main task of dosimetry is to monitor the effect of radiation upon people. Water can be the substance. In the case of photons, the ratio of the dose absorbed by soft biological tissue to the dose in water is 1.02 ±0.025 in the energy range indicated above. In view of the above conclusions, the simple chemical composition of water, and its general presence, water can be recommended as the standard substance.

When the constant rate of the air kerma is determined (the kerma replacing the previous quantity, i.e., the γ constant of a radionuclide), the rate of the kerma of the radiation unit has its lower limit given by the energy range of the photons to avoid the difficulties associated with the self-absorption of low-energy photons in air [4]. For the same reasons, a similar limit (Δ, keV) has been introduced in the definition of the photon equivalent.

The proposed definition of the photon equivalent makes it possible to express in a simple fashion the quantity which in the SI system can replace the γ constant of a radionuclide. The quantity can be termed the "photon constant of a radionuclide" and is defined as the photon equivalent of a radionuclide with the activity 1 Bq. The unit of the photon constant is photek·$Bq^{-1}$; 1 $R \cdot cm^2 \cdot h^{-1} \cdot mCi^{-1} \approx 6.95$ aphotek·$Bq^{-1}$, 1 photek·$Bq^{-1} \approx 0.144 \cdot 10^{18}$ $R \cdot cm^{-2} \cdot h^{-1} \cdot mCi^{-1}$. In the new units, the photon constant of $^{226}Ra$ is 65; of $^{40}K$, 5.6; of $^{60}Co$, 92; and of $^{137}Cs$, 23 aphotek·$Bq^{-1}$ [5]. The above-suggestions might be conveniently used in the transition to the SI system in the field of ionizing radiations.

## LITERATURE CITED


1. Radiation Safety Standards NRB-76 and Basic Health Regulations OSP-72/80 [in Russian], Énergoizdat, Moscow (1981).
2. B. M. Isaev and É. M. Tsenter, Izmer. Tekh., No. 9 (1980).
3. Radiation Safety, Quantities, Methods, Units, and Instruments [in Russian], Atomizdat, Moscow (1974).
4. ICRU Rep. 33, Radiation Quantities and Units, Washington (1980).
5. N. G. Gusev and P. P. Dmitriev, Quantum Radiation of Radioactive Nuclides [in Russian], Atomizdat, Moscow (1977).

# RUSSIAN JOURNALS IN THE PHYSICAL AND MATHEMATICAL SCIENCES

## AVAILABLE IN ENGLISH TRANSLATION

**ALGEBRA AND LOGIC**
*Algebra i Logika*
Vol. 23, 1984 (6 issues) ..... $360

**ASTROPHYSICS**
*Astrofizika*
Vol. 20, 1984 (4 issues) ..... $420

**AUTOMATION AND REMOTE CONTROL**
*Avtomatika i Telemekhanika*
Vol. 45, 1984 (24 issues) ..... $625

**COMBUSTION, EXPLOSION, AND SHOCK WAVES**
*Fizika Goreniya i Vzryva*
Vol. 20, 1984 (6 issues) ..... $445

**COSMIC RESEARCH**
*Kosmicheskie Issledovaniya*
Vol. 22, 1984 (6 issues) ..... $545

**CYBERNETICS**
*Kibernetika*
Vol. 20, 1984 (6 issues) ..... $445

**DIFFERENTIAL EQUATIONS**
*Differentsial'nye Uravneniya*
Vol. 20, 1984 (12 issues) ..... $505

**DOKLADY BIOPHYSICS**
*Doklady Akademii Nauk SSSR*
Vols. 274-279, 1984 (2 issues) ..... $145

**FLUID DYNAMICS**
*Izvestiya Akademii Nauk SSSR, Mekhanika Zhidkosti i Gaza*
Vol. 19, 1984 (6 issues) ..... $500

**FUNCTIONAL ANALYSIS AND ITS APPLICATIONS**
*Funktsional'nyi Analiz i Ego Prilozheniya*
Vol. 18, 1984 (4 issues) ..... $410

**GLASS AND CERAMICS**
*Steklo i Keramika*
Vol. 41, 1984 (6 issues) ..... $590

**HIGH TEMPERATURE**
*Teplofizika Vysokikh Temperatur*
Vol. 22, 1984 (6 issues) ..... $520

**HYDROTECHNICAL CONSTRUCTION**
*Gidrotekhnicheskoe Stroitel'stvo*
Vol. 18, 1984 (12 issues) ..... $385

**INDUSTRIAL LABORATORY**
*Zavodskaya Laboratoriya*
Vol. 50, 1984 (12 issues) ..... $520

**INSTRUMENTS AND EXPERIMENTAL TECHNIQUES**
*Pribory i Tekhnika Eksperimenta*
Vol. 27, 1984 (12 issues) ..... $590

**JOURNAL OF APPLIED MECHANICS AND TECHNICAL PHYSICS**
*Zhurnal Prikladnoi Mekhaniki i Tekhnicheskoi Fiziki*
Vol. 25, 1984 (6 issues) ..... $540

**JOURNAL OF APPLIED SPECTROSCOPY**
*Zhurnal Prikladnoi Spektroskopii*
Vols. 40-41, 1984 (12 issues) ..... $540

**JOURNAL OF ENGINEERING PHYSICS**
*Inzhenerno-fizicheskii Zhurnal*
Vols. 46-47, 1984 (12 issues) ..... $540

**JOURNAL OF SOVIET LASER RESEARCH**
*A translation of articles based on the best Soviet research in the field of lasers*
Vol. 5, 1984 (6 issues) ..... $180

**JOURNAL OF SOVIET MATHEMATICS**
*A translation of Itogi Nauki i Tekhniki* and *Zapiski Nauchnykh Seminarov Leningradskogo Otdeleniya Matematicheskogo Instituta im. V. A. Steklova AN SSSR*
Vols. 24-27, 1984 (24 issues) ..... $1035

**LITHOLOGY AND MINERAL RESOURCES**
*Litologiya i Poleznye Iskopaemye*
Vol. 19, 1984 (6 issues) ..... $540

**LITHUANIAN MATHEMATICAL JOURNAL**
*Litovskii Matematicheskii Sbornik*
Vol. 24, 1984 (4 issues) ..... $255

**MAGNETOHYDRODYNAMICS**
*Magnitnaya Gidrodinamika*
Vol. 20, 1984 (4 issues) ..... $415

**MATHEMATICAL NOTES**
*Matematicheskie Zametki*
Vols. 35-36, 1984 (12 issues) ..... $520

*continued on inside back cover*